Politecnico di Torino

Department of Environment, Land and Infrastructure Engineering

Changes of Extreme Precipitation and Temperature Indices Over Two Alpine Regions Using CMIP5 Climate Models

Master's Degree Thesis in

Environmental and Land Engineering

Candidate

Daniela Andrea Quintero García

Supervisors Prof. Alberto Viglione

Prof. Francesco Laio

July 2020

SUMMARY

General Circulation models (GCMs) are the main tools used to explore the climate system by modelling it at the global scale. They allow to study the past climate and generate future projections based on different emission scenarios. Studies based on GCMs simulations have shown that there is great variability in the expected climate change in different regions of the world. Also, the changes in average and extreme values of the atmospheric variables may differ. In this thesis we investigate the GCMs outputs in terms of temperature and precipitation extremes over two alpine areas, i.e., the Alps and the Andes, that are considered among the most vulnerable regions in the world. We evaluate the changes of temperature and precipitation over the period 1850-2100 as simulated by forty-nine models participating in the Coupled Model Intercomparison Project Phase 5 (CMIP5). We compute 27 climate extreme indices defined by the Expert Team on Climate Change Detection and Indices (ETCCDI) based on daily minimum and maximum temperatures and daily precipitation. In general, indices based on temperature indicate higher changes in the future for both regions when compared to the global changes. In particular the Alps are warming and are predicted to warm more than the Andes, both in terms of average temperature and of extreme temperature indices. For the precipitation based-indices, there is a wide disagreement about the sign of change in the Andes region, while the projections suggest an increase of extreme precipitation in the Alps. As expected, higher warming and precipitation extremes are more pronounced under RCP8.5 (worst-case emission scenario) as compared to RCP4.5 (intermediate emission scenario).

Meteorology has ever been an apple of contention,
as if the violent commotions of the atmosphere
induced a sympathetic effect on the minds
of those who have attempted to study them.

— Joseph Henry

ACKNOWLEDGMENTS

I would like to express my gratitude to *Prof. Alberto Viglione* and *Francesco Laio* for giving me the opportunity and responsibility to work on this project and for his continuous support and constructive suggestions during the development of this thesis work. I would also like to thank Walter Gallego for your continuous support along these years.

We acknowledge the World Climate Research Programme's Working Group on Coupled Modelling, which is responsible for CMIP, and we thank the climate modeling groups (listed in Table A.1) for producing and making available their model output. For CMIP the U.S. Department of Energy's Program for Climate Model Diagnosis and Intercomparison provides coordinating support and led development of software infrastructure in partnership with the Global Organization for Earth System Science Portals.

CONTENTS

LIST OF FIGURES

LIST OF TABLES

LISTINGS

Part I

THESIS

1

INTRODUCTION

Each of the last three decades has been successively warmer at the Earth's surface than any preceding decade since 1850 (Stocker et al. [32]). In the Northern Hemisphere, 1983-2012 was the warmest 30-year period of the last 1400 years. The human influence on the climate system is clear. Anthropogenic influences have contributed to observed increases in atmospheric moisture content in the atmosphere, changes in precipitation patterns, intensification of heavy precipitation, and warmer temperatures over land regions [31]. Those changes are linked to the increase in greenhouse gasses concentrations in the atmosphere, the positive radiative forcing, in changes in the global water cycle, reductions in snow and ice in glaciers, and in changes in climate extremes.

Extreme events, such as floods, heat waves, will have stronger impacts on sector related to climate such as water, agriculture, food security and forestry [11]. The fact that there is a possibility of climate extremes occurring and even intensifying in the future raises concern in society. Therefore, research on future climate and extreme events can be used to develop plans for risk control, better disaster risk management and social adaptation to climate extremes, reducing vulnerability, exposure, protecting human life and reducing economic damage.

Extremes are generally understood as very large and unusual deviations from the normal state of any system under consideration [29], extremes are realizations of the tail of the probability distribution of weather. They are generally more difficult to realistically represent in climate models. Climate extremes include windstorms (tropical cyclones and mid-latitude winter storms), floods, droughts and heat waves [3]. Thus, there is a clear incentive for studies related to extreme weather events and possible changes in their frequency and intensity as the climate changes during the 21st century. However, it is important to point out that there are few data available to make assessments of changes in extreme events, such as in their frequency or intensity, because these events are rare. The more rare the event, the more difficult it is to identify long-term changes. Some studies have been demonstrated that for a comparative change in the mean and variance of a univariate probability distribution, the frequency of these events is more sensitive to changes in variability than in the means.

Single extreme events cannot be directly attributed to anthropogenic climate change, as there is always the possibility that the event in question would have occurred without this contribution. However, for certain types

of regional, long-duration extremes such as warming and rainfall, it is possible that from the results of the climate model, the probability of such an extreme has changed due to anthropogenic climate forcing [11]. For instance, over the land, the range between dry and wet season precipitation has increased, particularly in the tropics [18]. In the case of the Alpine mountains extreme rainfall can trigger floods or landslides resulting in loss of life [4].

The frequency, spatio-temporal variability an intensity of climate extremes are expected to change [16]. For this reason it is important to analyse the past climate from observational data to better identify changes in the climate. For instance, daily precipitation and temperature have to be considered to asses meteorological extremes at a large spatial and temporal scale. It is important to point out that temperature extremes are associated with different atmospheric condition such as, quasi stationary antycyclonic circulation anomalies or atmospheric blocking in mid latitudes [29]. With the increase in temperature there are also changes in precipitation, for different reasons, for instance, changes in the energy balance induced by radiation leads to an increase in evapotranspiration, which contribute the atmospheric moisture content [29]. As the surface temperature increases by 1°C, the water retention capacity of the atmosphere increases by approximately 7% according to the Clausius-Clapeyron equation. However, the scaling rates of extreme precipitation and atmospheric water vapor with temperature are not the same (Lenderink and Van Meijgaard, 2008), this show that extreme precipitation is affected by different factors. Globally, the number of record-breaking events has increased faster than projected in a stationary climate, which fits with Clausius-Clapeyron's relation [16] [29].

Although models have many uncertainties, model simulations contribute to characterize the probability distribution of possible weather states in response to various climate forcings and thus help to assess their risks. Therefore, global climate models are used. This thesis assesses changes of CMIP5 climate models by applying ETCCDI climatic indices for precipitation and temperature over two alpine areas, the Andes mountains in Colombia, and the whole Alpine arc in Europe. Those regions in particular face potential impacts of climate change, which could affect food security and modify the water cycle in the region. Besides, climate change represents an important threat on biodiversity, particularly in the tropical Andes, which is the most biodiverse region on Earth [10]. The variables temperature and precipitation were used. For this purpose all available models are downloaded, processed, plotted and the results are compared with global scale tendency.

Two types of experiments were studied: 1) *Historical simulations*, which are integrations from 1860 to 2005 using realistic natural and anthropogenic forcings, emissions or concentrations of short-lived species and natural and anthropogenic aerosols or their precursors, besides land use changes, and 2) *two representative concentration pathway scenarios*. The first one is an interme-

diate scenario RCP4.5 which represents an increase in the radiative forcing from the end of the historical simulation to 2100 when the radiative forcing reaches 4.5 W/m^2 (approximately 650 ppmv). The second one is the more extreme RCP8.5 scenario with a corresponding range of CO_2 equivalent concentrations of 1370 ppmv.

The number of models per simulations varies considerably. For the *Historical* experiment are used 49 models, while the RCP4.5 and RCP8.5 scenarios are used 45 and 42 models, respectively.

The current work is organized into six chapters and one appendix. Chapter 2 is a theoretical background regarding Global Climate Models, and ETCCDI climate indices, in Chapter 3 is a theoretical climate context of the selected regions, in Chapter 4 data acquisition, software tools and processing data are described. The obtained results are shown in Chapter 5 and lastly, discussion and conclusions are presented in Chapter 6.

2

THEORETICAL BACKGROUND

2.1 GENERAL CIRCULATION MODELS (GCMS)

Numerical models also known as General Circulation Models are based on physical processes to simulate the transfer of energy and materials through the climate system [19]. They use mathematical equations to characterize how energy and matter interact in different parts of the ocean, atmosphere, cryosphere and land. The main components of the climate system considered in a climate model are [12]:

- **The atmospheric component**, simulating clouds and aerosols, which are related to the transport of heat and water around the globe.
- **The land surface component**, simulating surface characteristics such as vegetation, snow cover, soil water, rivers, and carbon storing.
- **The ocean component**, simulating the movement and mixing of currents, and biogeochemistry, since the ocean is the largest reservoir of heat and carbon in the climate system.
- **The sea ice component**, which modulates solar radiation absorption and air-sea heat and water exchanges.

Climate models separate Earth's surface into a three-dimensional grid of cells (Figure 2.1) representing specific geographic locations and elevations. The results modeled in each cell are passed to neighboring cells to model the exchange of matter and energy over time [14]. The size of the grid cells defines the resolution of the model, the smaller the size of the grid cells, the higher the level of detail in the model. A typical climate model could have e grid cells with a size of about 100 km on a side, though the vertical resolution have about 30 layers, since the atmosphere is thinner compared to the vast size of the planet. Thus, their resolution is quite coarse and many physical processes like precipitation occur at smaller scales and can not be properly . Therefore their known properties must be averaged over the larger scale in a technique known as parameterization. For this reason, the GCMs simulation are quite different to the same forcing, they fail to project high resolution climate, due to the way certain processes and feedback are modeled.
Climate models also include the element of time, called time step, which can be in minutes, hours, days, or years. the smaller the time step, the more detailed the results.

GCMs are based on global patterns in the ocean and atmosphere, and on historical records that occurred under similar patterns in the past [19].

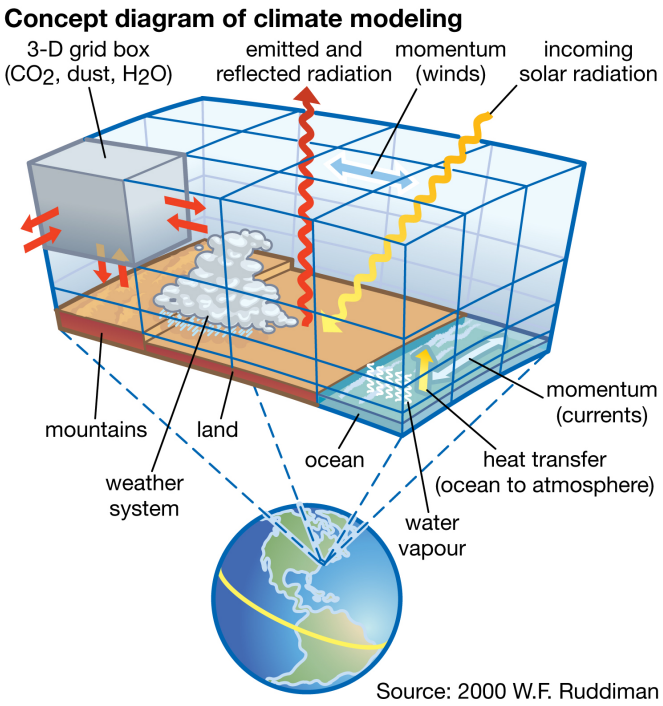

Figure 2.1: Main components of a global earth-system model.

One key difference between climate models and weather forecasts, is that climate models are probabilistic, indicating areas with higher chances to be warmer or cooler and wetter or drier than usual, whereas weather forecasts describe a detailed picture of the expected near future starting from present conditions.

2.2 COUPLED MODEL INTERCOMPARISON PROJECT (CMIP5)

The fifth phase of the Coupled Model Intercomparison Project (CMIP5) coordinated by the World Climate Research Program (WCRP) has produced a multi-model dataset designed to advance our knowledge of climate, its variability and change through the application of global models of the climate system [33]. Compares a great number of models from diverse modeling centers which perform simulations nder the same ensembles of initial and boundary conditions. These model datasets evaluate how realistic the models are in simulating the recent past, provide projections of future climate change (RCP scenarios), and include the quantification of some climate feedbacks such as ice-albedo, those related with clouds and the carbon cycle.

Scientists are questioning how climate will respond to increasing greenhouse gas concentrations through climate simulations. At present, our understanding of future climate change is summarized in the Report of the Intergovernmental Panel on Climate Change (IPCC AR5) (Stocker et al.) [32] which is based on complex climate model simulations. But, this complexity carry out imperfect simulations of the earth system. This report (AR5) exhibits that this imperfection is mainly due to the coarse spatial resolution

of climate models, which requires the parameterization of important small-scale phenomena such as atmospheric convection, and to the limited understanding of the physics of various climate processes, including the dynamics of clouds and sea ice.
CMIP5 peforms two large groups of climate change modeling experiments:

1. Long-term integration (century time scale).
2. Near-term integration (10-30) years, called decadal predictions experiments.

The *Long-term experiments* include an "AMIP run", a coupled "Control run", an "Historical run" that contains a period of 1850 to 2005 and is forced by observed atmospheric composition changes both with reflect anthropogenic (anthropogenic aerosols and greenhouse gases) and natural sources (such as volcanic activities, solar forcing, aerosol and emissions of short-lived species), moreover for the first time include time-evolving land cover. And for the period of the 21^{th} century four future projections simulations are used known as "Representative Concentrations Pathways (RCPs)" forced with specific emission concentrations [33]. These groups are usually started from multicentury preindustrial control (quasi equilibrium) integration, whereas the *Near-term experiments* are initialized with observed ocean and sea ice conditions, in this expriement there are two set of simulations. The first is a set of 10-yr hindcasts initialized from observed climate states near the years 1960, 1965, and every 5 yr to 2005 In these 10-yr simulations, it will be possible to evaluate the skill of the forecast system in predicting climate statistics for times when the initial climate state may exert some detectable influence.

Both experiments the long and near-term experiments are integrated using atmosphere-ocean global climate models (AOGCMs). The AOGCMs respond to specified, time-varying concentrations of various atmospheric constituents such as greenhouse gases and include an interactive representation of the atmosphere, ocean, land, and sea ice [33]. Some of these models are called Earth System models (ESMs) and are coupled to biogeochemical components that show the significant flows of carbon between ocean carbon stores, the atmosphere and the terrestrial biosphere. They in some cases also include interactive prognostic aerosol, chemistry, and dynamical vegetation components, including the changing land cover over time.

As reported in the chapter 12 of the Climate Change Physical Science Basis project [17] the *Long-term climate change projections* reflect how human activities or natural effects could influence the climate over decades and centuries. In this context, four RCPs scenarios were define, each one indicates the amount of climate forcing, expressed in Watts per square meter, that would result from greenhouse gases in the atmosphere in 2100. The lowest of the four RCP2.6, where the climate change is modest due to mitigation, peaks at 3.0 W/m^2 and then declines to 2.6 W/m^2 in 2100, the RCP4.5 (medium-low) and RCP6.0 (medium-high) stabilize after 2100 at 4.2 and 6.0

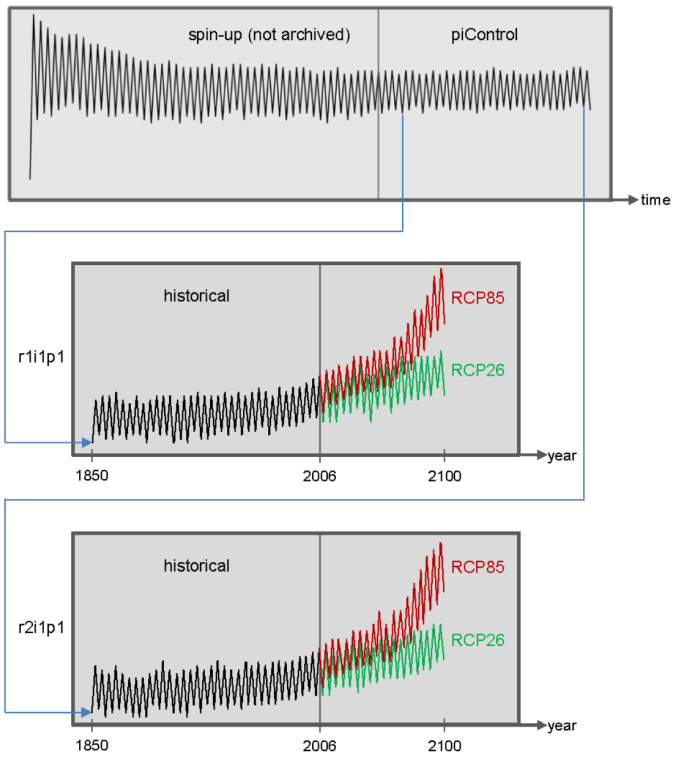

Figure 2.2: CMIP5 Long-Term group, the initial states are taken from the control run (piControl, pre-industrial control) were used to start the historical hindcast. (From ENES [8])

W/m^2 respectively, while RCP8.5 (highest) reaches 8.3 W/m^2 in 2100 on a rising trajectory. These scenarios are possible stories based on a range of projections of future population growth, technological development, and other forcing agents such as land use change that dependent on socioeconomic factors including global geopolitical agreements to control those emission.

These models provide essential information to assess climate change impacts at a global scale, but often this information come at a horizontal resolution of $100 - 300$ km, which is too coarse for many applications, particularly over complex terrain [36].

2.3 GLOBAL CLIMATE EXTREMES INDICES

According to IPCC, 2012 [11] climate extremes can be defined as the *'occurrence of a value of a weather or climate variable above (or below) a threshold value near the upper (or lower) ends of the range of observed values of the variable'*. There is strong evidence that the climate and its extremes are changing. Observational studies suggest that in some areas that have been analyzed, changes in some temperature extremes are observed and total rainfall is amplified in the tails in Figure 2.3 it is hypothesized changes in the distribution of temperature and show how minor changes can result in chamges in the tails. With regards climate models the results show changes in extreme events

for future climate, such as an increase in extreme high temperatures, a decrease in extreme low temperatures and an increase in intense precipitation events. In addition, in plants and wildlife, climate-induced extinctions, such as changes in species range, are being documented at an increasing rate.

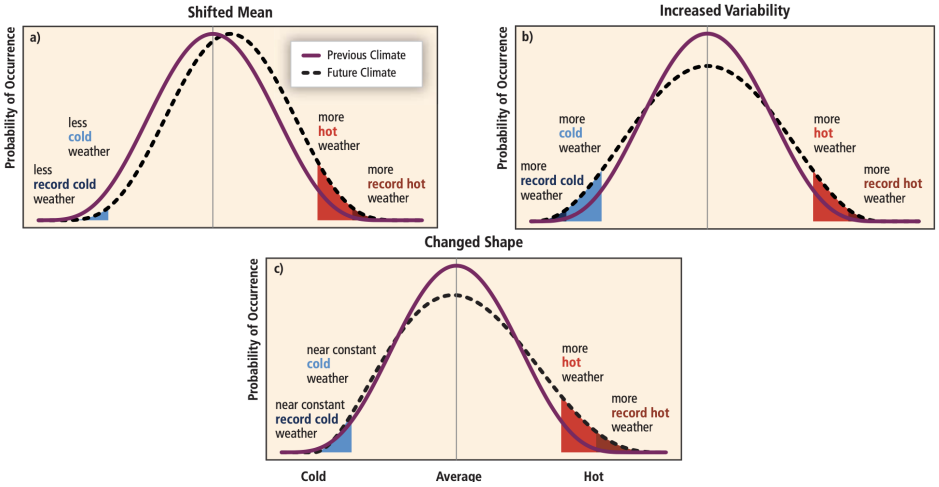

Figure 2.3: Changes in temperature distribution on extremes. Different changes in distributions between present and future climate and their effects on extreme values of the distributions: a) shift of the entire distribution toward a warmer climate. b) increased temperature variability, without shift of the mean. c) effects of an altered shape of the distribution, toward the hotter part of the distribution. From IPCC (2012) [11]).

Single extreme events cannot be directly attributed to anthropogenic climate change, as there is always the possibility that the event in question would have occurred without this contribution. However, for certain types of regional, long-duration extremes such as warming and rainfall, it is possible that from the results of the climate model, the probability of such an extreme has changed due to anthropogenic climate forcing [11]. Therefore, it is important to keep in mind the difference between detecting a change, and being able to attribute that change to some identifiable climate forcing factor. But it is difficult to associate a single extreme event with a specific cause, such as an increase in greenhouse gases, and because generally extreme events can occur even in unchanging climate, and because extreme events are often caused by a combinations of factors. [11]. However, what can be done is to attribute a change in the probability of the occurrence of a weather event to a particular cause for example an increase in greenhouse gases.

Climate extremes include windstorms (tropical cyclones and mid-latitude winter storms), floods, droughts and heat waves [3]. Thus, there is a clear incentive for studies related to extreme weather events and possible changes in their frequency and intensity as the climate changes during the 21st century. However, it is important to point out that there are few data available to make assessments of changes in extreme events, such as in their frequency or intensity, because these events are rare. An extreme weather event is defined

"rare" when between the 10th or 90th percentile of a probability density function estimated from observations. Thus, the more rare the event, the more difficult it is to identify long-term changes.

Climate models simulate extreme temperatures and heat waves well and are similar to the spread between observation-based estimates in most regions. However, extreme events often occur on weather time scales that require daily resolution data to accurately evaluate possible changes. For this reason, A WMO CCl/CLIVAR expert team (ETCCDI) on climate change detection, monitoring and indices has defined 27 climate indices (see Table A.2) focusing on extreme and heavy events. These daily based indices focus to investigate changes in intensity, duration and frequency of extreme climate events.
ETCCDI indices are divided into four categories listed in table 2.1 : 1) *"Absolute"*, based on a relevant temperature value, which describe the hottest or coldest day of a year, or the annual maximum 1 day or 5 day precipitation; 2) *"Threshold"*, which count the number of days when a fixed temperature or precipitation threshold is exceeded, e.g, frost days; 3) *"Duration"*, which describe the length of wet, dry, warm and cold periods; and 4) *"Percentile-based threshold*", which describe the exceedance rates above or below a threshold which is defined as the 10^{th} or 90^{th} percentile derived from the base period. The advantages of using ETCCDI Indices is that they are easy to understand and allow an easy comparison of trends between different regions. We calculated a total of twenty-seven extreme indices. All of them are calculated based on daily time series of three variables (TX, TN, Pr).

2.3.1 *Temperature Indices*

- **FD**: number of frost days, count the days when daily minimum temperature is below 0°C. This index is often used for climate studies.
- **SU**: number of summer days, count the days when daily maximum temperature is greater than 25°C.
- **ID**: count of days when daily maximum temperature (TX) is below 0°C
- **TR**: count of days when daily minimum temperature (TN) is above 20°C. Generally occur with periods of heat (mainly in extra-tropical regions) [28].
- **GSL**: number of days between the start of the first spell of warm days (six or more days with mean temperature above 5°C)in the first half of the year, and the start of the first spell of cold days (six or more days with mean temperature below 5°C) in the second half of the year.
- **TXx**: the maximum of TX, represent the warmest day of a year, month or season.
- **TNx**: the maximum of TN, represent the warmest night of a year, month or season.

- **TXn**: the minimum of TX, represent the coldest day day of a year, month or season.
- **TNn**: the minimum of TN, represent the coldest night of a year, month or season.
- **WSDI**: count the days with at least 6 consecutive days when TX is above 90^{th} percentile.
- **CSDI**: count the days with at least 6 consecutive days when TN is above 10^{th} percentile.
- **DTR**: yearly mean difference between TX and TN

Percentiles: are the exceedance rates above or below a thresholds, calculated for a 5 day sliding window on each day in the base period (by definition 1961-1990) [28]. The bootstrapping method is applied for the base period. The percentiles indices include:

- **TN10p**: (cold nights) percentage of days when TN < 10^{th}percentile.
- **TX10p**: (cold days) percentage of days when TX < 10^{th}percentile.
- **TN90p**: (warm nights) percentage of days when TN < 90^{th}percentile.
- **TX90p**: (warm days) percentage of days when TX > 90^{th} percentile.

2.3.2 *Precipitation Indices*

- **RX1day**: monthly or annual maximum of 1 day precipitation accumulations.
- **RX5day**: monthly or annual maximum of 5 day precipitation accumulations. It can be used to describe changes in potential flood risks.
- **SDII**: precipitation intensity, is the precipitation amount on wet days (pr> 1 mm) divided by the number of wet days.
- **R10mm**: number of days with more than 10 mm/day of precipitation.
- **R20mm**: number of days with more than 20 mm/day of precipitation, describe extreme precipitation.
- **Rnnmm**: is a threshold defined by the user. I defined two threshold values, R1mm and R30mm. Is the number of days when precipitation is greater than 1 mm/day and 30 mm/day.
- **CDD**: maximum number of consecutive days when pr < 1 mm/day.
- **CWD**: maximum number of consecutive days when pr > 1 mm/day.

- **R95p**: annual total precipitation accumulated on days when when daily precipitation is greater than 95^{th} percentile threshold computed in a reference period, by definition 1961-1990.
- **R99p**: annual total precipitation accumulated on daays when daily precipitation is greater than 99^{th} threshold computed in a reference period.
- **PRCPTOT**: daily precipitation amount in a period.

Table 2.1: Categories for the Climate indices (CEIs) from [7].

Absolute	**Threshold**	**Duration**	**Percentiles**
TXx	FD	CSDI	Tx10p
TXn	ID	WSDI	Tx90p
TNn	SU		Tn10p
	TR	CDD	Tn90p
DTR		CWD	R95p
SDII	R1mm		R99p
	R10mm		
RX1day	R20mm		
RX5day			
PRCPTOT			

Some studies have concluded that the majority of land areas have had decreases of cold extremes indices and increases in warm extremes indices since about 1950 [32]. The change in the distribution of night temperatures seems to be greater than the daytime temperatures, whereas in terms of mean distributions are simply to increase. On the other side, studies reveals changes in precipitation extremes are less confidence than temperature, in that there are large areas that show increasing trends, while other regions show decreasing.
Analysis of regions with sufficient data such as Europe indicate increases in the frequency and intensity of extreme events in recent decades, but results differ widely across regions and seasons. For instance, the Mediterranean indicate that droughts have increased. Figure 2.4 shows some of the observed changes (intensity and frequency) in climate extremes. Overall, temperature and precipitation extremes seem to be increasing. However, also drought events seem to be increasing in some regions.

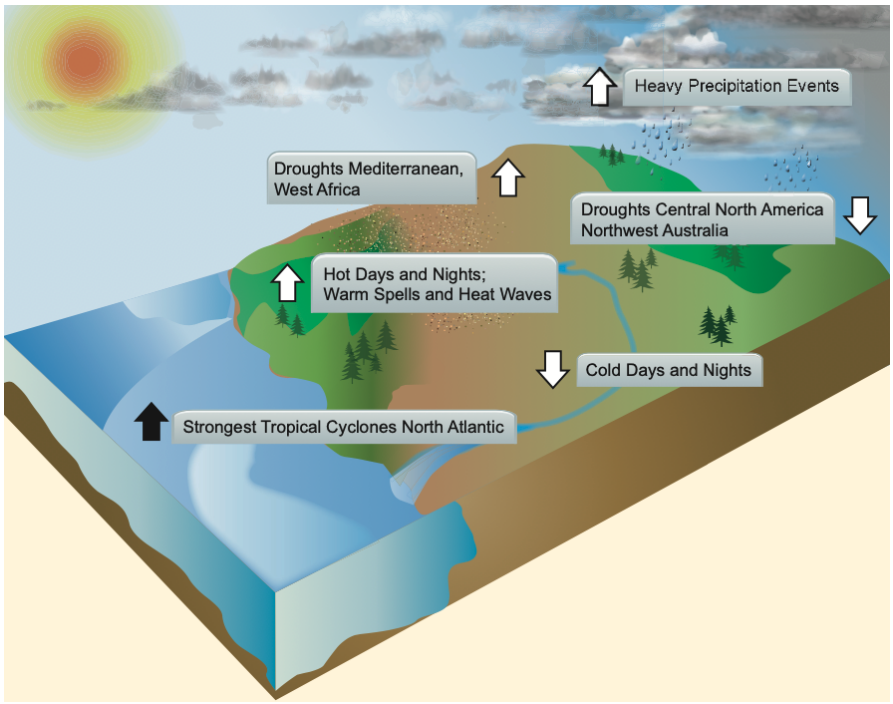

Figure 2.4: Observed trends of various climate extremes generally since the middle of the 20^{th} century (the direction of the arrows indicates the sign of the changes). From [11].

3

SELECTED REGIONS AND RELATED WORK

This chapter discusses the existing studies related to the goal of this thesis. Firstly, we will provide a background of the focus regions, i.e., the Alpine and the Andes mountains, discussing the studies that have been conducted and their climate context.

All models are used on their original resolution. It is important to mention that the grid resolution of the climate model products is insufficient to properly represent the spatial variability of complex areas topographically, such as the two study regions.

3.1 ALPINE REGION

The domain for this study cover the whole Alpine mountains, ranges 4 to 15°E in longitude and from 43.5 to 49.5°N in latitude (see Figure 3.1). The climate regime in the northern Alps is mostly affected by weather systems originating from the Atlantic Ocean, whereas the south is primarily influenced by the Mediterranean ocean [36]. The climate is very sensitive to global warming, because of the presence of snow, glaciers, and his high mountains. Some meteorological variables that contributes to the characterization of the Alpine climate (like the temperature, precipitation, global radiation and relative humidity) will be affected by global warming [1]. A review of the climate change in the European Alps [1] show that simulations under the A1B emission scenario produce a warming of about 0.25°C per decade until the middle of the 21st century and an accelerated warming of 0.36°C per decade in the second half of the century. And will lead changes in the seasonality of precipitation, intensification in rainfall extremes, and more flooding in winter, as well as reduction in snow cover and the permafrost retreat will be probably more frequent. These events will be cause a reduction of return period in future projections. But this will depend on the season and the location, because the projected changes may be opposite in different areas. In general, precipitation is expected to decrease in summer specially in southern regions, and on the other side, is expected more intense precipitation extremes in autumn and in the northern parts of the Alps.

Another study Zubler et al. [36] evaluate the distribution of climate change signals of the CMIP5 models in terms of temperature and precipitation in the Alpine region and results indicates that different methods of "model selection" have a significant influence in the temperature spread at the end of the century 2070-2099 compared to the reference period 1980-2009, excluding models with low resolution show a difference in spread of more than 1°C confronted to a selection strategy in which all models are included and given

the same weight. In this study is demonstrated that the selection of models has a considerable impact on the resulting climate change projections. The results shows that the selection of "good" models is viable and can maintain the spread of the ensemble, and climate change signals for temperature are stronger for the "good models" selection.
This study reveals that the increases in temperature are around 1.0-4.7°C over the northern Alps and 1.0-5.5 °C over the south for the RCP4.5 scenario. And the RCP8.5 the increased warming correspond to 2.1 to 8.9°C in the north and by about 2.1 to 9.5 °C in the south.The study reveals that CMIP5 models do not indicate a common sign of change in average seasonal mean of rainfall. They suggested that it may be because the Alps are located in a transition zone between the drying in the Mediterranean and the wetting of northern Europe [36]. In addition, in winter and spring the majority of Global Climate Models (GCMs) have tendency to increase in rainfall over the north of the Alps. In summer, Regional Climate Models (RCMs) project drier weather, whereas GCMs project wetter conditions. Zubler et al. conclude that the selection of the model is to some extent subjective depending on the characteristics to consider. For instance, topographical and hydrological aspects. It was also shown that independence in models does not exist, since they are related to some extent to each other.

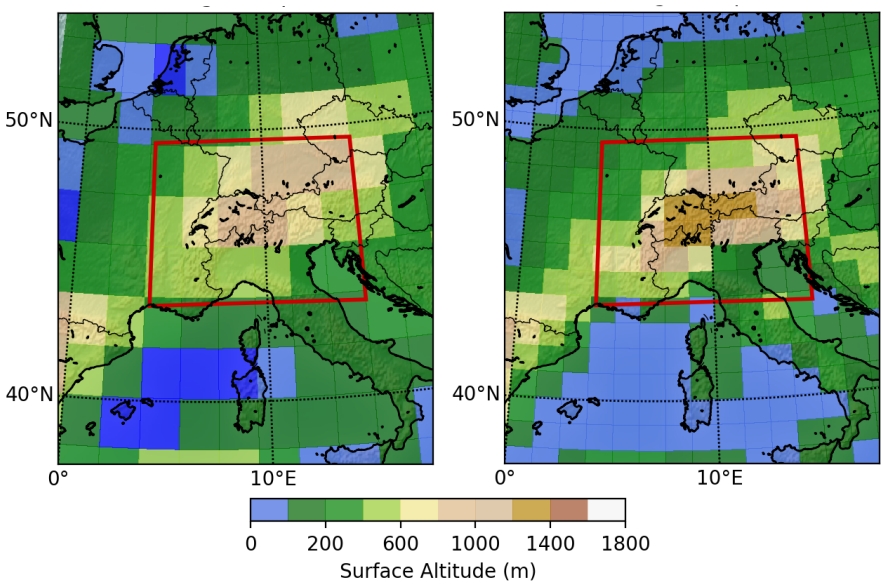

Figure 3.1: Topography of the Alpine region in m a.s.l. at the example of the CCSM4 model with resolution 0.94°x1.25° on the left side, and CMCC-CMS model with resolution 3.71°x3.75° on the right side.

In another study Terzago et al. [34] evaluate the reliability in reproducing the main drivers of snow processes and to explore the ability to reproduce the snow water equivalent distribution over this area, from reanalyses and remote sensing data. In addition, they analyse simulations from the latest generation of regional and global climate models (RCM, GCM), participating in the EURO-CORDEX and the CMIP5 respectively. Then is compared

with observational data (EOBS) and with the remote sensing and reanalysis outputs. The results showed that the spatial distribution of snow over time is represented quite differently by reanalysis and EOBS data. The GCM projections show a larger reduction of snow compared to the RCM projections that show less snow reductions.
They found that GCMs with spatial resolutions equal to or finer than 1.25° in longitude are more consistent with the satellite ensemble and reanalysis products in terms of mean square error and standard deviation than GCMs with lower resolution, i.e. with cell grid greater than 1.25°. The high resolution models form a more homogeneous group without extreme values. Moreover, the CMIP5 ensemble do not take into proper account elevations above 1500–2000 m a.s.l. which are not represented in most models. In general, GCM projections agree in showing a strong reduction of snow resources by the mid-21st century in the RCP8.5 scenario, especially in the spring season. The uncertainties on the amplitude of the snow water equivalent change are large, but the signal is coherent across all models.

In another study Brönnimann et al. [4] studies the seasonal occurrence of extreme precipitation events in the Alps using regional and climate models. They focus on the maximum Rx1day per decade, the annual mean temperature, temperature at the event day and the event date. A typical Rx1day event can be caused by the passage of a cold front related to an elongated depression or cut-off low situation with destabilization and prefrontal convective activity, also are associated with the convergence and elevation of moist air, originating in the Mediterranean region [4].
The results show no increase in annual maximum 1-day precipitation events (Rx1day) over the last 400 years using different types of ensembles such as CCC400, COSMO, CMIP5, CORDEX-11 and CORDEX-44. By the other hand, also is showed an increase of 10%–20% in the ensemble mean for a high emission scenario, and the annual mean temperature shows an increase of 4-6°C at the end of the century, corresponding to an increase of 30-50% in rainfall extremes, but does not have sense. For this reason they considered only the temperature on the day of the Rx1day event, in which they found a slight increase in temperature, 3°C for the CMIP5 experiment and just 1°C for COSMO. During Rx1day events they found that these events in summer occurs when the days is a bit colder than average, while in winter this events occur on days warmer than average. They showed that there is a tendency for fewer events to occur during June and July and more during the neighbouring months, that is to say, they sift towards the cold season, and during the mid summer the event become rare. These events show a decrease by 10% in the past and a decrease around 30% in the future scenario.

Conversely, when they analyse rare events (the highest Rx1day) they find that these events are more concentrated in the middle of the summer in the present period. In the ensemble CCC400 these events occurs mostly during the entire summer, whereas in CMIP5 occurs mostly in the early autumn.

In general, there is no change in the frequency of occurrence or intensity for moderate extremes (events with a frequency of once per year), they just change in their seasonality with a small change in intensity. They become more frequent in early summer and early autumn, i.e when it is cooler. On the contrary, the most extreme events change in intensity and not in seasonality. If the intensity of heavy precipitation events depends on thermodynamics conditions, such as saturation specific humidity, it will follow the Clausius-Clapeyron relation, but with the event day temperature, not with the annual mean temperature. In the Alpine region, moderate extreme rainfall may not increase as much as expected when applying a Clausius-Clapeyron, this indicates that other factors are also important, they are not exclusively thermodynamically limited. In addition, in the future climate they found that Rx1day occur less frequently in summer and more frequently in spring and autumn. Conversely 10-year events (most extreme events) show their highest frequency in summer and increase significantly in intensity in the future projection.

In another study Rajczak, Pall, and Schär [23] analysed a set of 10 Regional Climate Models driven by six GCMs to asses changes in heavy and extreme precipitation for the future climate (2070-2099) based in the 19070-1999 period for Europe and the Alpine region, by using statistical measures. Were used four empirical indices to capture the climatology of precipitation, such as the mean precipitation, wet-day frequency, wet-day intensity and the 90% quantile of the frequency distribution of wet days. The simulation show an increase in mean amount and wet day frequency in the north of Europe, whereas show a decrease in the south. In the case of extreme events their frequency increases, but it is observed to be stronger in the south. In the Mediterranean the average rainfall is projected to decrease in spring and autumn, but it increases in extreme events. With regard the Alps all models robustly project a greater intensity during autumn, with the exception of summer and the southern alpine region. All RCMs projections indicates a decrease in mean precipitation and intensity during summer over the the Alps.

Climate changes in the Alpine region will lead negative impacts on society, economy and ecosystems. More intense precipitation extremes can be results in severe flooding and therefore in damage to human life and infrastructure.

3.1.1 *Climate context*

The European Alps is a mountain range stretching along an arc of about 1200 km. This mountains are characterized by extensive lowlands, deep valleys and peaks over 4800 m. the long-term space-time variability of the Alpine climate and its influence on various sectors has long been of great scientific interest. Because of this it is one of the world's longest observation time series of climate parameters. the Alps are affected by four main climatic in-

fluences: from the west flows the relatively mild, moist air of the Atlantic; cold polar air descends from northern Europe; continental air masses, cold and dry in winter and hot in summer, dominate in the east; and, to the south, warm Mediterranean air flows northward [35]. Due to interactions between the mountains and the general circulation of the atmosphere features such as the breaking of gravitational waves, the blocking of heights and föhn winds are generated [6]. Temperature extremes and annual precipitation are related to the physiography of the Alps. The complex topography of this region determines strong gradients in climate parameters in short distances, causing major transitions over land areas; from vegetation and soil to snow and ice.

Most mountain ranges are poorly populated due to the harsh climate. Traditional agricultural practices were the mainstay of the mountain economy for centuries. But these practices are rapidly disappearing. It has an environmental and social value, because the amount of water delivered by the Alps allocates 40 % European Union consumption. At present, human activities are impacting this environment, these include mass tourism, afforestation and deforestation, the damming and channelling of alpine rivers and the construction of roads [2]. Another large pressure for this region is the climate change. Due to the high ecological and climatic vulnerability of mountains, a small change could have devastating effects on their capacity to absorb and retain water. There is already evidence that glaciers are shrinking; further shrinkage could lead to significantly longer dry periods in the lowlands and marked changes in mountain vegetation.

In general, Alpine glaciers have been decreasing . The Italian Alpine have decreased their area up to 20-22% related to a reference period from 1990-2003 [6]. From 1850 to 2005. The Alpine glaciers have lost almost 50% of their area. In terms of volume have lost on average 1% of their volume per year since 1975. Besides the permafrost in the Alps is affected by global warming, leading to a feedback positive, thus lower snowfall and winter season resulting in more thawing of the permafrost. Moreover, changes in hydrology at higher altitudinal levels will change the stability of the mountains, making them much more unstable, especially where the incidence of precipitation phenomena increases, most often leading avalanches and landslides [6].

The fourth report of the IPCC [32] shows that global warming would bring warming temperatures and more humid conditions in winter, and warmer summers. In some studies Soncini and Bocchiola [30] indicate that a more pronounced decrease in the volume of snowfall in the Italian Alps is expected by 2060. As regard changes in the rainfall pattern of the Alpine region (higher intensity in extreme rainfall events) could have negative effects on socio-economic aspects. For instance, destruction of the crops planted, significant damage to structures and building. Therefore, provoking economic damage to the population.

3.2 ANDES REGION

The study domain covers equator -9.5 °N and 71°W-78°W (Figure3.2). There are many studies related to the Andean region, since it has been identified as one of the most vulnerable regions in South America and recent extreme seasons and recent extreme events are significantly impacting biodiversity and many sectors of the economy in some countries.

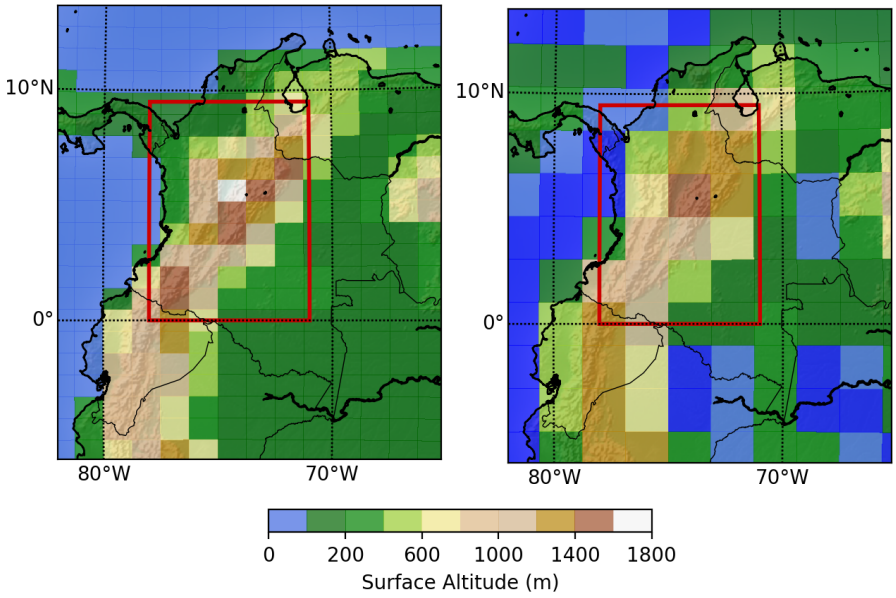

Figure 3.2: Topography of the Andes region in m a.s.l. at the example of the CCSM4 model with resolution 0.94°x1.25° on the left side, and CMCC-CMS model with resolution 3.71°x3.75° on the right side.

There are few studies that evaluate the performance of CMIP5 GCMs over the Andes in Colombia. Sierra, Arias, and Vieira [27] evaluated the ability of some CMIP5 models to represent mean seasonal rainfall and its interannual variability in northern South America. the results indicate that the models with the best representation of the ITCZ (Intertropical Convergence Zone) and the local low-level jets over northern South America are able to realistically simulate the main characteristics of the seasonal rainfall pattern. But in general, the ENSO (El Niño-Southern Oscillation) frequency is still not well captured by CMIP5 models. Some studies reveals that the most of the CMIP5 models represent correctly the total amount of rainfall over the Amazon during the wet season (DJF), but only HadGEM2-ES, HadGEM2-CC, and CCSM4 represent correctly the amounts of rainfall during the dry and transition seasons [27]. Finally, The models NorESM1-M and HadGEM2-CC represent properly the sea surface temperature and ITCZ location over the Pacific Ocean and HadGEM2-ES shows one of the smallest biases of the ITCZ.

Elseways, another study Palomino et al. [22] analyzes summer precipitation projections in Colombia using statistical downscaling (SD) models and

raw GCMs models under RCP2.6, RCP4.5 and RCP8.5 scenarios and during the period 1971-2000 and were compared with observed values. The results show that the simulation of the five raw GCMs has considerable biases, possibly due to the inadequate representation of the physical processes of precipitation and the low spatial resolution in this area because of the complex topography. For the regional analysis the model MIROC5 and HadGEM2-AO overestimated the rainfall values in all regions of the country, whereas CNRM-CM5 and MPI-ESM-LR underestimated the precipitation. However, CESM1(CAM5) provided an appropriate estimation of precipitation in most of the regions. Overall, all GCMs agreed with rainfall values are higher than the observed ones. By the other hand, the SD model showed to be able to better reproduce the field of precipitation in Colombia in a more realistic way. Regarding the precipitation for SD models in the future scenarios for the period 2071–2100 showed significant increases in precipitation, in particular in the pacific central coast and central south region.

Schoolmeester et al. [24] [21] summarized findings of other studies and indicates that some regions such as the northwestern of Colombia, Ecuador and Peru will expect more precipitation than observed in the present climate, while a decrease is likely in the northeastern Andes of Venezuela and Colombia. Another studies for South America based on dynamical downscaling models cited in [21] agree a general warming over the entire Andes on the future projection ranging from 1° to 5° by the end of the 21st century depending on the RCP scenario.

The difficulty of Global Climate Models to adequately project rainfall changes in the Andes is highly associated with their coarse spatial resolution (100-300 km). It is important to apply high resolution modeling tools that allow to solve more complex topographies, to understand the role of local processes of precipitation and temperature changes in response of global warming. Schoolmeester et al. [24] indicates that this changes in mean temperature, precipitation and the glaciers melting in the Andes, will cause effects on run-off and consequently on the availability of water for society and industry.

3.2.1 *Climate context*

The European Alps is a mountain range stretching along an arc of about 1200 km. This mountains are characterized by extensive lowlands, deep valleys and peaks over 4800 m. the long-term space-time variability of the Alpine climate and its influence on various sectors has long been of great scientific interest. Because of this it is one of the world's longest observation time series of climate parameters. the Alps are affected by four main climatic influences: from the west flows the relatively mild, moist air of the Atlantic; cold polar air descends from northern Europe; continental air masses, cold

and dry in winter and hot in summer, dominate in the east; and, to the south, warm Mediterranean air flows northward [35]. Due to interactions between the mountains and the general circulation of the atmosphere features such as the breaking of gravitational waves, the blocking of heights and föhn winds are generated []. Temperature extremes and annual precipitation are related to the physiography of the Alps. The complex topography of this region determines strong gradients in climate parameters in short distances, causing major transitions over land areas; from vegetation and soil to snow and ice.

Most mountain ranges are poorly populated due to the harsh climate. Traditional agricultural practices were the mainstay of the mountain economy for centuries. But these practices are rapidly disappearing. It has an environmental and social value, because the amount of water delivered by the Alps allocates 40% European Union consumption. At present, human activities are impacting this environment, these include mass tourism, afforestation and deforestation, the damming and channeling of alpine rivers and the construction of roads [2]. Another large pressure for this region is the climate change. Due to the high ecological and climatic vulnerability of mountains, a small change could have devastating effects on their capacity to absorb and retain water. There is already evidence that glaciers are shrinking; further shrinkage could lead to significantly longer dry periods in the lowlands and marked changes in mountain vegetation.

In general, Alpine glaciers have been decreasing . The Italian Alpine have decreased their area up to 20-22% related to a reference period from 1990-2003 [6]. From 1850 to 2005. The Alpine glaciers have lost almost 50% of their area. In terms of volume have lost on average 1% of their volume per year since 1975. Besides, the permafrost in the Alps is affected by global warming, leading to a feedback positive, thus lower snowfall and winter season resulting in more thawing of the permafrost. Moreover, changes in hydrology at higher altitudinal levels will change the stability of the mountains, making them much more unstable, especially where the incidence of precipitation phenomena increases, most often leading avalanches and landslides [6].

The fourth report of the IPCC [32] shows that global warming would bring warming temperatures and more humid conditions in winter, and warmer summers. In some studies Soncini and Bocchiola [30] indicate that a more pronounced decrease in the volume of snowfall in the Italian Alps is expected by 2060. As regard changes in the rainfall pattern of the Alpine region (higher intensity in extreme rainfall events) could have negative effects on socio-economic aspects. For instance, destruction of the crops planted, significant damage to structures and building. Therefore, provoking economic damage to the population.

4 DATA, SOURCES, SOFTWARE AND DEVELOPED SCRIPTS

This chapter introduces the analyzed data, the sources to obtain it and the software tools and libraries used for its manipulation.

4.1 DATA

All of the CMIP5 models that fitted the needs of variable and experiment availability were used, in total, 50 out of the 61 CMIP5 models.

We use historical monthly and historical daily simulations (1850–2005) and two future daily climate projections (2006–2100) known as RCP4.5 and RCP8.5. We chose Precipitation and Temperature variables as they are good indicators of climate change, they are required for the calculation of the Global climate Indices and they have been used extensively in the literature. Table 4.1 summarizes the used datasets.

Table 4.1: Chosen Datasets

Project	CMIP5	
Model	All available	
Experiment	Historical	
	RCP4.5	
	RCP8.5	
Time frequency	Daily	
	Monthly	
Realm	Atmosphere	
Ensemble	r1i1p1 when available	
Variable (long name)	tas	(Near surface air temperature)
	tasmin	(Maximum temperature)
	tasmin	(Minimum temperature)
	pr	(Precipitation)

- **Ensembles:** There are multiple CMIP5 experiments, called ensemble calculations, which are the result of using several initial states. These ensemble calculations facilitate the quantification of the climate/internal variability of simulation data related to a single model, that is to say ensembles models allow to measure uncertainty since climate model simulations depend on the initial state [8]. The ensemble members are named in the rip-nomenclature, r for *realization*, i for *initialisation* and

p for *physics*, followed by an integer.
For this work, one run was chosen from each model (usually $r1i1p1$ when available). For models without $r1i1p1$ ensemble, others was used.

- **Near surface air temperature:** Measures the air temperature usually 2 meters above the ground [K]
- **Maximum temperature:** Measures daily-maximum (usually 2 meters) near-surface air temperature [K]
- **Minimum temperature:** Measures daily-minimum (usually 2 meters) near-surface air temperature [K]
- **Precipitation:** Measures the precipitation flux in liquid and solid phase that falls from the clouds [kg/m^2s]

Depending on the type of analysis performed, a different combination of variable, experiment and frequency was used, as shown in table 4.2. The total number of models available for each analysis is also given. A full list the models and some additional is present in Apendix A, table A.1

Table 4.2: Selected data for each analysis

Variable	Frequency	Experiment	N° Models	Analysis
pr	Daily	Historical	33	ETCCDI Climate Indices
		RCP4.5	31	
		RCP8.5	33	
tasmin	Daily	Historical	33	ETCCDI Climate Indices
		RCP4.5	31	
		RCP8.5	33	
tasmax	Daily	Historical	34	ETCCDI Climate Indices
		RCP4.5	32	
		RCP8.5	34	
pr	Monthly	Historical	49	Evaluation of models and
tas		RCP4.5	45	change in precipitation
		RCP8.5	42	and temperature

4.1.1 *The NetCDF format*

The datasets are provided as NetCDF (Network Common Data Form) files, a binary and header-based data format. The file extension is .nc. NetCDF is a file format for storing multidimensional scientific data (variables) such as temperature, precipitation, humidity, pressure, wind speed, and direction.
Coordinate variables and data variable are defined in the file header. Each data file contains one data variable (e.g. tas) and the coordinate variables

longitude, latitude, altitude, time.

NetCDF is the format most frequently used for storing climate model output as well as some observational data.This type of format is self-describing, network-transparent, directly accessible, and extendible. Self-describing means that a netCDF file includes information about the data it contains (also know as meta data). Network-transparent means that a netCDF file is represented in a form that can be accessed by computers with different ways of storing integers, characters, and floating-point numbers. Direct-access means that a small subset of a large dataset may be accessed efficiently, without first reading through all the preceding data. Extendible means that data can be appended to a netCDF dataset without copying it or redefining its structure [20].

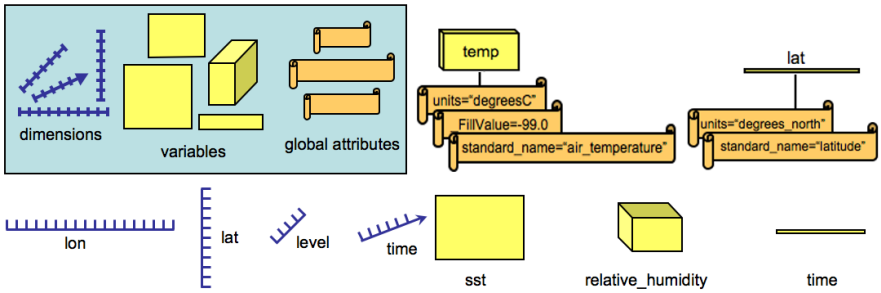

Figure 4.1: Gridded datasets: NetCDF data format from [20]

4.1.2 *Sources*

The CMIP5 datasets used in this work were obtained from the *obs4MIPs* project. Datasets from each model are hosted on servers all around the world, most of them belonging to the same institute producing the data. However, the datasets are accessible from a single website thanks to the Earth System Grid Federation (ESGF) at `https://esgf-node.llnl.gov/projects/cmip5/`.

The Earth System Grid Federation (ESGF) Peer-to-Peer (*P2P*) enterprise system is a collaboration that develops, deploys and maintains software infrastructure for the management, dissemination, and analysis of model output and observational data. ESGF's primary goal is to facilitate advancements in Earth System Science. It is an interagency and international effort led by the Department of Energy (DOE), and co-funded by National Aeronautics and Space Administration (NASA), National Oceanic and Atmospheric Administration (NOAA), National Science Foundation (NSF), and international laboratories such as the Max Planck Institute for Meteorology (MPI-M) German Climate Computing Centre (DKRZ), the Australian National University (ANU) National Computational Infrastructure (NCI), Institut Pierre-Simon Laplace (IPSL), and the Centre for Environmental Data Analysis (CEDA).[9]

The ESGF website offers the possibility to explore the available datasets by different criteria. One may search using any combination of model, variable, experiment, frequency (e.g., monthly, daily, 3 hourly), and modelling realm (e.g., atmosphere, ocean, sea ice). The Table 4.1 shows the criteria used to filter the desired data.

4.1.3 *Data Acquisition*

To access the models data from the ESGF website, one must first register, indicating how the data will be used and agreeing to specific "terms of use". Some of the models will release their data for "unrestricted" use, whereas others will limit use to "non commercial research and educational" purposes. Through the registration, it will be possible to inform users of errors found in model output and of data that have been removed or updated.

After registration, it is possible to use the website filtering and navigation tool (figure 4.2), in order to select the desired datasets to be downloaded. Using the filters described in table 4.1 the correct data was selected.

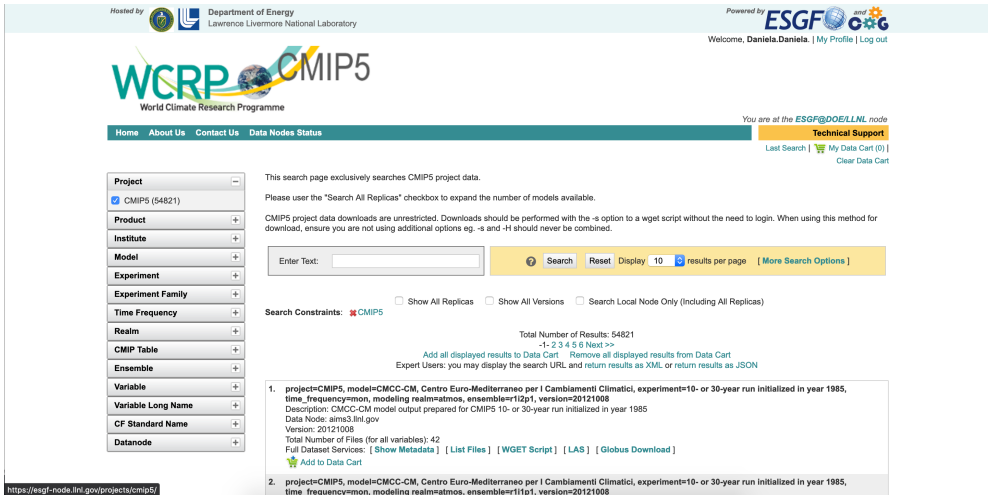

Figure 4.2: Earth Science Grid Federation (ESGF) Website.

Once the data has been identified, an .sh script is provided. This script allows to download multiple data files sequentially, using the UNIX standard **wget** program, available in different Operating Systems.

The script also offers automatic download retries in case of connectivity issues, and an integrity check based on the standard **md5 checksum**, to verify if the data is downloaded properly.

The website also support web browser HTTP download, but it is only recommended when a single file needed, or if it is not possible to run the provided script. In this case it is necessary to verify the checksum manually, to avoid working with incomplete or corrupted files.

4.2 SOFTWARE TOOLS

In the development of this thesis, several software tools were required. They can be divided into four sub-categories:

- Scripting.
- NetCDF data manipulation.
- General data manipulation and visualization.
- Other support tools and environments.

4.2.0.1 *Scripting*

When manipulating large quantities of information, automatizing the processing is crucial to speed up the development and reduce the amount of human errors. This can be achieved easily using a high level language for scripting, as Python.

The main automatized task are.

- File retrieval: Loop through folders in the file system to find the files to be processed. In this case NetCDF files.
- Perform bulk operations on those files.
- Define helper functions that will be used in multiple parts of the analysis.
- Generate and save results (images and reports)

4.2.0.2 *Python*

Python is a general purpose language. It is easy to learn and widely used in science. It is an interpreted language, therefore, it is much easier to make rapid changes and test those changes. Python has been embraced by the earth science community for analysis, visualization and data exploration. Advantages of using python are:

- As it is a high level language, the code is smaller, therefore there is less chance for errors.
- It is cross platform so it can be used in different host operating systems.
- There is a multitude of information, support forums and tutorials online.
- It is widely used in the scientific community, therefore there are a lot of specialized libraries.
- Its use is not limited to a particular science field, on the contrary it is interdisciplinary. This benefits the user as it increases the amount of available tools.
- It is constantly under review and development.

In specific, the latest available Python version at the moment was used: Python 3.8.3

4.2.1 *NetCDF manipulation*

When working with data files it is not advised to operate directly on them. It is better to use tools and libraries if available because:

- If files are binary, as in most of the cases, they can not be opened as plain text files, and specific libraries are required for reading the data.
- The use of existing libraries speeds up the development phase.
- If the libraries are coming from a trustworthy source, they have been debugged, reviewed and improved, so they are much more reliable than developing an ad hoc solution.

For NetCDF manipulation, we used two main set of tools, CDO and NCO.

4.2.1.1 *Climate data operators (CDO)*

The Climate Data Operator (CDO) software is a collection of many operators for standard processing of climate and forecast model data [25]. There are more than 700 operators available. They include statistical and arithmetic functions, data selection, Modification of meta data, subsampling tools, spatial interpolation and climate indices. It is a UNIX command line interface and has been tested on many UNIX/Linux systems, Cygwin, and MacOS-X. The CDO is developed and maintained by the Max-Planck-Institut, and there is a good amount of information in tutorials and support forums on how to use it.

CDO and Python: The CDO operators are installed on the host system as a binary, and can be accessed natively from a shell. However, its use from a shell limits the possibilities, and as recommended by the CDO developers [5], it is advised to use a more powerfull alternative. CDO offers a wrapper around the cdo binary for Python and Ruby. For Python it is available on the official repositories, through pip.

netCDF4-Python: To use CDO on Python, a pre-requisite is the input/output file manipulation library netCDF4-Python. This is available as a precompiled package for most linux/unix distribution, and on pipe.

CDO and Global Climate Indices: The latest official release of CDO (currently cdo 1.9.8) does not include the updated cdo operators for the calculation of the global climate indices as defined by the expert team (ETCCDI). However, CDO developer Fabian Wachsmann has already released ETCCDI complaint operators. These new operators are available in the development branch of cdo (currently cdo 1.9.9*rc*3). Instructions on how to install and use the new operators are available at the gitlab repository cdo_cei [26]. As advised in the tutorial, we use the the cdo dev channel of conda forge.

4.2.1.2 *NetCDF Operators (NCO)*

To a less extend, the NCO tool is also used. NCO is a package of command line operators that manipulates generic NetCDF data and supports some Climate and Forecast (CF) conventions. NCO utilities are intended to be as

generic as possible; they do not impose any limitations on the size or type of data. The utilities are used mostly to examine quickly .nc files meta data and content directly from the shell.

4.2.2 *General data manipulation and visual representation*

In order to manipulate and visualize the data, python offers a selection of libraries, some of them specific to data science. This libraries are not strictly related to the NetCDF file format, but thanks to the netCDF4-Python and CDO libraries, it is possible to read the .nc files, and convert the data to standard NumPy or xarray variables. After the data is in a more familiar python format, it is possible to operate on it (if the required operation is not already offered by the cdo library), and create a plot or map using the Matplotlib library.

Here are the main libraries used and a short description:

- **PathLib and OS:** In order to access, read, delete and manipulate files in the operating system, python offers the PathLib and OS libraries. With them, the developed script is not dependent on the used operating system.
- **NumPy**: is an efficient container of generic multi-dimensional data. Offers comprehensive mathematical functions, random number generators, linear algebra routines, Fourier transforms, etc.
- **Matplotlib**: Used for the timeseries, region maps and bar plots. With Matplotlib it is easy to customize legend, add custom text with information and change color and font sizes as desired.

4.2.3 *Other support software*

Some miscellaneous support software that facilitated the development of this thesis and is worth mentioning:

4.2.3.1 *The unix environment and the Bash shell*

This thesis was developed on a Unix environment, more specifically macOS Catalina. The Unix environment and the bash shell allow for an easy integration and use of the other software tools (cdo operator, python scripts, git, wget). Besides, the Bash shell also offers the possibility of scripting for quick bulk file manipulation. All of the tools used on the thesis can be installed on an open source Linux environment as well. Windows installation should also be possible using some third party software, but it is recommended to stick to Unix.

4.2.3.2 *Virtual environments: Conda and Brew*

To facilitate the installation of the required software libraries and dependencies, a virtual environment is recommended. In Unix, the most common options are Conda and Brew; both of them work pretty similarly. The user creates a virtual environment in which one can install as many packages and libraries without affecting the Operating System. If something goes wrong, one can easily remove the virtual Env and start over. This is particularly useful for the installation of the new cdo Global Climate Indices operator, that are available in the development branch of cdo, via Conda.

4.2.3.3 *Git: version control system*

In any project that involves programming, it is fundamental to have some sort of versioning control. Git is the most popular and widely used tool for this purpose, and it allows to keep track of modifications on the source code of the project. It is available in Linux, Windows and MaC, and there are several web services that allow for the remote storing of the code (GitHub, GitLab etc), which can be used as a simple backup, or for distributed development. Git is easy to use and offers the appropriate tools for small individual projects and for more complex collaborative endeavourers.

4.2.3.4 *Environment setup*

To begin working with netcdf files and python, cdo and some additional libraries need to be installed. In Mac OS this can be achieved using a virtual environment with conda, which also allows for the installation of the cdo development branch required for the calculation of the ETCCDI indices. In listing 4.1 the basic setup is shown. For Linux OS some other packages may be required.

Listing 4.1: Environment Setup

```
# Follow official instructions to download Miniconda bash script)
# Make sure to downlaod the python3 version of the script
bash Miniconda3-latest-MacOSX-x86_64.sh

# Create env and install cdo dev: https://slides.com/wachsylon/cdoetccdi#/3
conda create --name cdoenv conda-forge/label/dev::cdo -c conda-forge

# Activate environmen
conda activate cdoenv

# pip install all the required packages
pip install cdo
pip install numpy
pip install netCDF4
pip install matplotlib
pip install https://github.com/matplotlib/basemap/archive/master.zip
pip install PyQt5
```

4.3 DATA PRE-PROCESSING

After the data has been downloaded, the following step is to do some checks and preparations on the NetCDF files.

- **Simple file consistency checks:** Using the commands `cdo info`, `cdo sinfo` and `ncdump -h` it is possible to obtain some general information of the file, like number of timestamps and parameter name. This check is important to make sure the correct data is downloaded.
- **Region selection:** With the command `cdo sellonlatbox` it is possible to select the desired regions, in coordinates. This step is the first one performed, to avoid working with the whole global data in the following steps, which would take too much time.
- **Units conversions:** For some of the analysis, the units need to be converted. For temperature, from Kelvin to Celsius degrees. For precipitation, from $[kg/m^2s]$ to $[mm/day]$. This is possible using arithmetic operations like `cdo subc` and `cdo mulc`, and changing the units name in the cdo files with `cdo chunit`.
- **Time format conversions:** Not all the models use the same calendar and reference time, so to allow operations among files from different models, these two parameters need to be converted. This can be achieved with the commands `cdo setreftime 1850-01-01,00:00:00` and `cdo -setcalendar,standard`
- **Timestamps merging:** Some of the models provide the data in multiple files, especially if the frequency is daily. These files need to be glued together using the command `cdo mergetime`.
- **Variables deletion**: The GFDL models family has some additional time variables that are not really necessary, and can interfere with future commands. They can be deleted from the netcdf files using `cdo delete,name=average_DT,average_T1,average_T2`

4.3.1 *Files organization*

As in this project we are working with a huge quantity of files, the organization of them is very important. After the nc files are preprocessed, they are stored in folders using a hierarchical structure that follows Experiment, Model, Param, Region, as shown in figure 4.3

From this folder structure the required files are read and processed as needed. Output results are written to a secondary location to keep everything organized.

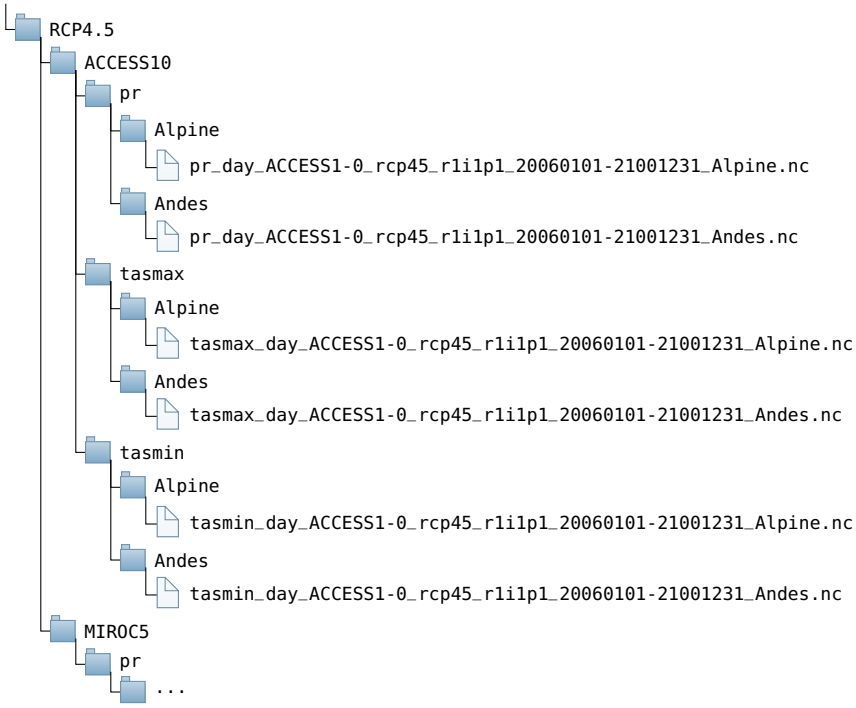

Figure 4.3: Folder structure for netcdf files storage

4.4 DATA PROCESSING

4.4.1 *Common commands*

Some common operations used during the data processing are:

- **Spatial average:** In order to produce a timeseries, an spatial average needs to be performed. This can be achieved using, `cdo fldmean` which is used to calculate the weighted average of the area.
- **Temporal average:** In order to produce a map, a time average needs to be performed. This can be done using `cdo timmean`
- **Date selections:** Sometimes it is useful to perform a certain operation over some range of years, or considering only a few months (seasons). this can be done with the commands `cdo selyear` and `cdo select,season`
- **Reading parameters:** Usually parameters are manipulated using cdo commands. However, when the variables need to be plotted, they have to be read into python np arrays. This can be achieved by reading the netcdf file, extracting the variables and closing the file again, as shown in listing 4.2
- **Models ensemble:** The models ensemble is performed using the median, which corresponds to the 50th percentile. This can be found with `cdo enspctl,50`

Listing 4.2: Opening netcdf file and reading parameters

```
data_in = Dataset(file_path, mode='r') # read the netcdf in file_path

pr = data_in.variables[index['pr']][:] # read precipitation var

# Read Time information
time = data_in.variables['time'][:]
time_uni = data_in.variables['time'].units
time_cal = data_in.variables['time'].calendar

# Read latxlon information
lons = fh.variables['lon'][:]
lats = fh.variables['lat'][:]

fh.close() # Close the file
```

- **Change grid:** As different models have different resolutions, when the models need to be ensembled regionally, their grids need to be adapted. As reference, the grid from the MIROC5 model was used, as it has a good resolution, and the model was used in all of the analysis.

4.4.2 *Commands for ETCCDI Indexes*

Most of the indices are calculated with an ad hoc ETCCDI cdo command. Some indices do not required an especial command and can be calculated using standard cdo commands. Finally, for some indices the ECA version of the command was used, as the ETCCDI version did not work as expected. This is summarized in in table 4.3.

Table 4.3: cdo commands used to calculate the 27 ETCCDI Indices

index	cdo command	index	cdo command
FD	`cdo etccdi_fd`	SU	`cdo etccdi_su`
ID	`cdo etccdi_id`	TR	`cdo etccdi_tr`
GSL	`cdo eca_gsl`	TXx	`cdo yearmax`
TNx	`cdo yearmax`	TXn	`cdo yearmin`
TNn	`cdo yearmin`	TN10p	`cdo etccdi_tn10p`
TX10p	`cdo etccdi_tx10p`	TN90p	`cdo etccdi_tn90p`
TX90p	`cdo etccdi_tx90p`	WSDI	`cdo eca_hwfi`
CSDI	`cdo eca_cwfi`	DTR	`cdo monmean -sub`
Rx1day	`cdo etccdi_rx1day`	Rx5day	`cdo etccdi_rx5day`
SDII	`cdo etccdi_sdii`	R10mm	`cdo etccdi_r10mm`
R20mm	`cdo etccdi_r20mm`	Rnnmm	`cdo etccdi_r1mm`
CDD	`cdo etccdi_cdd`	CWD	`cdo etccdi_cwd`
R95pTOT	`cdo etccdi_r95p`	R99pTOT	`cdo etccdi_r99p`
PRCPTOT	`cdo yearsum`		

4.4.3 *Workflow for indices calculation*

The workflow for an index calculation is described as follows:

1. **Individual Models** Some operations need to be performed at model level:
   a) **Index calculation:** The fist step in the process is to traverse the folder hierarchy described in figure 4.3, searching for the appropriate file (taking into account experiment, model and parameter). Then the index is calculated for that file using the corresponding cdo command (see table 4.3).
   b) **Index processing:** The obtained file has to be processed to obtain:
      i. Time Series and anomaly. Calculating a regional average, the file is reduced to a timeseries. Then, the Anomaly is obtained by subtracting the mean value from the baseline period (1961 – 1990).
      ii. Maps and anomaly. Calculating the temporal average over the periods of interest, we obtain a map. Then, the reference map is substracted from the maps of the periods of interest in order to obtain their anomaly.
2. **Models ensemble:** Models from the same experiment are 'merged' by calculating the 50th percentile (median).
   a) For the Time Series, besides the median, the 25th and 75th percentiles are also calculated
   b) For the maps merging, a grid matching operation is required.
3. **Graphs:** Three different types of graphs are generated, using the python library **Matplotlib**. For the indices that produce a result in days or in precipitation units, the relative change[%] w.r.t the baseline period is also calculated, as it can be helpful to visualize and understand better the results. For the indices in temperature units, the relative change is not calculated, as it is not meaningful. For the temperature percentile indices, the results are already in exceedance rate[%] so the relative change is not necessary.
   a) **Timeseries** To help the analysis, for each Region the following data is drawn in the same plot:
      i. Ensemble median from the Historical, RCP4.5 and RCP8.5 experiments.
      ii. A moving average of 10 years on the ensemble median.
      iii. A shading of the region between 25th and 75th percentiles.
      iv. The timeseries from all of the models in the 3 experiments (in high transparency).

With this, it is easy to compare differences between experiments, and check the variability of the models. An additional axis with the relative change is added in the right for the indices that require it.

b) **Maps:** For each of the regions and periods of interest, a map is generated, using the **Basemap** python library. For the indices that require a relative change analysis, additional maps are generated. The colorbar colors and limits are automatically configured for each index taking into account the minimum and maximum values, and to ease the comparative analysis between different regions, periods of time and RCP projections, some of the maps share the same colorbar settings.

c) **Bar Plots:** As a final tool for comparisons we use the bar plot. For each index a barplot with the value by in the year 2090, for each region and RCP experiment is generated. Additionally, the values from global calculations (taken from the website [15]) are added. For indices that require a relative change analysis, an additional barplot is generated.

5 RESULTS

In this chapter, different results in form of graphs (time series and regional maps) are shown and analyzed. The annual trends obtained from monthly data are covered first. They are useful to understand the variability of the models, specially in the precipitation case.

The second part of the chapter is dedicated to assess the climate extreme indices obtained from daily data. Most of the indices show clear tendencies towards a warmer climate, and a small tendency towards higher rainfall.

5.1 ANNUAL TRENDS OF THE AVERAGE TEMPERATURE AND PRECIPITATION

The following trends calculated using the monthly data available from each model for the parameters tas and pr are analyzed, for regions Alpine and Andes:

- Annual mean trends for the historical period, 1850 to 2005
- Temperature and precipitation anomalies for the historical period
- Future climate projection for two RCPs scenarios

The figures in the next paragraphs have all the same structure. The x-axis shows the years from 1850 to 2005 for the historical experiment and $2006 - 2100$ for the future projections. The y-axis presents the corresponding temperatures and precipitations yearly values calculated from the monthly mean values. The solid lines represents the models with higher resolution, and the dashed lines represent the rest of them. Due to the great variability between the models, in the graphs a smoothed version of the time series (moving average window of eight years) is shown instead.

5.1.1 *Historical annual average temperature and precipitation*

Figure 5.1 shows the annual average temperature in the Alps and the Andes. Despite the large variability between models, a slight increase is observed for both regions. In the Alps the average annual temperature goes from 6 to 12 degrees Celsius, while in the Andes the temperature ranges from 22 to almost 25 degrees Celsius.

Regarding the precipitation, in figure 5.2 it is observed that in the Andes the values are higher than in the Alps. About the tendency, it is hard to tell, because there is very large variability between the models.

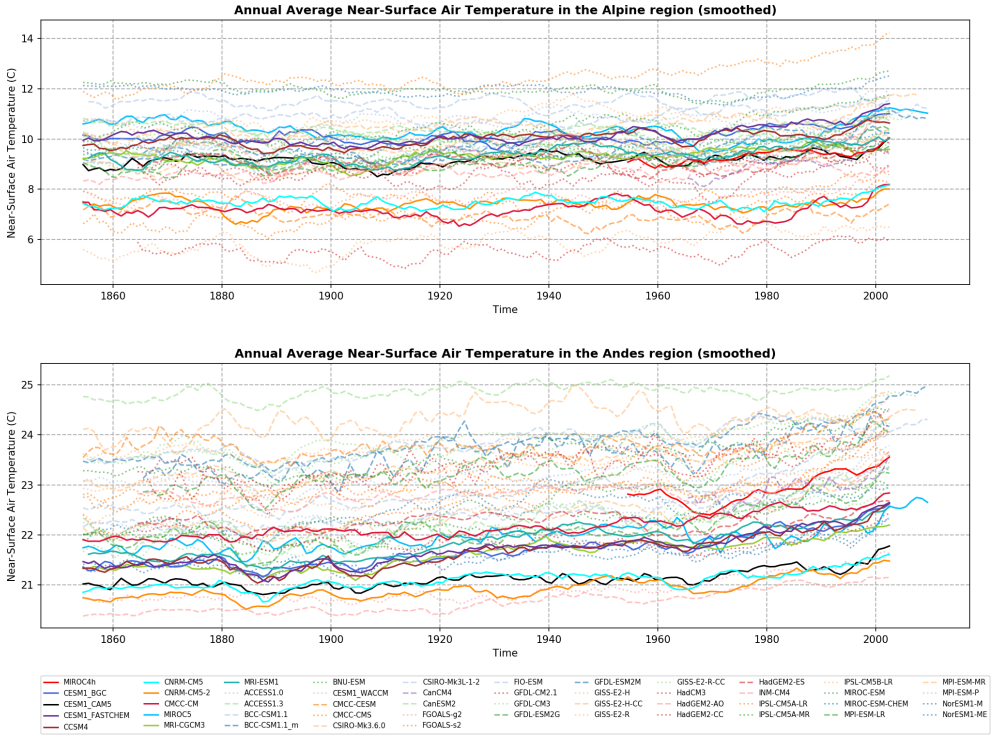

Figure 5.1: Annual Alpine and Andes temperature trends from 1850 to 2005 of forty-nine CMIP5 models.

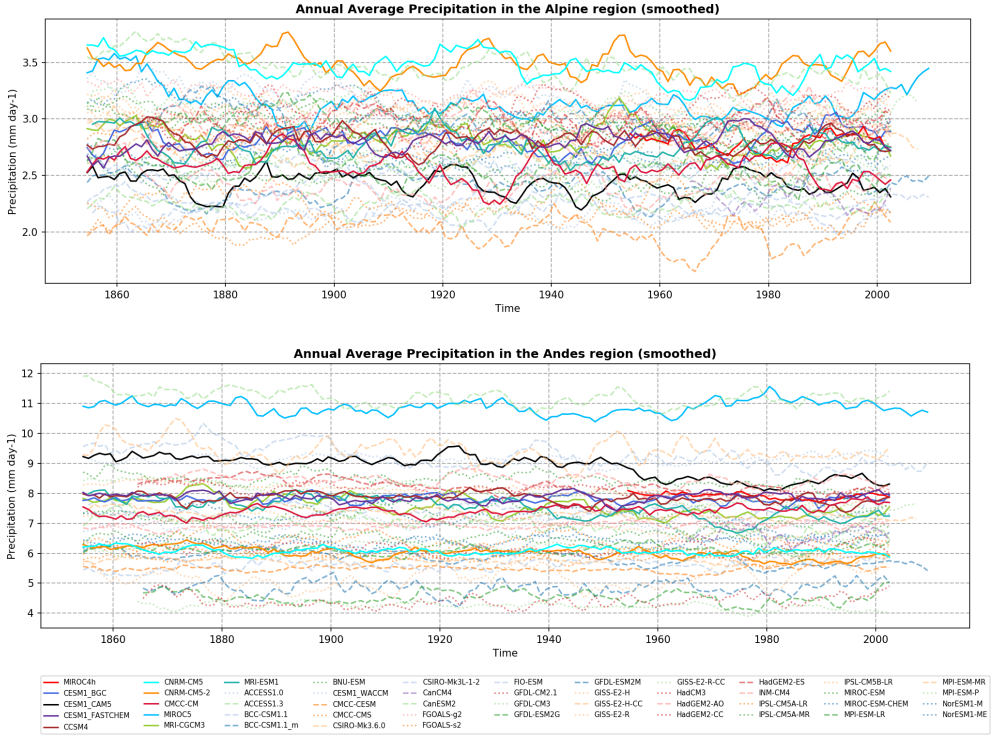

Figure 5.2: Annual Alpine and Andes precipitation trends from 1850 to 2005 of forty-nine CMIP5 models.

5.1.2 *Historical temperature and precipitation anomalies*

To eliminate part of the variability between models, the anomaly is calculated, by subtracting the average value from the baseline period from the whole times series. This results in a graph where it is easier to appreciate the trend. In the figure 5.3 it is observed that from the beginning of the time series until the baseline period the temperature anomaly in Andes is mostly negative. In the Alps this trend is not observed and the temperature remains relatively unchanged. On the contrary, for the values after the baseline period it is evident in that in both regions there is rise in the temperature.

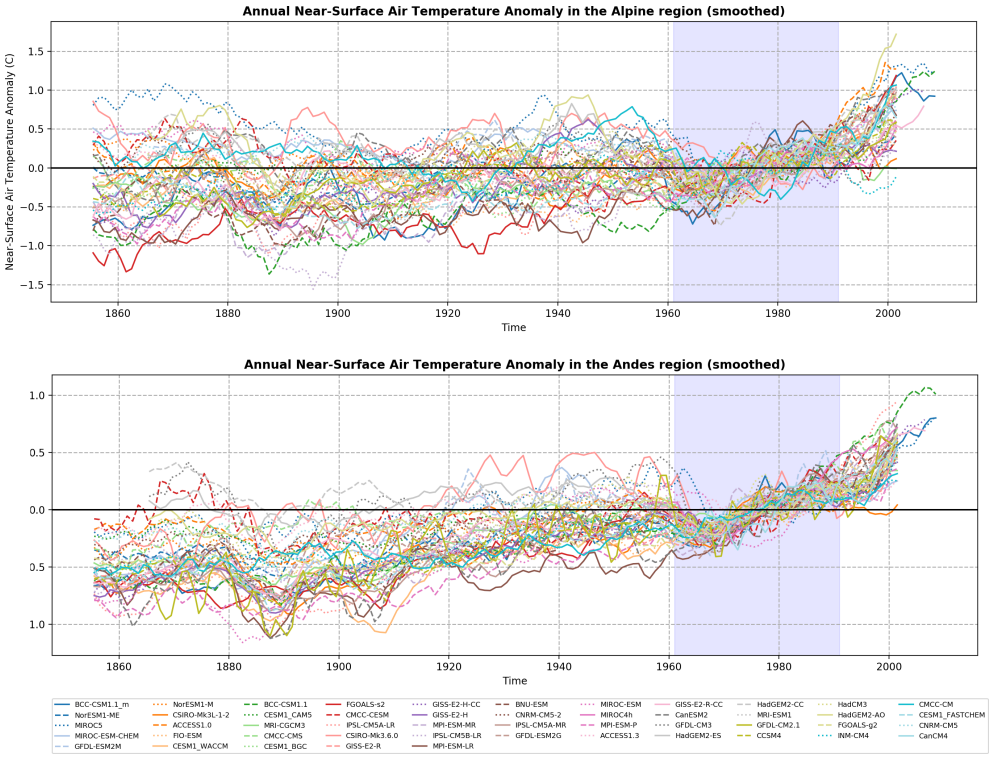

Figure 5.3: Temperature anomaly for the Alps and the Andes relative to 1961 to 1990 of forty-nine CMIP5 models. The shaded area covers the reference period. To guide the readers eye one horizontal line is added at the y=0 value.

Figure 5.4 illustrates the precipitation over the Alps and Andes. Even with the anomaly, high variability between the models is still present. The largest uncertainty is observed in the Andes. There is however a small tendency in both regions over the last fifty years of the simulation where a change to a drier climate is observed.

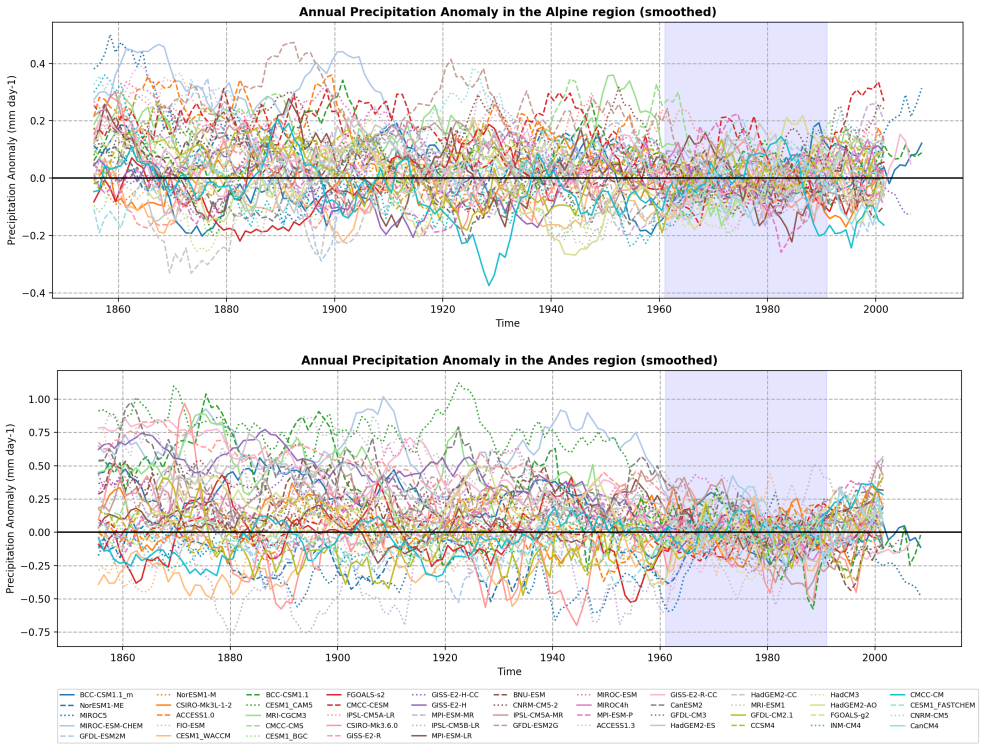

Figure 5.4: Precipitation anomaly for the Alps and the Andes relative to 1961 to 1990 of forty-nine CMIP5 models. The shaded area covers the reference period. To guide the readers eye one horizontal line is added at the $y = 0$ value.

5.1.3 *Future climate projections*

Future projections of the regional climate are subject to different sources of uncertainty due to the natural variability of the climate system, unknown future GHG emissions, and simplifications in global climate models. Figures 5.5 and 5.6 indicates that in there is appreciable inter-model uncertainty in the magnitude of the projected future changes predominantly over the Alpine region. Furthermore, it shows that the models with lower resolution tend to overestimate the warming, mainly in the Andes region. As expected, the RCP8.5 projections shows a higher increase.

As far as precipitation is concerned, figures 5.7 and 5.8 illustrate great variability among the models and no trend is clear. However, it is observed that the rainfall in the Alps is much more variable compared to it in Andes which where it is more stable over time.

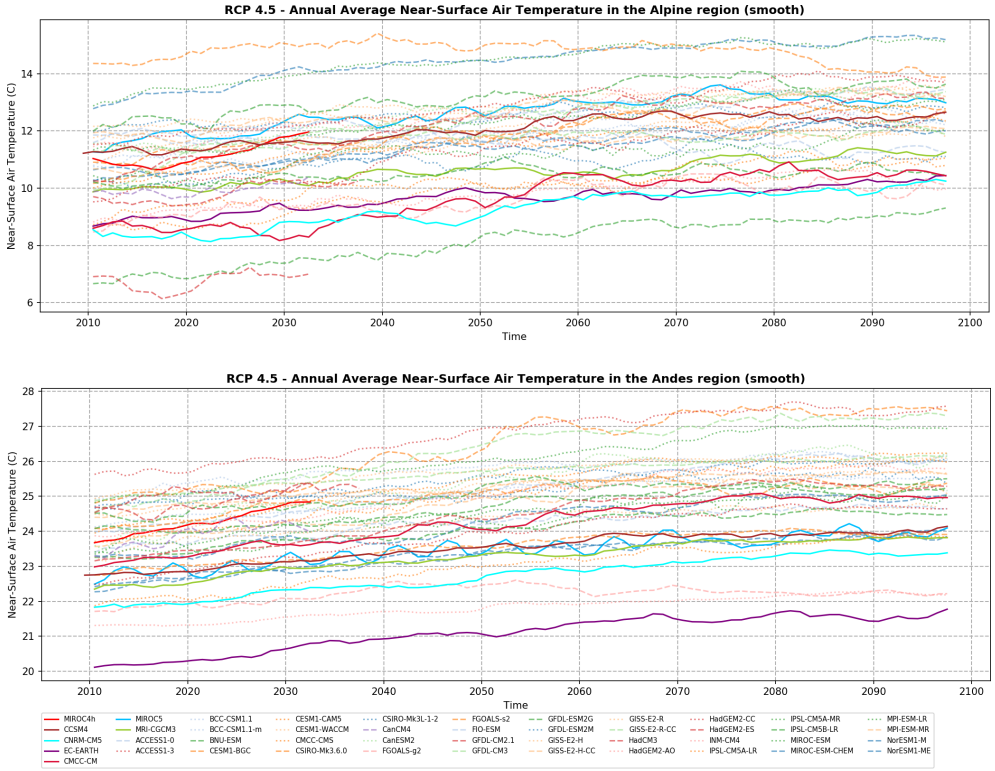

Figure 5.5: Temporal evolution in Alpine and Andes regions driven by the emissions scenario RCP4.5 from 2006 to 2100 of forty-five CMIP5 models.

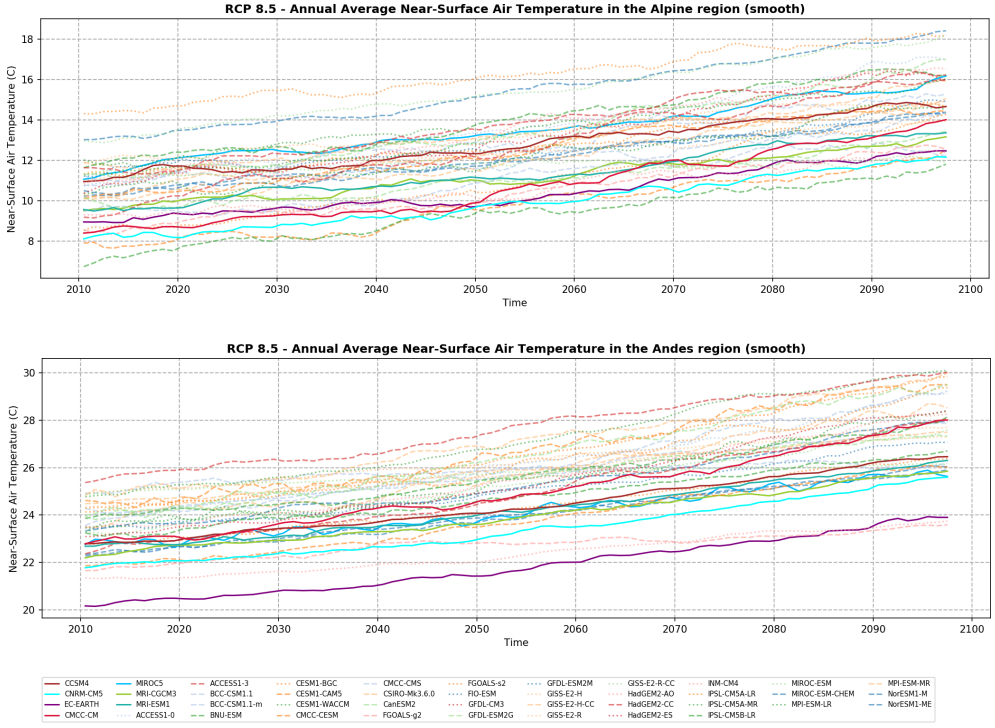

Figure 5.6: Temporal evolution in Alpine and Andes regions driven by the emissions scenario RCP8.5 from 2006 to 2100 of forty-five CMIP5 models.

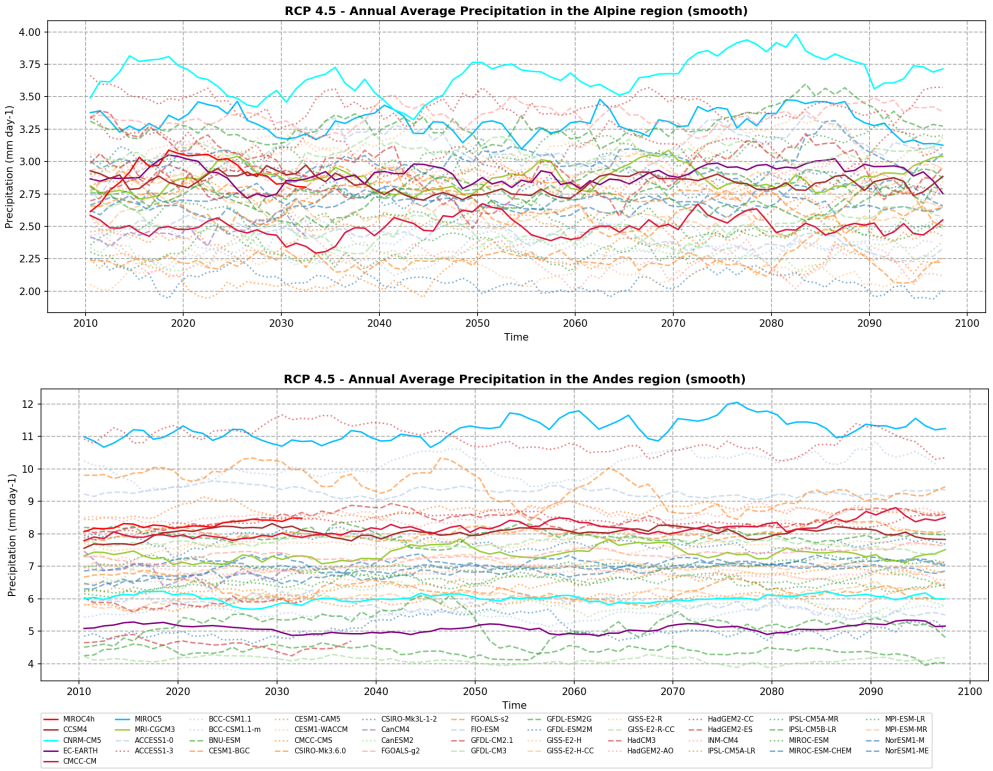

Figure 5.7: Evolution in precipitation over the Alps and Andes driven by the emission scenario RCP4.5 from 2006 to 2100 of forty-five CMIP5 models.

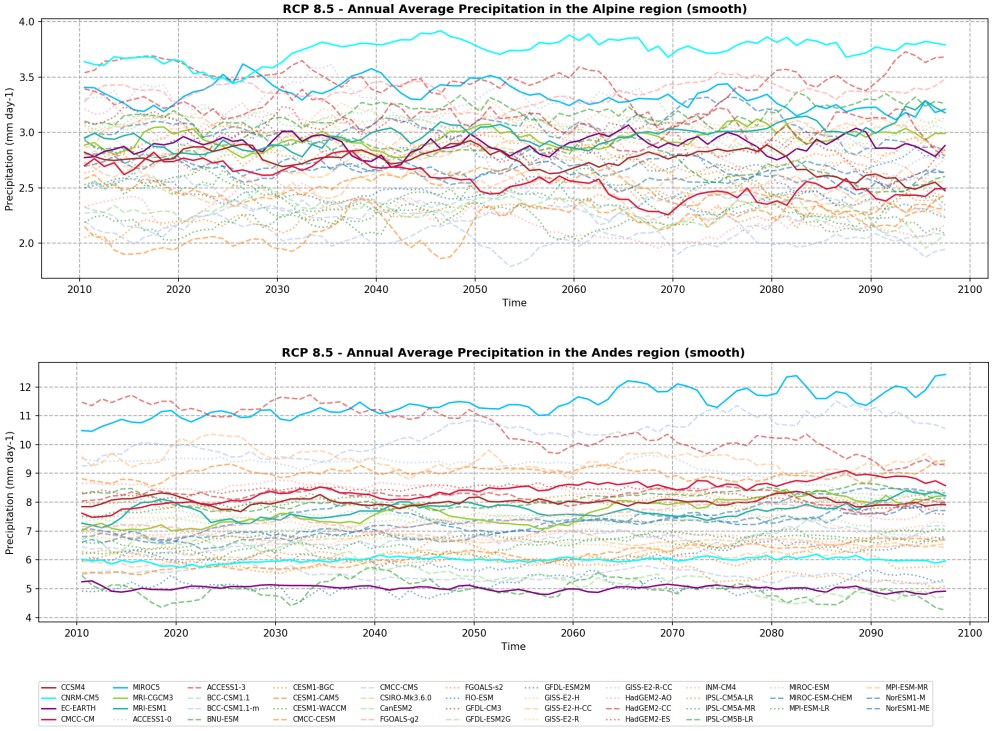

Figure 5.8: Evolution in precipitation over the Alps and Andes driven by the emission scenario RCP8.5 from 2006 to 2100 of forty-five CMIP5 models.

In comparison to monthly values, daily data provides more detailed information on meteorological conditions. By analyzing daily maximum and minimum temperature, and precipitation, it is possible to detect changes in key indicators, like the 27 ETCCDI indices which are calculated an analyzed in this chapter for both regions.

Each region is studied individually, beginning with the Alps. The indices are represented graphically in terms of temporal evolution and spatial pattern in three different time periods (past: 1861-1890, present: 1990-2020, future: 2061-2090). The historical and the two RCPs experiments are combined to obtain a higher time span: 1861-2090. The values are presented as anomalies relative to the reference period 1961-1990.

5.2 ETCCDI INDICES IN THE ALPS

5.2.1 *Number of Frost Days*

In Figure 5.9 it is observed that in the past the number of frost days was constant over time, at around 81 days below 0°C in a year, as it was during the reference period. However, after 1990 a continuous reduction in the frost days is observed, by about 18 and 15 days less for both scenarios in the year 2020; and 29 and 44.7 days less for the RCP4.5 and RCP8.5 respectively at the end of the century, which represent a relative decrease of 36% and 55%.

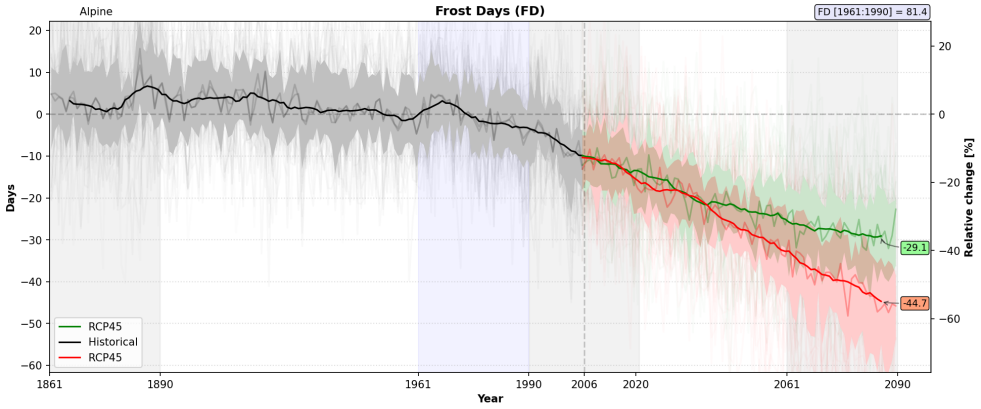

Figure 5.9: The multimodel median of changes in **Frost Days** displayed as differences to the reference period, averaged over the Alpine region. The vertical shading indicates the reference period, and the three 30 year periods considered in the analysis (1861-1890, 1991-2020 and 2061-2090). For each RCP, besides the median, the figure shows the 25^{th} - 75^{th} percentiles area (read and green shading), and a smoothed version (moving window of 10 years). On the top right, the value average value in the reference period.

Figure 5.10 shows the spatial behavior of the Frost Days in the Alpine region, for the four chosen time periods. The spatial differences are more noticeable in the RCP scenarios, where the decrease in Frost Days is higher in the north-east region. However, by looking at the relative change, the decrease becomes more homogeneous. This is because, the north-east region,

with higher altitudes, has more Frost Days in the reference period, and loses more frost days in the future projections. Consistently with the timeseries, the RCP8.5 scenario shows more change than the 4.5 counterpart.

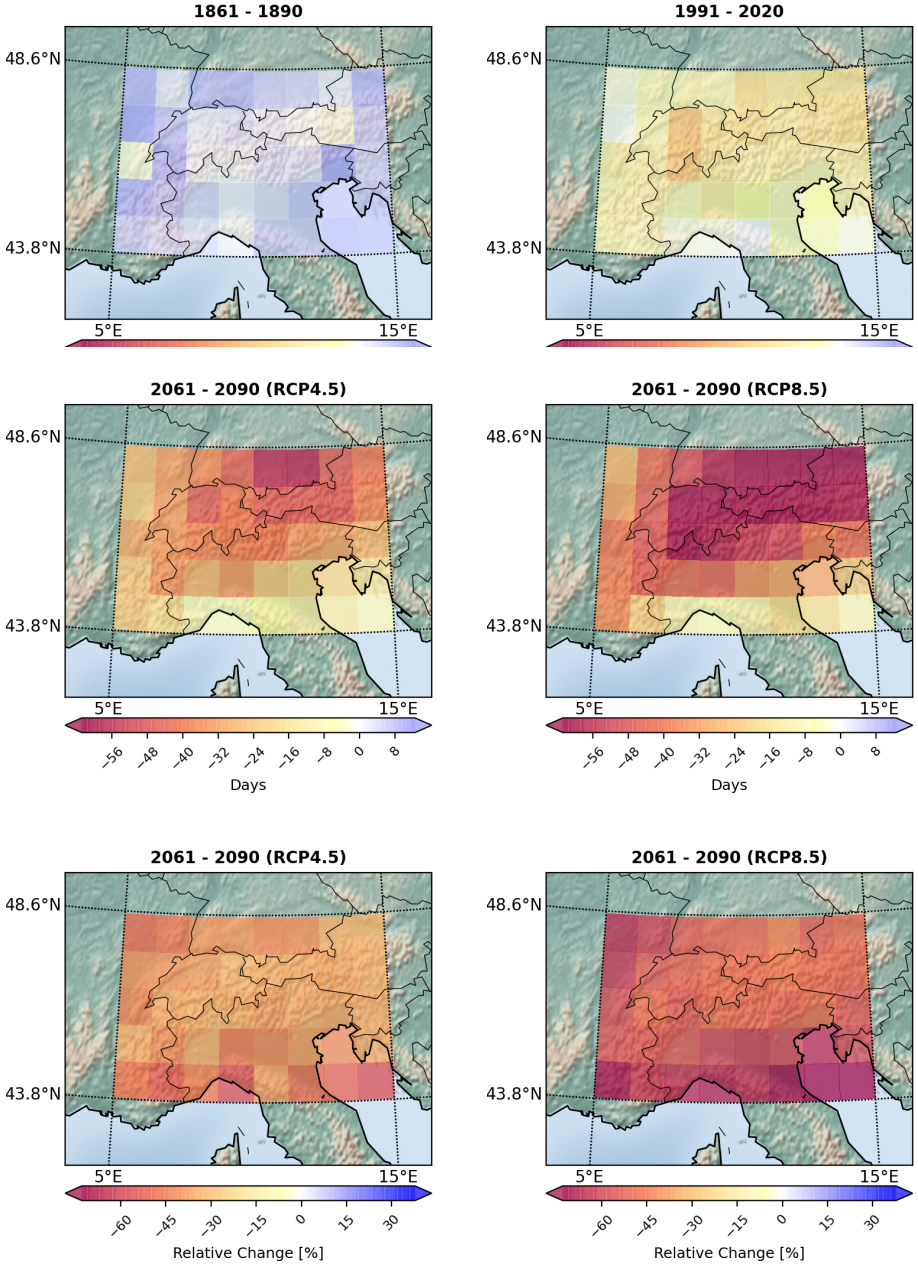

Figure 5.10: The multimodel median of changes in **Frost Days** relative to the reference period for the Alpine region, temporally averaged over the three analyzed time periods. The top four maps show the change in the index's units, while the bottom two are in percentage.

5.2.2 *Number of Summer Days*

The number of summer days, i.e the days where the daily maximum temperature is greater than 25°C (Figure 5.11) has remained constant throughout the years in the historical experiment. On the contrary, after 1990 a constant increase is observed. At the beginning both RCPs have a similar increase, but later the RCP8.5 has a more inclined growth, reaching values of 66 days by the end of the century, which is equivalent to a 214% increase with respect to the reference period (on average 31 days). For the RCP4.5 the increase of 36 days which corresponds to 116% of relative change.

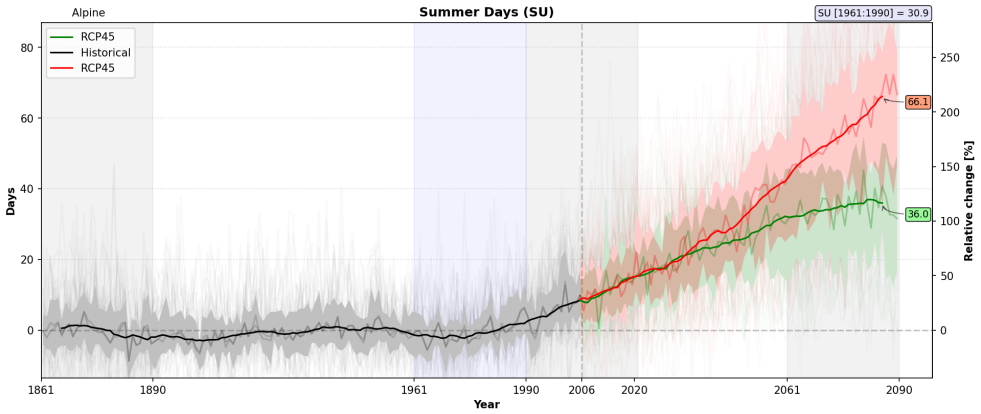

Figure 5.11: The multimodel median of changes in **Summer Days** displayed as differences to the reference period, averaged over the Alpine region.

The spatial pattern is pretty uniform in the whole area when looking at the increase in days, as can be observed in figure 5.12. Both the flats and high elevation regions are affected by the increase in summer days. On the other hand, when looking at the relative change, the northern region shows more changes, as in the reference period, it has fewer Summer Days. As expected, the changes are more pronounced in the and RCP8.5 experiment.

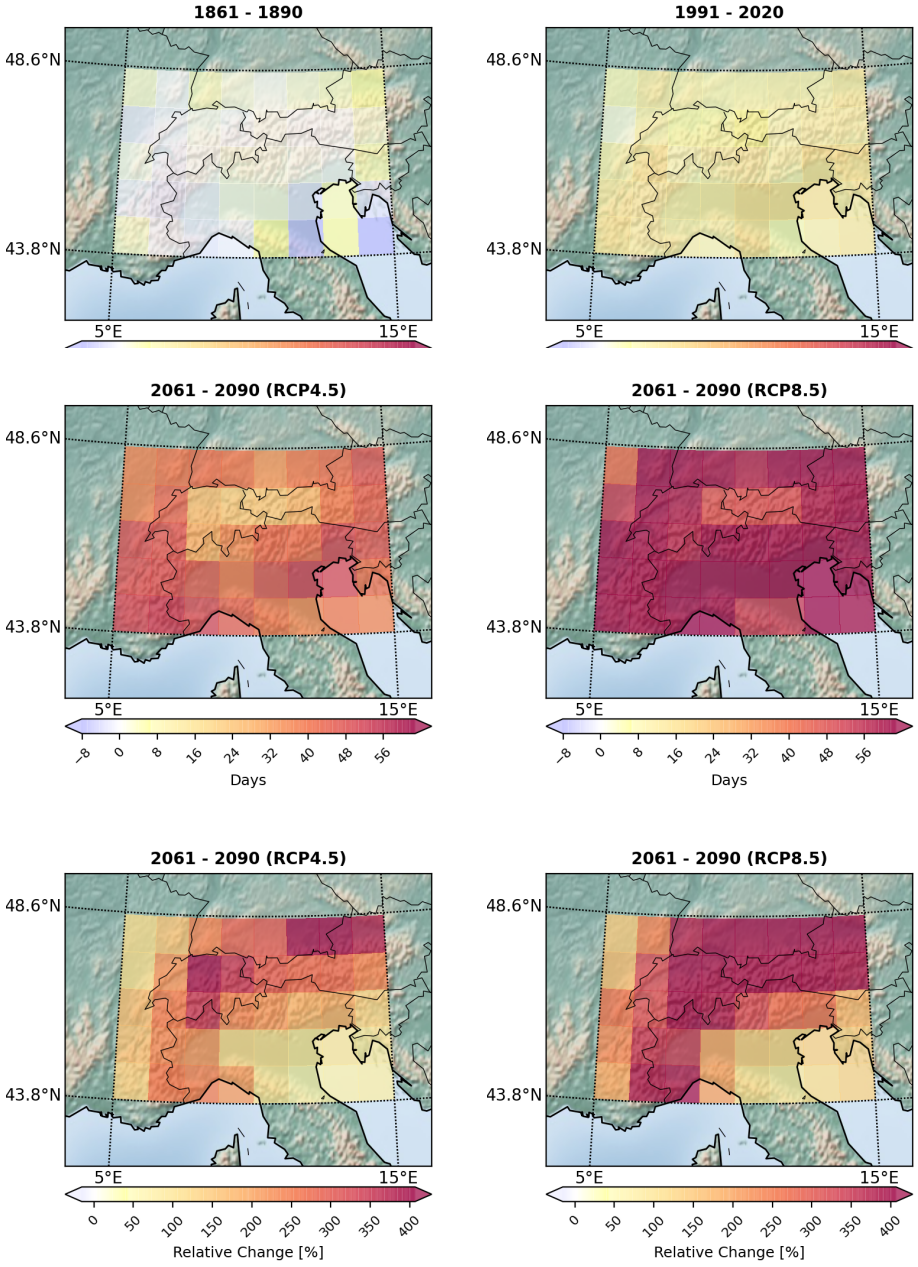

Figure 5.12: The multimodel median of changes in **Summer Days** relative to the reference period for the Alpine region, temporally averaged over the three analyzed time periods. The top four maps show the change in the index's units, while the bottom two are in percentage.

5.2.3 *Number of Icing Days*

Figure 5.13 shows a gradual decrease in the number of days with daily maximum temperature is below 0°C. In this index both RCPs have similar trend from 2006 to 2041. By the end of the 21st century the RCP8.5 scenario has a larger decrease corresponding to 15 days while in RCP4.5 is of 11.6 days. These changes correspond to 67% and 52% of relative change. Compared to

frost days, the number of days lost is lower, but in relative change the change is higher (for Frost Days it is 54% and 35%).

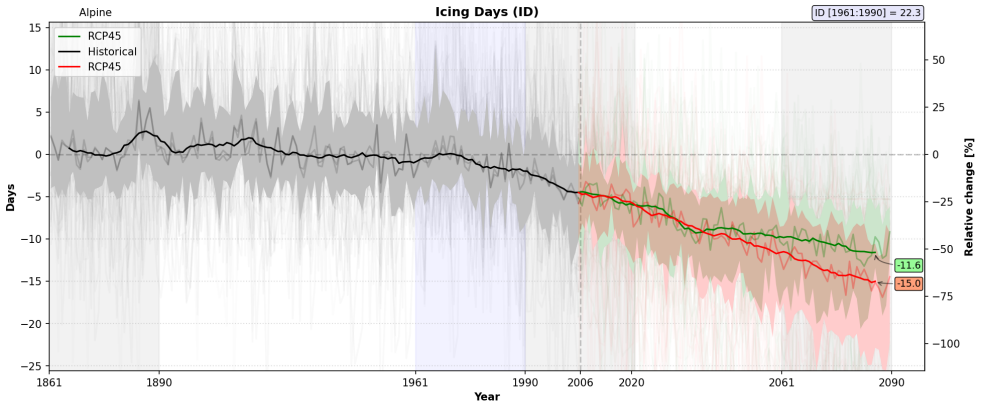

Figure 5.13: The multimodel median of changes in **Icing Days** displayed as differences to the reference period, averaged over the Alpine region.

Similarly to Frost Days, the Icing Days show a lot of variation when looking at the changes in number of days, and more homogeneity when analyzing the relative changes. The northern region shows the major loses in number of days, while the southern regions show very little change, as they had close to zero Icing Days in the reference period to begin with.

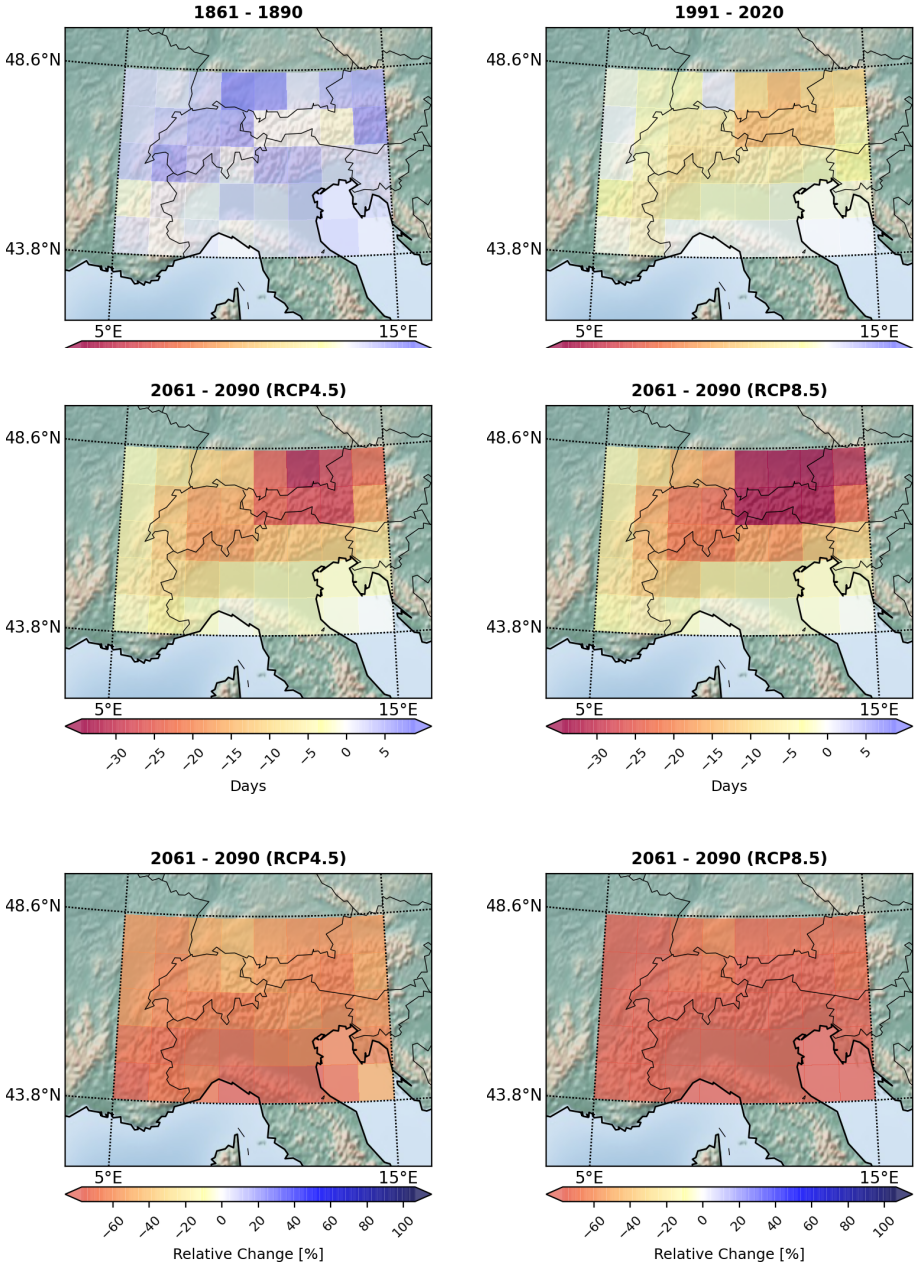

Figure 5.14: The multimodel median of changes in **Icing Days** relative to the reference period for the Alpine region, temporally averaged over the three analyzed time periods. The top four maps show the change in the index's units, while the bottom two are in percentage.

5.2.4 *Number of Tropical Nights*

There is an increase in the number of days with minimum temperature greater than 20°C, by about 10 days in both scenarios in the middle of the 21st century. The change reaches 16 days and 37.6 days for the RCP4.5 and RCP8.5 respectively by the end of the century. Compared with the TR average of 8 days in 1961-1990, these values correspond to a relative change

of 193% and 453%. In this index the values show large variability between models.

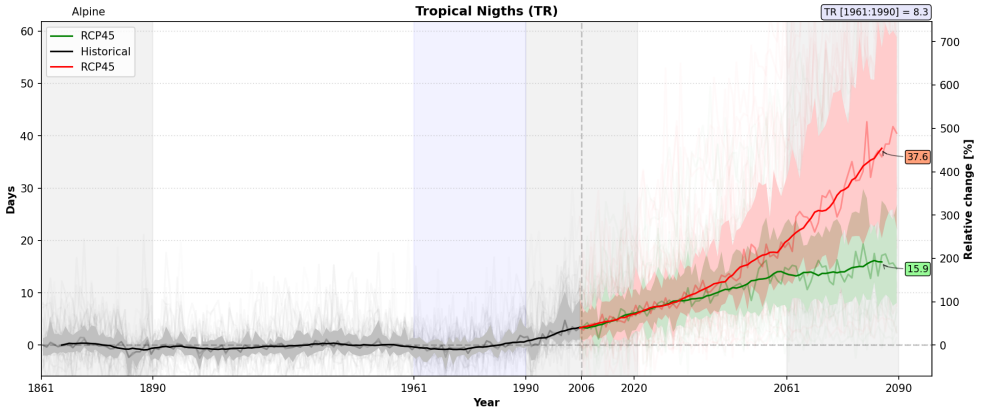

Figure 5.15: The multimodel median of changes in **Tropical Nights** displayed as differences to the reference period, averaged over the Alpine region.

From figure 5.16, the spatial behavior shows a larger increase in the number of tropical nights in the southern region. In the northern region the increase seems small, but it is worth noticing that in the reference period, this area presents virtually zero tropical nights. As expected, the increase is larger for the RCP8.5, for the whole region.

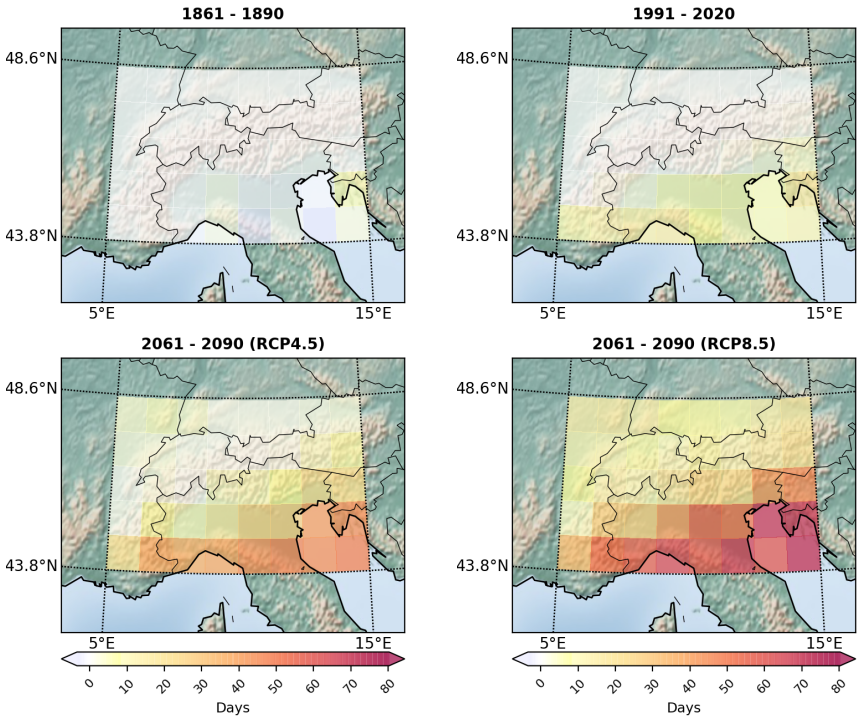

Figure 5.16: The multimodel median of changes in **Tropical Nights** relative to the reference period for the Alpine region, temporally averaged over the three analyzed time periods.

5.2.5 *Growing season length*

As observed in figure 5.17 GSL is expected to increase, as a direct result of the increase in temperature. In the past climate there are no significant changes. However, from about the year 1900 a steady increase is observed. GSL is expected to increase by 35.8 days and 59 days in RCP4.5 and RCP8.5 by the year 2090, compared to the mean 262-day base period.

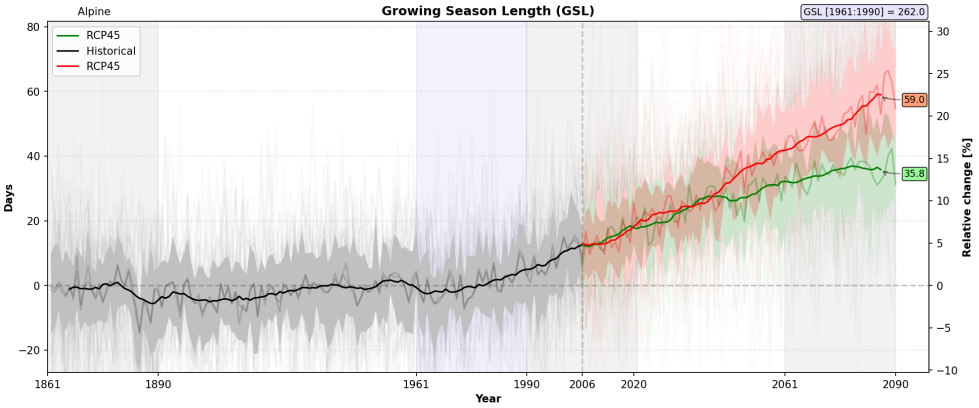

Figure 5.17: The multimodel median of changes in **Growing Season Length** displayed as differences to the reference period, averaged over the Alpine region.

From figure 5.18 the spatial variability shows that in the past the warm period was smaller than the base period. In the future the number of days increases mostly in the northern part of the Alps.

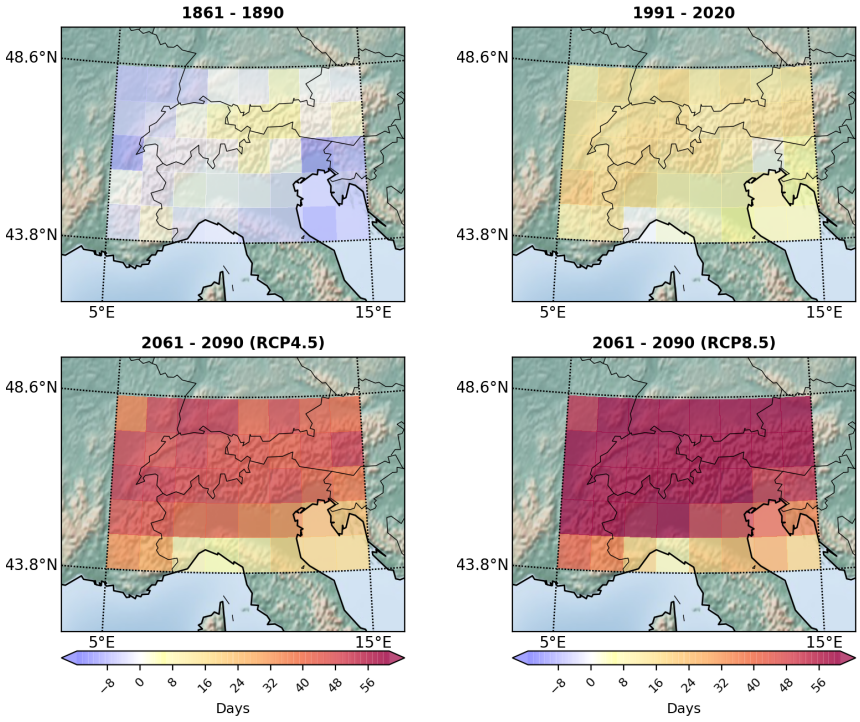

Figure 5.18: The multimodel median of changes in **Growing Season Length** relative to the reference period for the Alpine region, temporally averaged over the three analyzed time periods.

5.2.6 *Yearly Maximum Value of Daily Maximum Temperature*

The CMIP5 simulation show a constant trend in the past (see Figure 5.19 slightly below the average of the reference period (by about 30°C of TXx). On the contrary, future projections show a significant increase in the maximum values of temperature annually for both scenarios, showing an increase of 3.8°C for RCP4.5 and 7.2°C for RCP8.5. For this index the models have great uncertainty about how much the temperature increase would be for the days with daily maximum temperature, these increase can range from 2°C to 6°C for the RCP4.5 scenario. And from 6°C to 10°C for the RCP8.5 considering the 25th and 75th percentiles of each simulation.

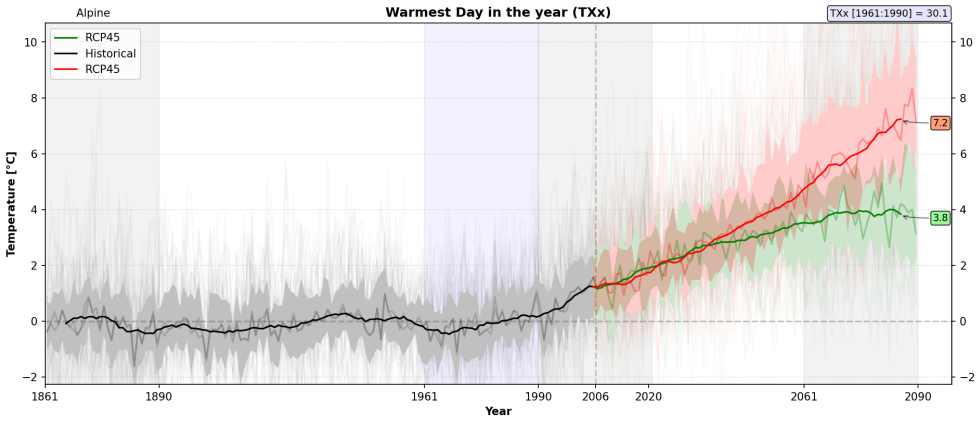

Figure 5.19: The multimodel median of changes in **Yearly Maximum Value of Daily Maximum Temperature** displayed as differences to the reference period, averaged over the Alpine region.

The spatial variability for TXx is displayed in the figure 5.20. It is observed that the temperature increases homogeneously throughout the region, a few more in the high part of the mountains . As expected, in scenario RCP8.5 the temperature increases further.

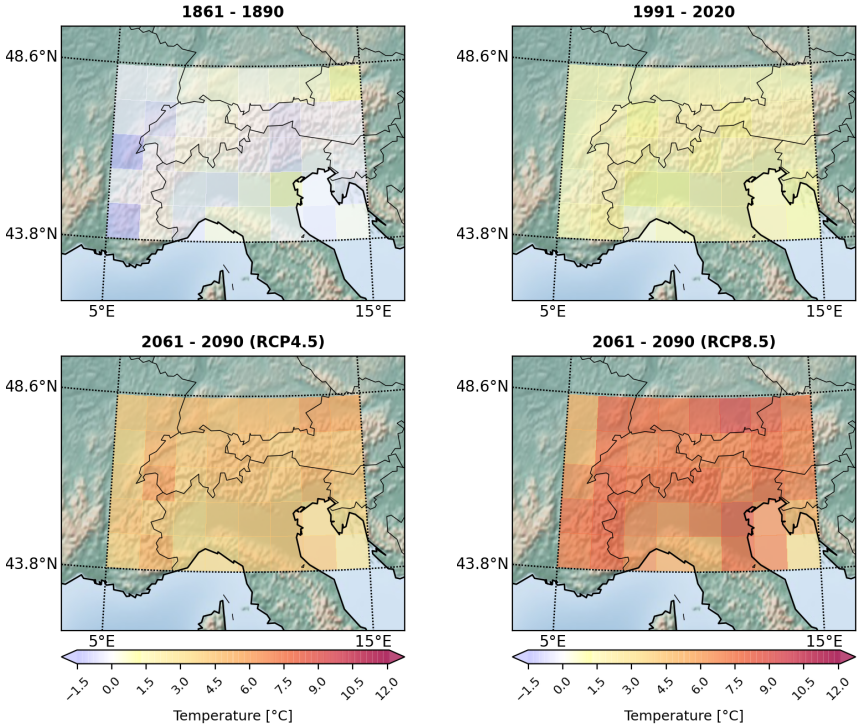

Figure 5.20: The multimodel median of changes in **Yearly Maximum Value of Daily Maximum Temperature** relative to the reference period for the Alpine region, temporally averaged over the three analyzed time periods.

5.2.7 *Yearly Maximum Value of Daily Minimum Temperature*

In figure 5.21 shows the trend in TNx. It is expected to increase less than the TXx (figure above). Since 1990, a continuous increase in the minimum daily temperature has been observed. In the the present period 1990-2020 both scenarios have a similar behavior. By the end of the 21st century, the median temperature is expected to increase by 3.2°C and 6.1°C in the *RCP*4.5 and *RCP*8.5 respectively.

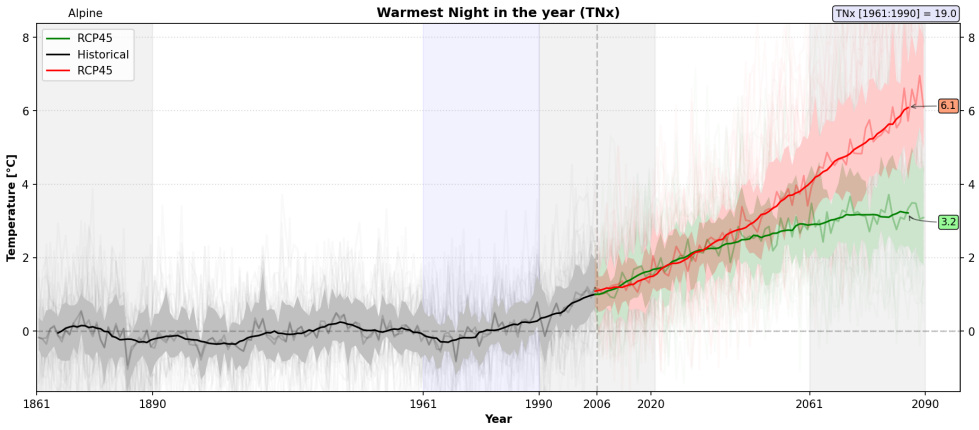

Figure 5.21: The multimodel median of changes in **Yearly Maximum Value of Daily Minimum Temperature** displayed as differences to the reference period, averaged over the Alpine region.

From figure 5.22 the spatial behavior shows that the temperature increases homogeneously in the whole region, a little more in the northeast.

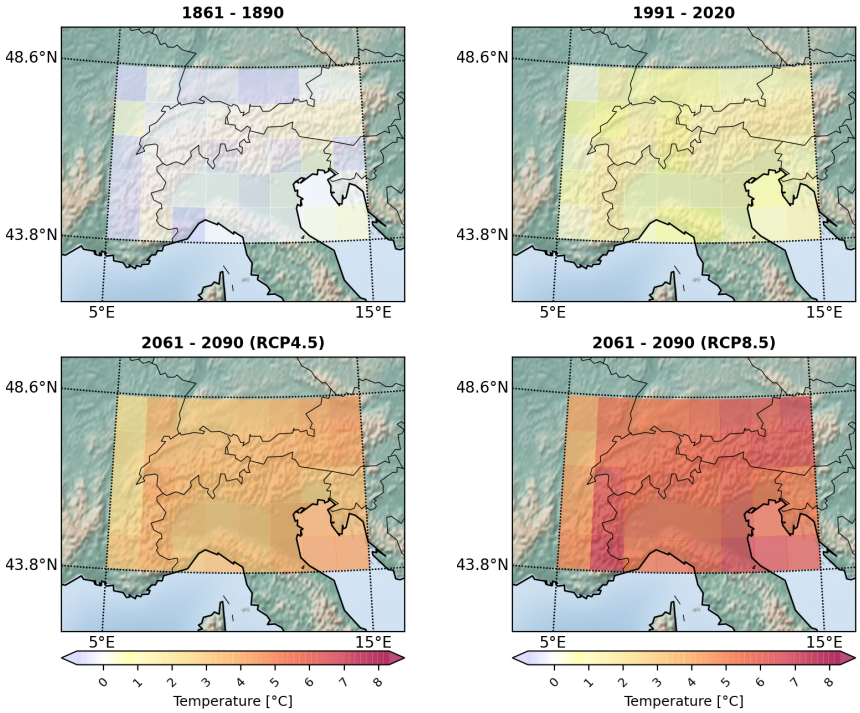

Figure 5.22: The multimodel median of changes in **Yearly Maximum Value of Daily Minimum Temperature** relative to the reference period for the Alpine region, temporally averaged over the three analyzed time periods.

5.2.8 *Yearly Minimum Value of Daily Maximum Temperature*

In figure 5.23 the trend is also expected to gradually increase form 1990, the median increases most in RCP8.5 with 5.6°C closely followed by the RCP4.5 with an increase of 3.6°C, compared to the median of −5.2°C of TXn in the reference period.

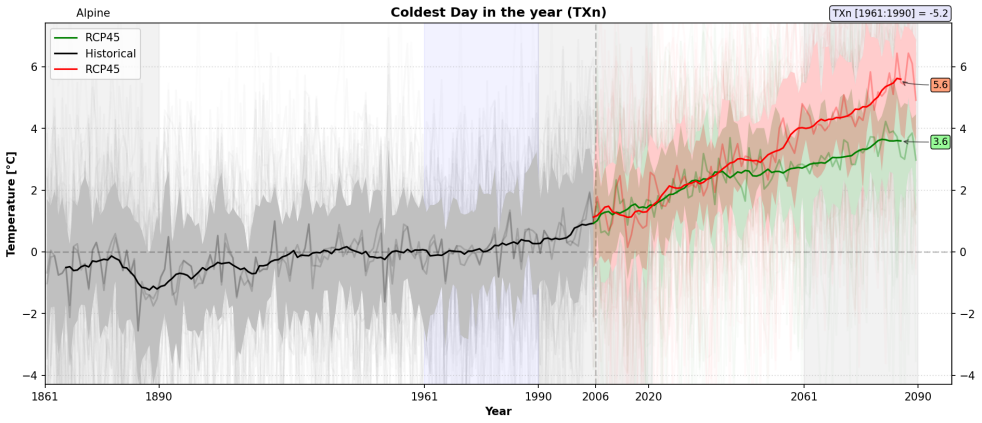

Figure 5.23: The multimodel median of changes in **Yearly Minimum Value of Daily Maximum Temperature** displayed as differences to the reference period, averaged over the Alpine region.

From figure 5.24 As can be seen from the above indices, the temperature increases uniformly throughout the region over the years, with slightly more warming in the northeast.

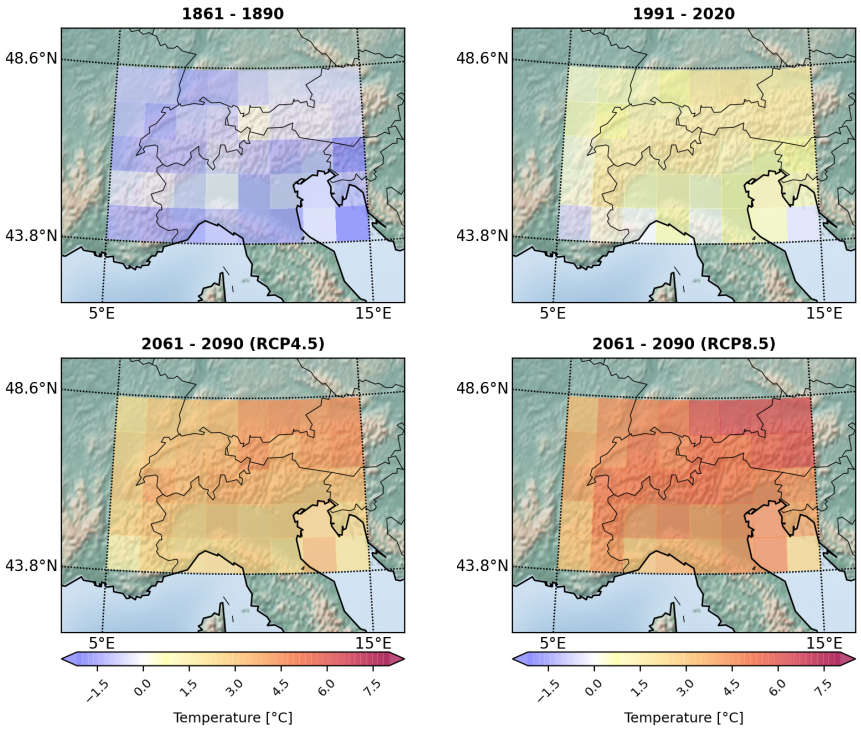

Figure 5.24: The multimodel median of changes in **Yearly Minimum Value of Daily Maximum Temperature** relative to the reference period for the Alpine region, temporally averaged over the three analyzed time periods.

5.2.9 *Yearly Minimum Value of Daily Minimum Temperature*

The annual minimum of TN (Figure 5.25) shows a constant temperature in the past climate which is similar to the average temperature of the reference period. On the other hand, future projections show an increase at the end of the century by 4.5°C and 6.6°C in rcp4.5 and RCP8.5 respectively, in comparison to the mean TNn of the reference period (−12°C).

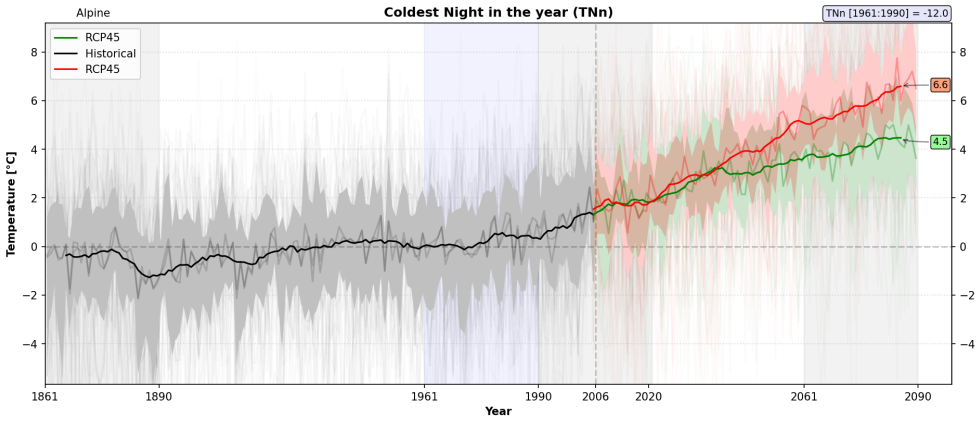

Figure 5.25: The multimodel median of changes in **Yearly Minimum value of Daily Minimum Temperature** displayed as differences to the reference period, averaged over the Alpine region.

From figure 5.26 shows large temperature changes, in the past TNn was much lower than the reference period. The biggest increases are projected in RCP8.5 in the northeast region, with an increase of 9°C.

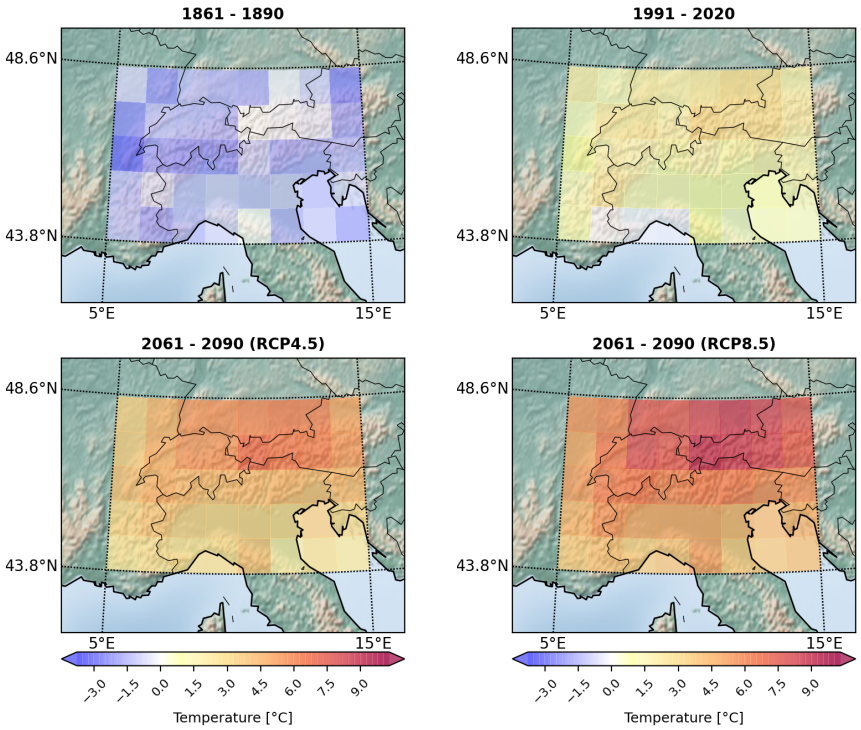

Figure 5.26: The multimodel median of changes in **Yearly Minimum Value of Daily Minimum Temperature** relative to the reference period for the Alpine region, temporally averaged over the three analyzed time periods.

5.2.10 *Percentage of Days when TN < 10^{th} Percentile*

The percentage of cold nights is expected to decrease as shown in figure 5.27. From the historical simulation it is observed that the percentage of cold nights is slightly higher in the past than in the reference period, and since 1961 there has been a steady decrease. From the RCP experiments the decrease continues in both scenarios with similar trend. In the middle of the 21^{st} century the RCP8.5 scenario begins to decrease more rapidly reaching the year 2090 without any cold nights. On the other hand, the RCP4.5 projection indicates that there will be only 1.7%.

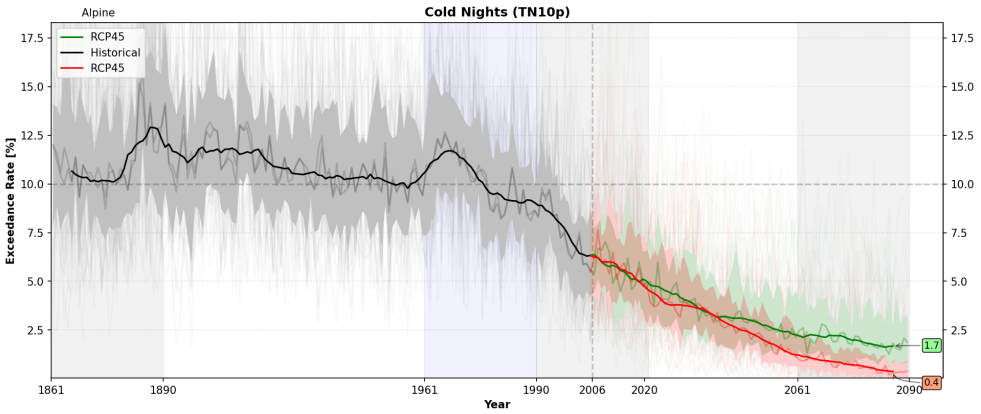

Figure 5.27: The multimodel median of changes in **Percentage of Days when Daily Minimum Temperature is lower than the 10^{th} Percentile** displayed as differences to the reference period, averaged over the Alpine region.

The spatial variability for Tn10p can be observed in Figure 5.28, From the 1861-1890 image the cold nights were about 13% colder compared to the base period, especially the northern part was particularly cold. Since the second image, which represents the time present (1991-2020), a modest and uniform warming is observed in the whole area. In both future projections it is expected that only 3% and 41.5% of the nights will be cold (compared to the base period) in RCP4.5 and in RCP8.5 respectively.

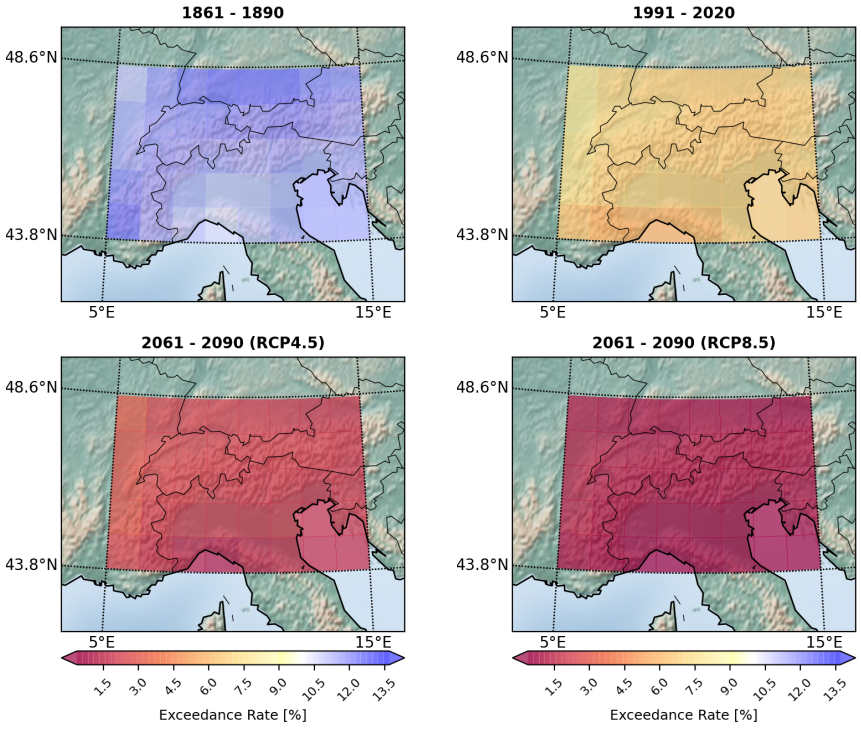

Figure 5.28: The multimodel median of changes in **Percentage of Days when Daily Minimum Temperature is lower than 10th Percentile** relative to the reference period for the Alpine region, temporally averaged over the three analyzed time periods.

5.2.11 *Percentage of Days when TX < 10th Percentile*

The behavior of cold days simulated by the CMPI5 models is shown in Figure 5.29. There is no noticeable change in the exceedance rate of cold days in the range from 1861 to the reference period, according to the historical data. Around the year 1980 we start to see a steady decrease in the value. It is important to notice that the data from 1980 to 2005 has been taken from the historical experiment and not from the RCP projections.

The decreasing trend continues in both RCPs projections, with RCP8.5 showing a higher change, as expected. By the end of the 21st century, RCP4.5 predicts less than 2.5% of days that qualify to be in 10th percentile of the reference period, and in RC*P*8.5 there will virtually be no days.

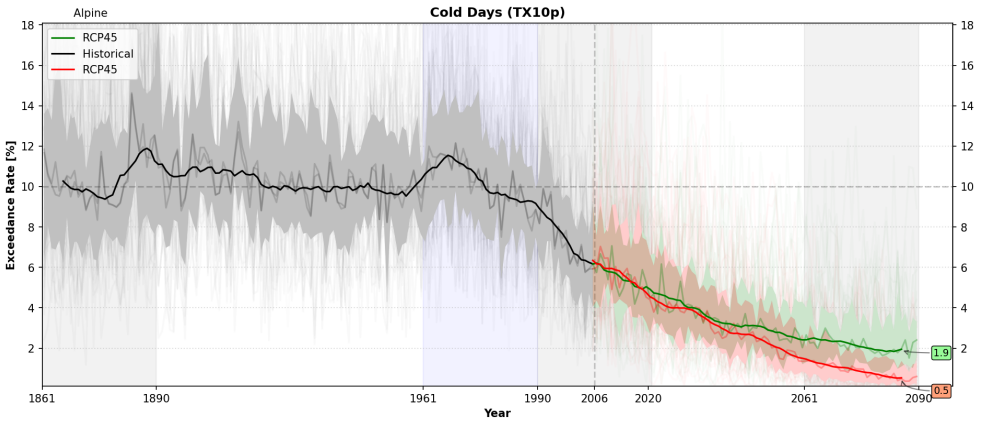

Figure 5.29: The multimodel median of changes in **Percentage of Days when Daily Maximum Temperature is lower than the 10th Percentile** displayed as differences to the reference period, averaged over the Alpine region.

From Figure 5.30 the percentage of temperature exceedance of TN10p is presented. From the 1861-1890 image it can be observed no exceedance rate in percentage of days northern part. As what concerns in future scenarios the increasse exceedance rate is homogeneous across the whole area.

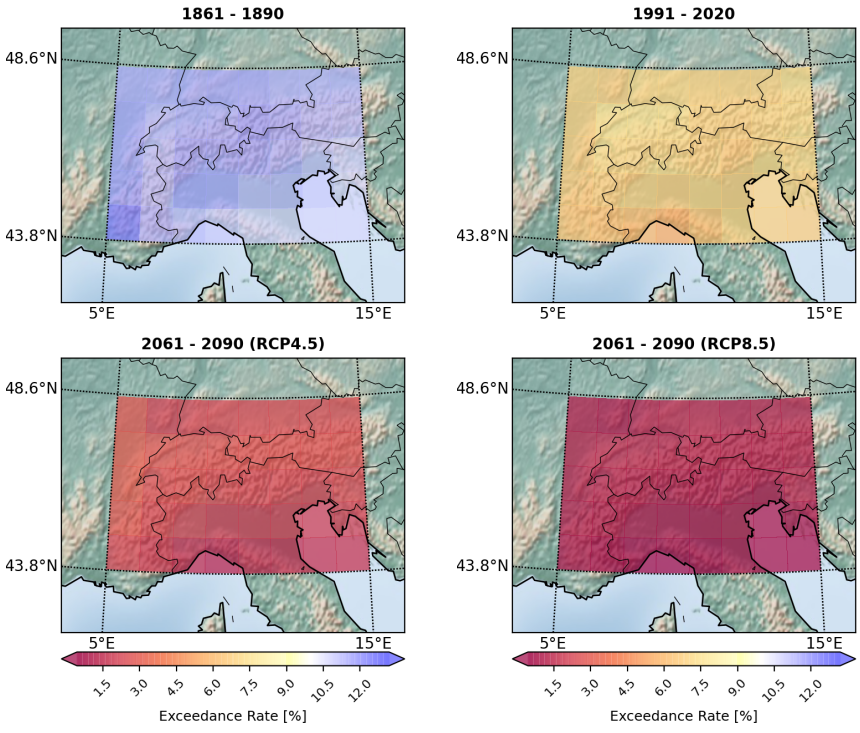

Figure 5.30: The multimodel median of changes in **Percentage of Days when Daily Maximum Temperature is lower than 10th Percentile** relative to the reference period for the Alpine region, temporally averaged over the three analyzed time periods.

5.2.12 *Percentage of Days when TN > 90^{th} Percentile*

The behavior of warm nights is shown in Figure 5.31. There is no observed significant changes in the historical simulation. However, from 1990*s* we start to see a strong increase in the percentage of warm nights compared to the 90_{th} percentile of TN of the reference period. In the year 2090 there is an exceedence rate of 38.4% for the RCP4.5 and 54.5% for the RCP8.5.

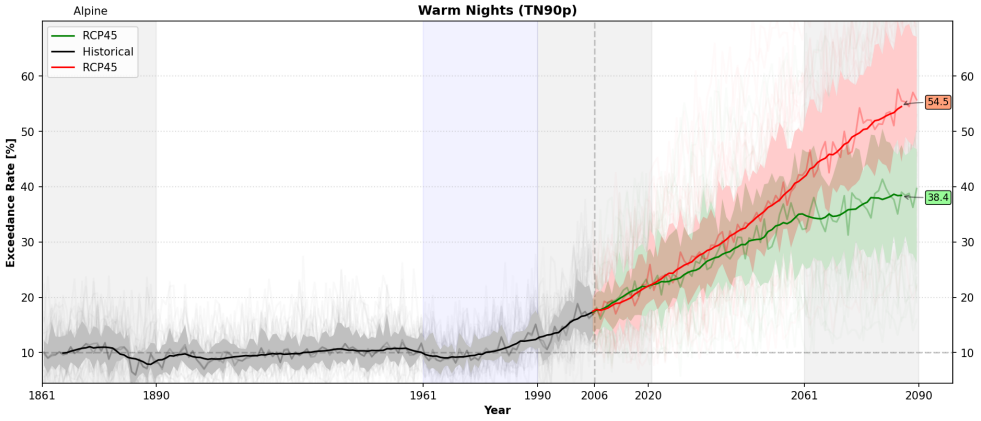

Figure 5.31: The multimodel median of changes in **Percentage of Days when Daily Minimum Temperature is greater than the 90^{th} Percentile** displayed as differences to the reference period, averaged over the Alpine region.

The spatial variability for Tn10p can be observed in the Figure 5.32. The highest increases in the exceedance rate of warm nights are projected to be in the southern part.

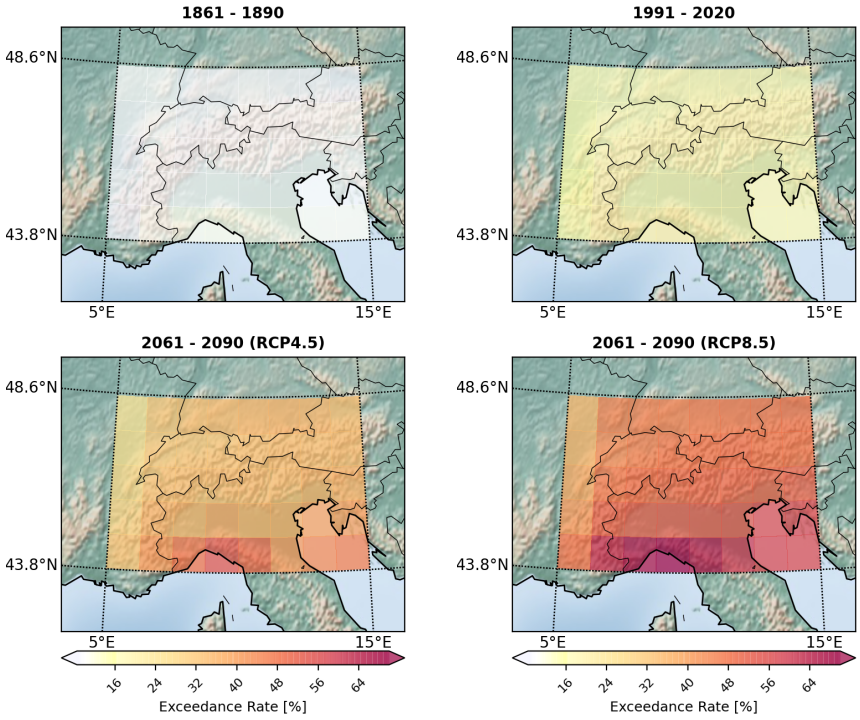

Figure 5.32: The multimodel median of changes in **Percentage of Days when Daily Minimum Temperature is greater than 90th Percentile** relative to the reference period for the Alpine region, temporally averaged over the three analyzed time periods.

5.2.13 *Percentage of Days when TX > 90th Percentile*

The warm days behavior is presented in Figure 5.33, as well as warm nights, there is no noticeable change in the historical simulation from 1861 to 1980. Then from the beginning of 1990 we see a steady increase in the values, mostly in RCP8.5 with a median exceedence rate of 56.3% and for the RCP4.5 an increase of 39% in comparison to the reference period.

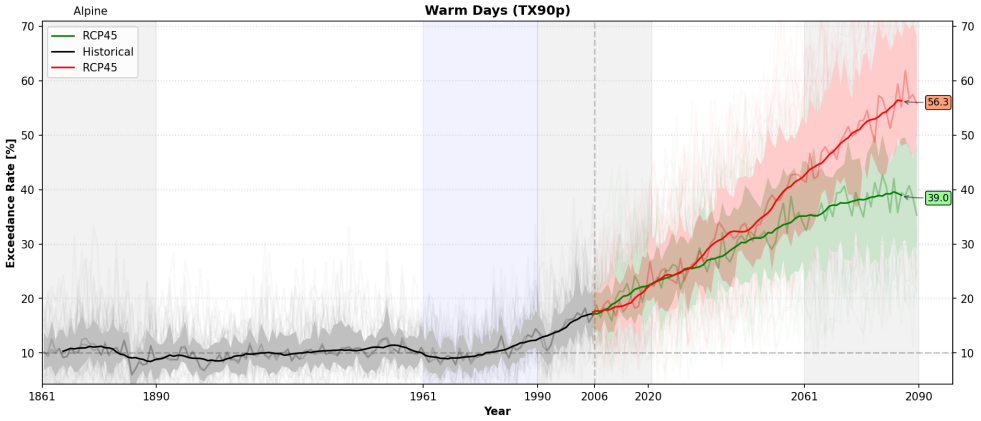

Figure 5.33: The multimodel median of changes in **Percentage of Days when Daily Maximum Temperature is greater than the 90th Percentile** displayed as differences to the reference period, averaged over the Alpine region.

From Figure 5.34 the highest increases in the exceedance rate of warm days is also projected to be in the southern part, and the lowest increases in the northwestern part.

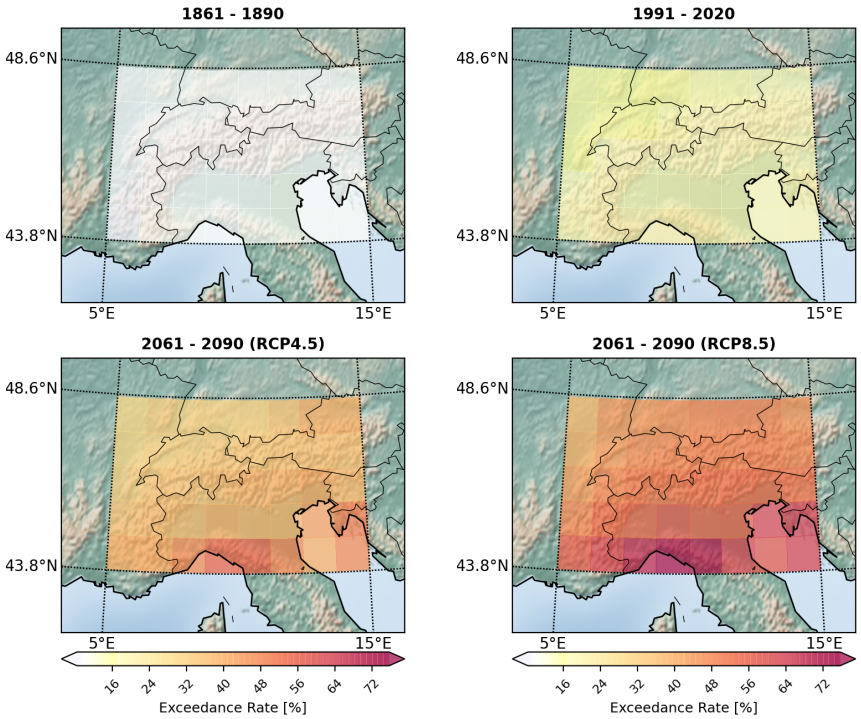

Figure 5.34: The multimodel median of changes in **Percentage of Days when Daily Maximum Temperature is greater than 90th Percentile** relative to the reference period for the Alpine region, temporally averaged over the three analyzed time periods.

5.2.14 *Warm Spell Duration Index*

Consistent with temperature changes warm spell duration (WSDI) is expected to increase in the two RCPs scenarios (Figure 5.35). WSDI increase under RCP8.5 scenario of 68.7 days, and under RCP4.5 with about 131.5 days by the year 2090 related to the reference period (6.1 days), these changes corresponds in a relative change of about 1100% and 200% respectively.

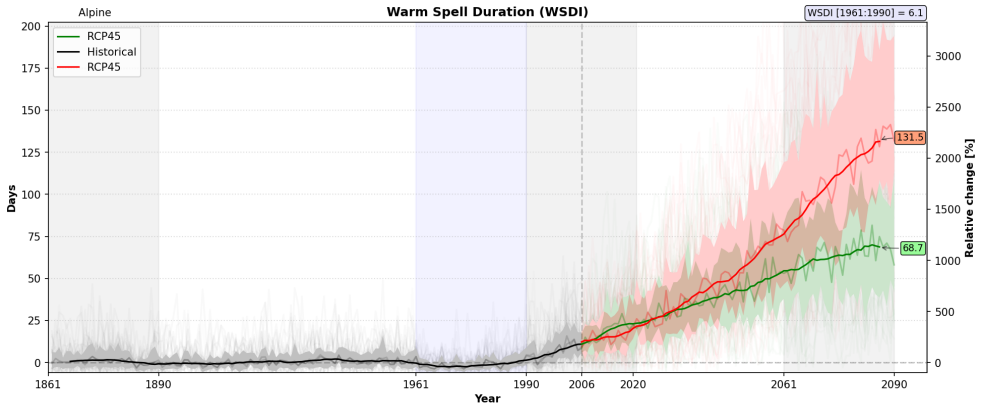

Figure 5.35: The multimodel median of changes in **Warm Spell Duration Index** displayed as differences to the reference period, averaged over the Alpine region.

Spatial variability of WSDI index is illustrated in Figure 5.36, as expected from the previous indices the biggest increase of warm periods is located in the southern part of the Alps.

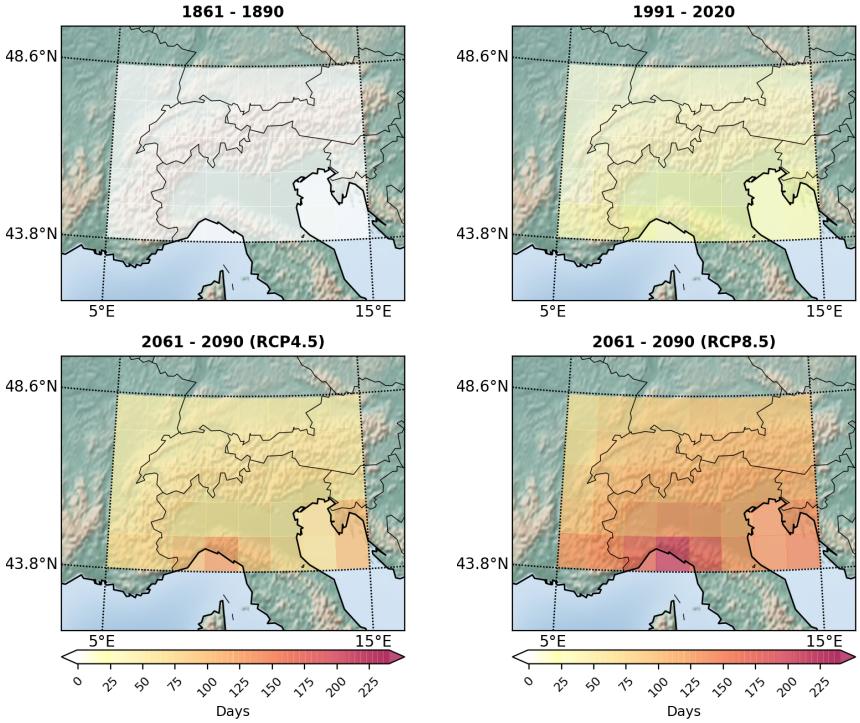

Figure 5.36: The multimodel median of changes in **Warm Spell Duration Index** relative to the reference period for the Alpine region, temporally averaged over the three analyzed time periods.

5.2.15 *Cold Spell Duration Index*

Consistent with the previous index, CSDI is projected to decrease in both future scenarios (Figure 5.37). This decreases start from the year 1960 and

cotinuous to decrease until arrive to -4.7 days and -5.4 days in RCP-4.7 and RCP8.5 respectively.

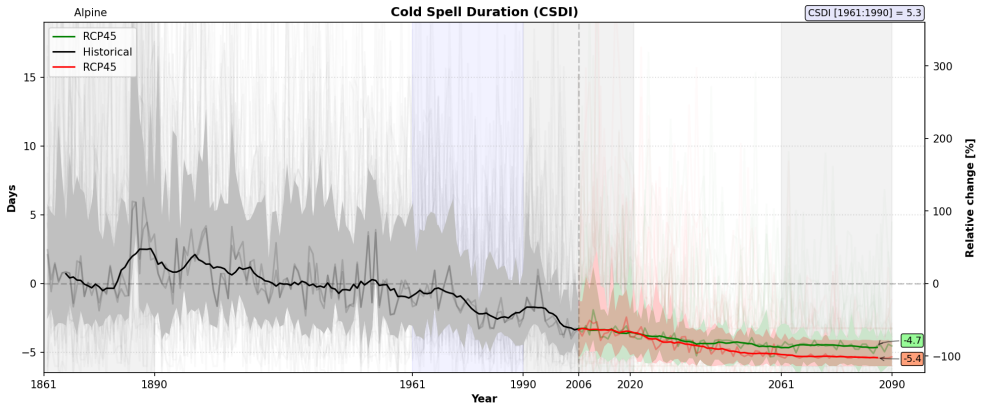

Figure 5.37: The multimodel median of changes in **Cold Spell Duration Index** displayed as differences to the reference period, averaged over the Alpine region.

From Figure 5.38 we see that the largest decrease of CSDI is by about 6 days in the southern region.

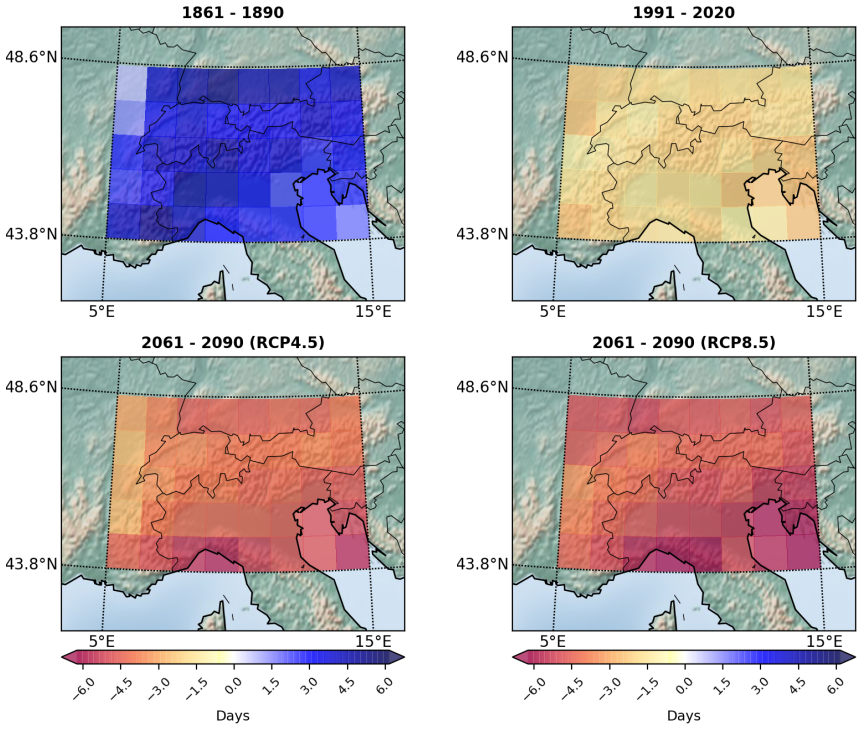

Figure 5.38: The multimodel median of changes in **Cold Spell Duration Index** relative to the reference period for the Alpine region, temporally averaged over the three analyzed time periods.

5.2.16 *Daily Temperature Range*

The Figure 5.39 show a slight increase in the yearly mean difference between TX and TN in the future projections. For both projections there is a very similar increase until the middle of the century. Then RCP8.5 increases faster, and by the end of 2090 both projections reach an increase of 0.3°C and 0.5°C compared to the DTR of the reference period (in mean 7.2°C). It is also observed that there is a great variability among the models, for historical simulation and future projections.

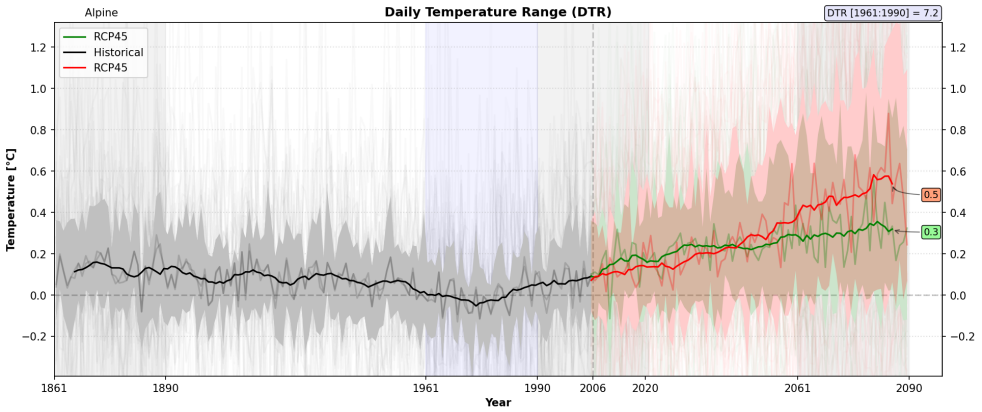

Figure 5.39: The multimodel median of changes in **Daily Temperature Range** displayed as differences to the reference period, averaged over the Alpine region.

As we can see in Figure 5.40 the temperature does not increase homogeneously in the whole region. For RCP8.5 In the southeast region the minimum temperature increases more than the maximum temperature. on the contrary, in the northwest and central region the maximum temperature increases more than the minimum.

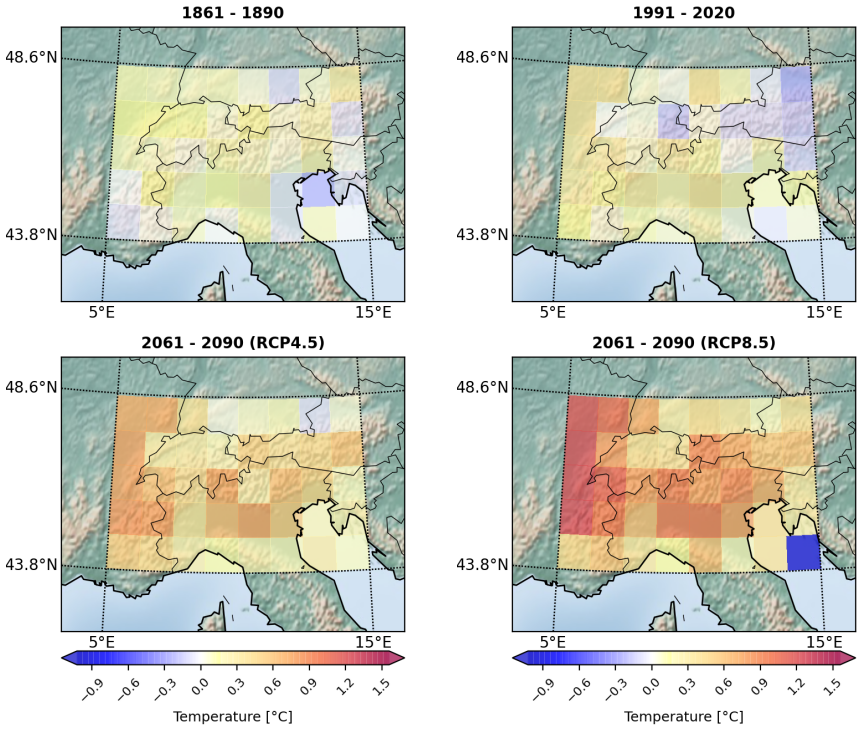

Figure 5.40: The multimodel median of changes in **Daily Temperature Range** relative to the reference period for the Alpine region, temporally averaged over the three analyzed time periods.

5.2.17 *Yearly Maximum* 1-*Day Precipitation*

The behavior of annual maximum of 1 day precipitation is presented in Figure 5.41. From the historical simulation there is no noticeable changes. However since 1990 we start to see constant increase in the values. For both RCPs scenarios there are similar increases, slightly higher in RCP8.5, reaching an increase of about 4.2 mm and 6.2 mm in RCP4.5 and RCP8.5 respectively, corresponding in a relative change of 12.6% and 18.6% relative to the reference period (in mean 33.3 mm).

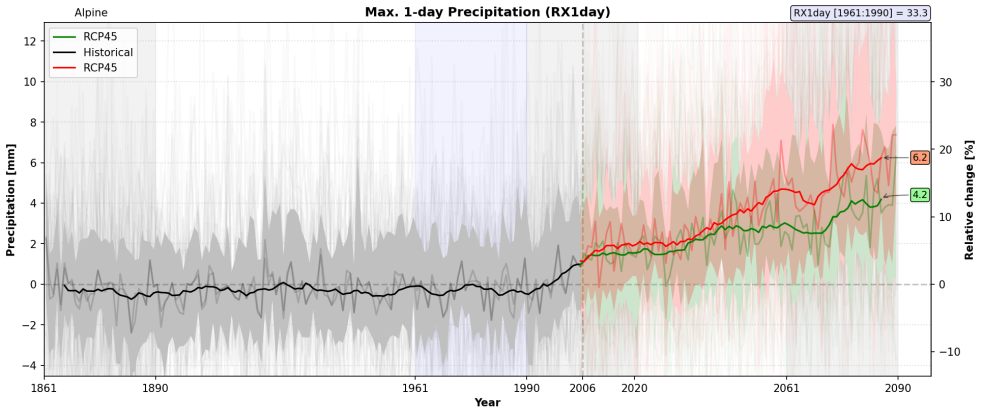

Figure 5.41: The multimodel median of changes in **Maximum 1-Day Precipitation** displayed as differences to the reference period, averaged over the Alpine region.

From Figure 5.42 the precipitation does not increase homogeneously in both scenarios. In RCP4.5 greatest temperature values are projected in the northeast region. Whereas in RCP8.5 almost the entire alpine region increases uniformly. The largest increases are expected For RCP8.5 In the southeast region the minimum temperature increases more than the maximum temperature. on the contrary, in the northwest and central region the maximum temperature increases more than the minimum.

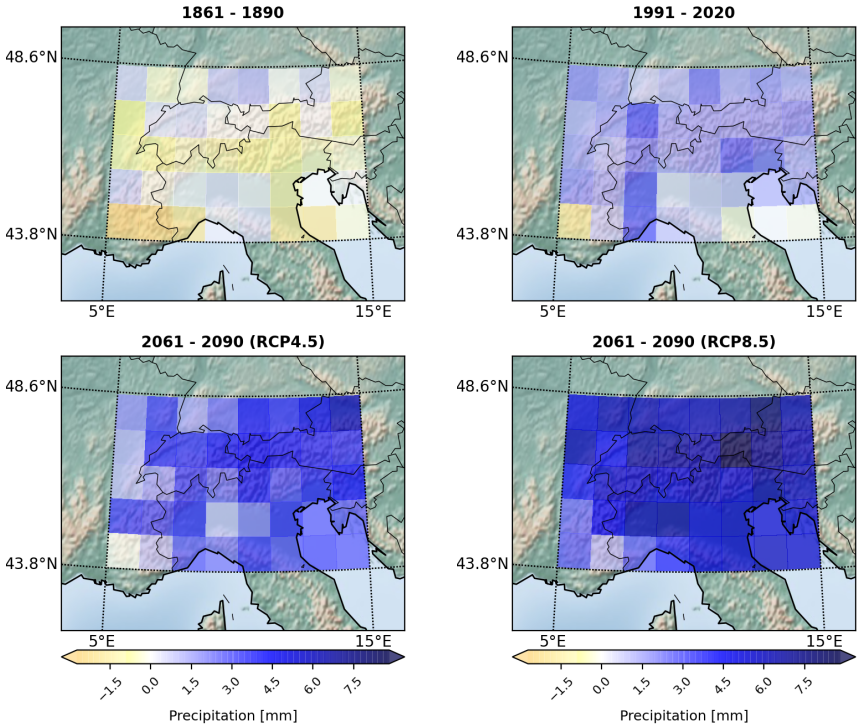

Figure 5.42: The multimodel median of changes in **Maximum 1-Day Precipitation** relative to the reference period for the Alpine region, temporally averaged over the three analyzed time periods.

5.2.18 *Yearly Maximum 5-Day Precipitation*

The annual maximum precipitation of 5 days behavior (**??** tend to increase in the 21st century. RX5day represents a more extreme condition. In the historical experiments there are not changes in precipitation. But in the future projections there are significant increases in the values of rainfall, the RCP4.5 reaches an increase of 6.3 mm which corresponds in a relative change of 8.7%, while RCP8.5 reaches a value of 6.3 mm, wich corresponds 10.4% in a relative changes as differences from the reference period of 72.2 mm in mean.

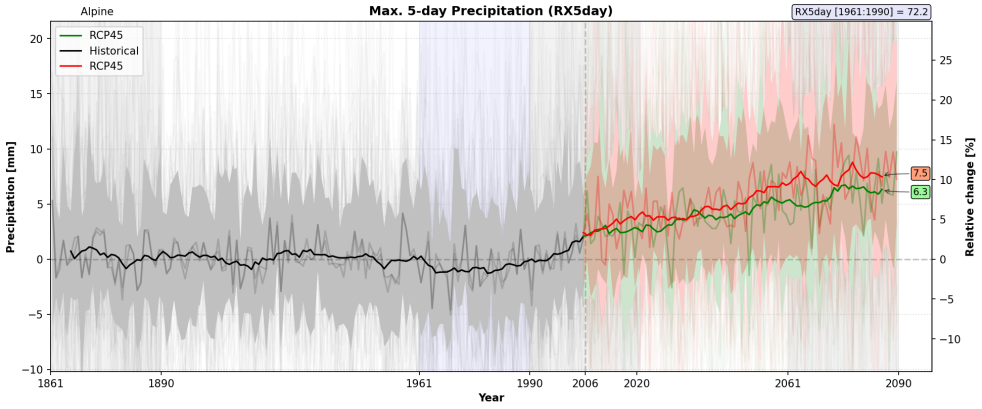

Figure 5.43: The multimodel median of changes in **Maximum** 5**-Day Precipitation** displayed as differences to the reference period, averaged over the Alpine region.

As we can see in Figure 5.44 precipitation increases in most of the region, except in the southwest, where there is a small decrease.

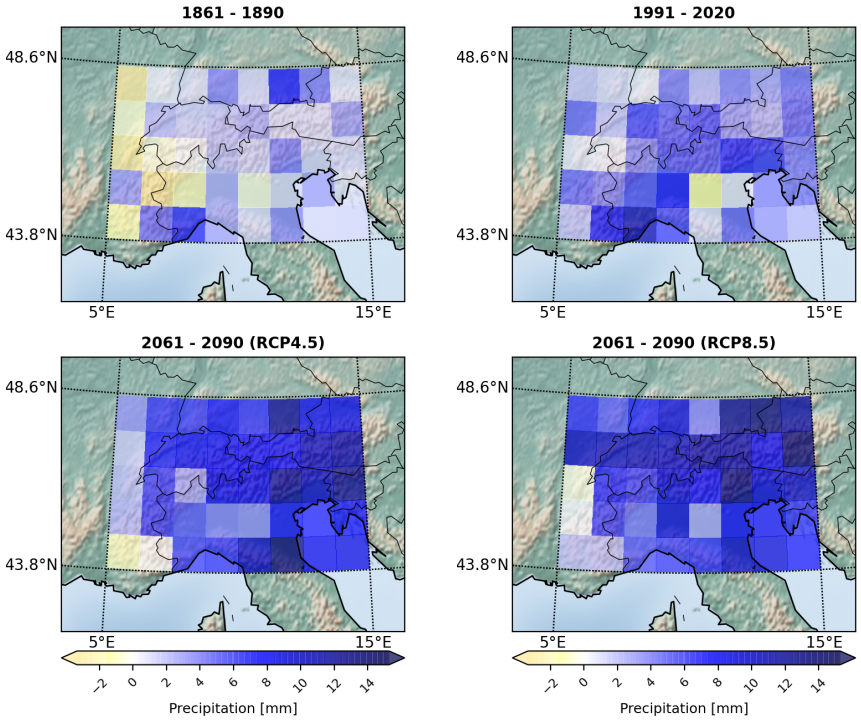

Figure 5.44: The multimodel median of changes in **Maximum 5-Day Precipitation** relative to the reference period for the Alpine region, temporally averaged over the three analyzed time periods.

5.2.19 *Simple Precipitation Intensity Index*

Simple daily precipitation is projected to increase (Figure 5.45), we start to see a slight steady increase from 1990, in the future projections median increase is to 0.4 mm/day in the RCP4.5 scenario and 0.6 mm in RCP8.5, which represent a relative change of 6.8% and 10.2% respectively if compared to the reference period.

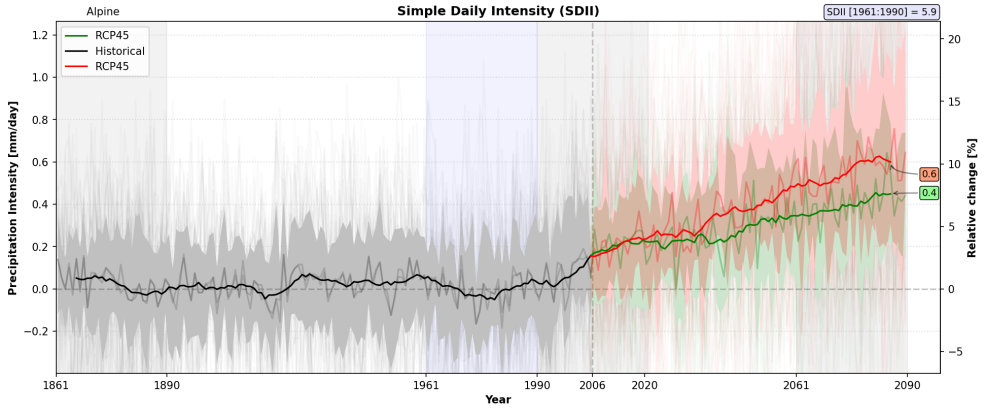

Figure 5.45: The multimodel median of changes in **Simple Daily Intensity** displayed as differences to the reference period, averaged over the Alpine region.

Spatial variability of SDII is illustrated in Figure 5.46 very heavy precipitation is expected in the whole Alps in RCP8.5 scenario, mostly in the northern part.

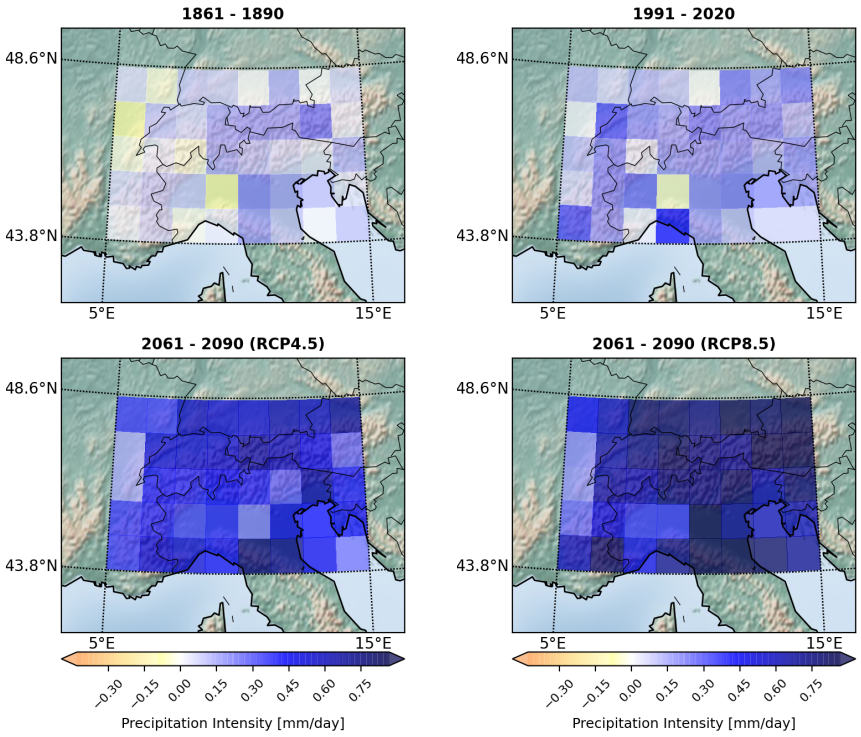

Figure 5.46: The multimodel median of changes in **Simple Daily Intensity** relative to the reference period for the Alpine region, temporally averaged over the three analyzed time periods.

5.2.20 *Annual Count Of Days When PRCP* $\geqslant$ 10 *mm*

The trend of heavy precipitation with more than 10 mm in a day seems to be slightly above average in the historical simulation compared to the reference period. For future projections the increase in heavy rainfall is slightly greater than in the past climate. In addition, in RCP8, 5 the tendency is to increase, until the year 2060, then start to decrease until arrive in 2090 to 1.1 days, which corresponds to a relative change of 4.3%. Instead, in RCP4.5 there is a steady increase reaching an increase of 2.7 days, which corresponds to a relative change of 10.5% relative to the reference period of average of 25.6 days of rainfall intensity annually.

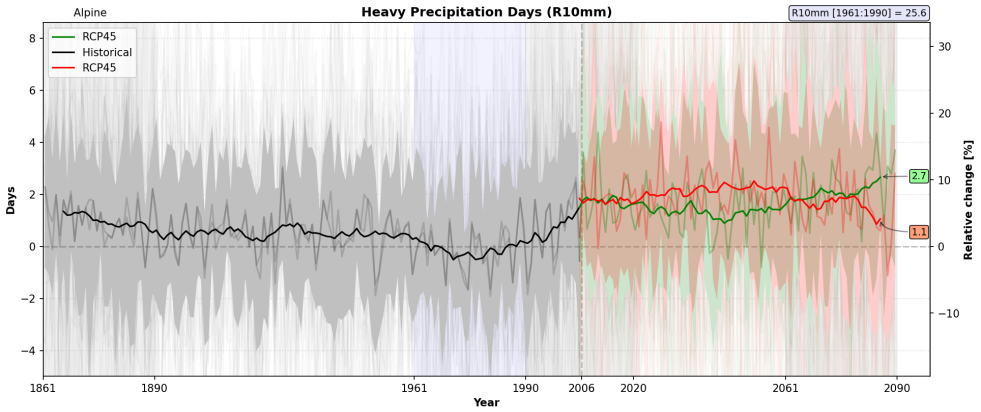

Figure 5.47: The multimodel median of changes in **Heavy Precipitation Days** displayed as differences to the reference period, averaged over the Alpine region.

Spatial variability of R10 mm is displayed in Figure 5.48, precipitation does not increase homogeneously all over the region. In both RCPs scenarios, the greatest increases in precipitation are projected to be in the northern part of the Alps, and in the southwestern part the opposite occurs, there is a decrease of days with heavy precipitation.

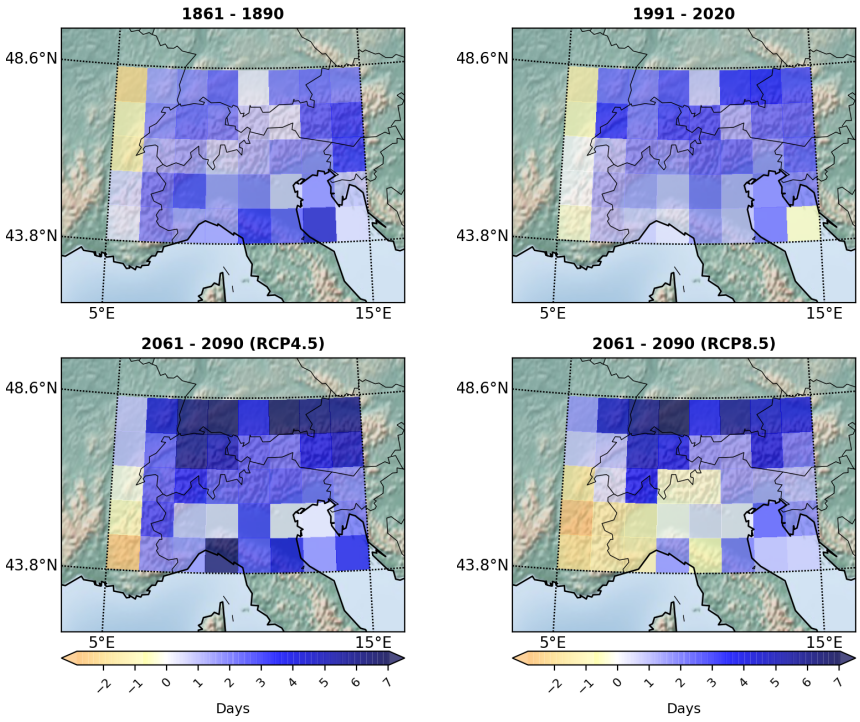

Figure 5.48: The multimodel median of changes in **Heavy Precipitation Days** relative to the reference period for the Alpine region, temporally averaged over the three analyzed time periods.

5.2.21 *Annual Count Of Days When PRCP ⩾ 20 mm*

The behavior of very heavy precipitation index 5.49 has significant increases in comparison to the reference period, since the year 2000, precipitation values have been steadily increasing, and it is expected to continue in future projections. In RCP4.5 is expected to increase 1.2 days (approximately 10.5%) and 1.4 days (approximately 27.5%) in both RCPs scenarios, compared to the reference period with an average of 5.1 days.

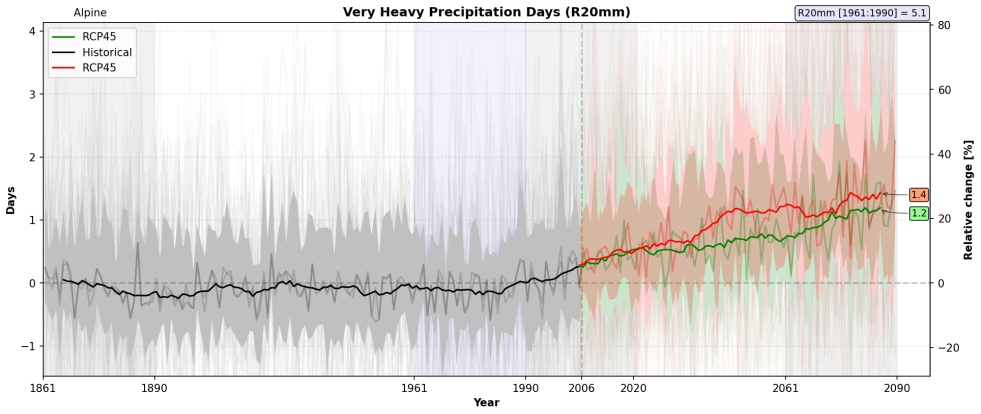

Figure 5.49: The multimodel median of changes in **Very Heavy Precipitation Days** displayed as differences to the reference period, averaged over the Alpine region.

Spatial variability of R20 mm is displayed in Figure 5.50, consistently with r10mm, the greatest increases in precipitation are projected to be in the northern part of the Alps, and in the southwestern part the increase is much lower.

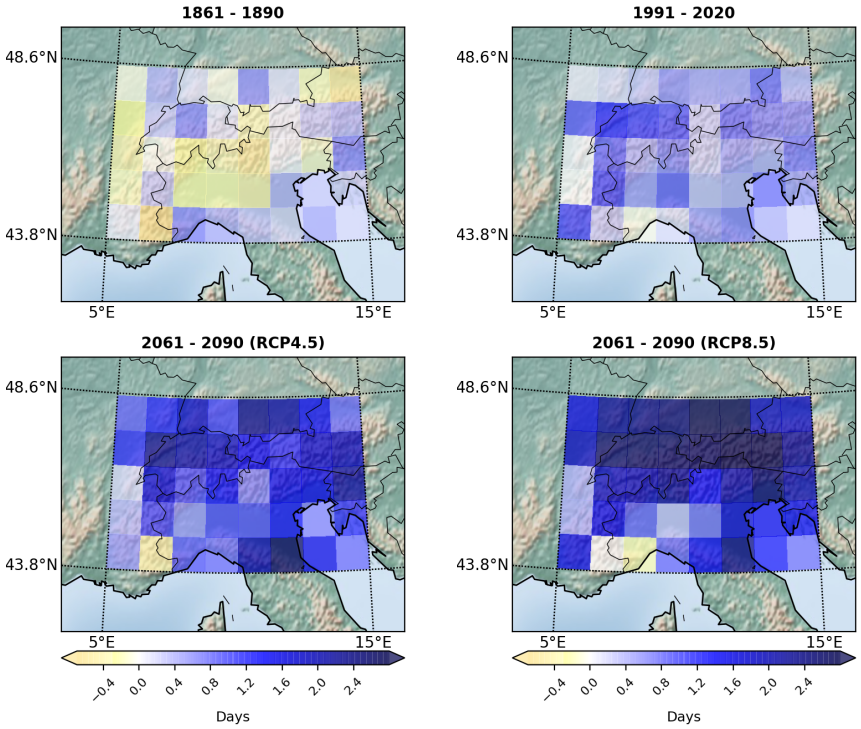

Figure 5.50: The multimodel median of changes in **Very Heavy Precipitation Days** relative to the reference period for the Alpine region, temporally averaged over the three analyzed time periods.

5.2.22 *Annual Count Of Days When PRCP ⩾ nnmm*

In this case we calculate R1mm, to evaluate changes in wet days. From Figure 5.51 we can see a steady decrease in wet days from 2006. In RCP4.5 a decrease of 4.4 days is expected, and in RCP8.5 a decrease of 16.6 days.

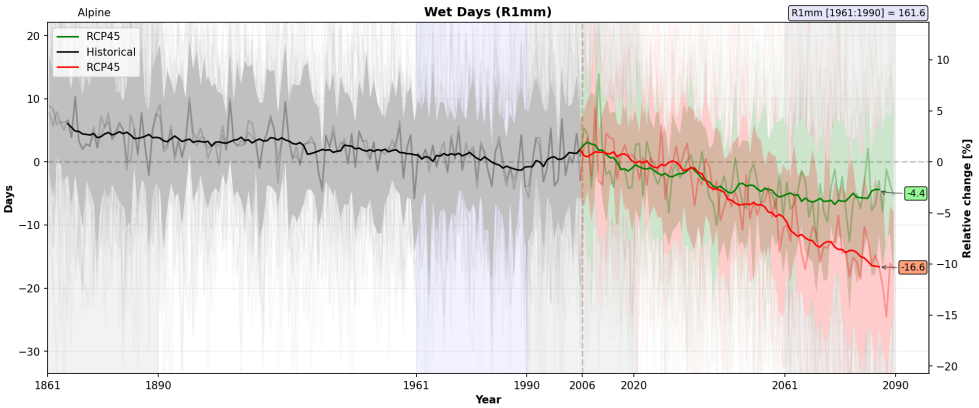

Figure 5.51: The multimodel median of changes in **Wet Days** displayed as differences to the reference period, averaged over the Alpine region.

In Figure 5.52, Spatial variability of R20 mm is presented. The biggest decrease is projected in the center and southern part of the Alps, this is consistent with r10mm.

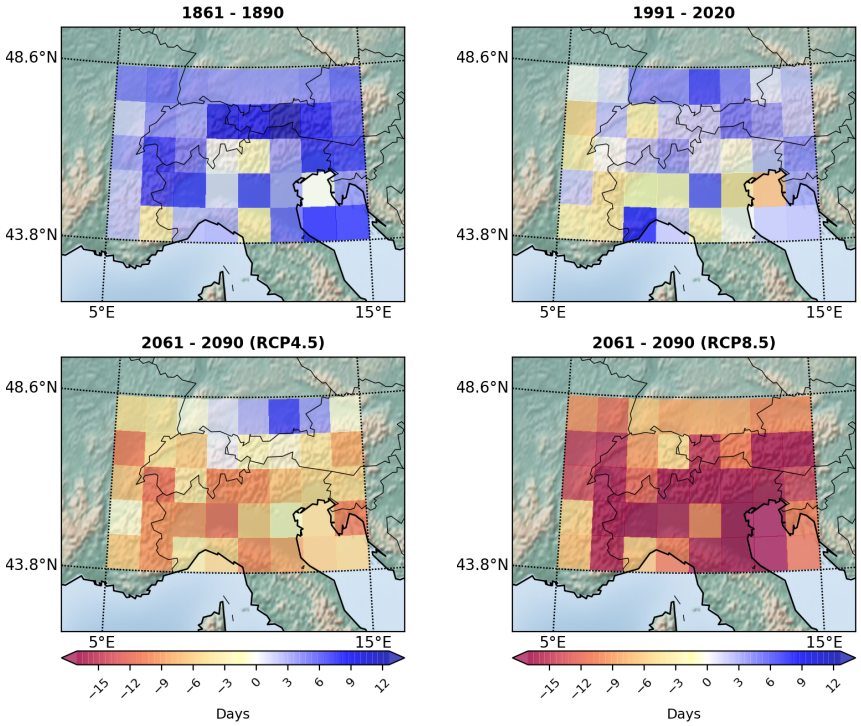

Figure 5.52: The multimodel median of changes in **Wet Days** relative to the reference period for the Alpine region, temporally averaged over the three analyzed time periods.

5.2.23 *Maximum Length Of Dry Spell*

The behavior of maximum lenth dry spell 5.53 has significant increases in comparison to the reference period (21.3 days). In RCP4.5 there is an increase of 0.9 days and in RCP8.5 an increase of 4.1 days by the year 2090.

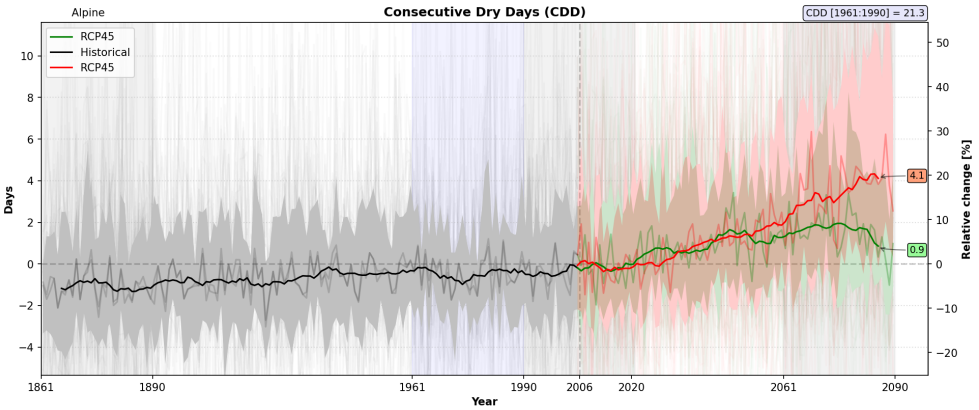

Figure 5.53: The multimodel median of changes in **Wet Days** displayed as differences to the reference period, averaged over the Alpine region.

In Figure 5.54, Spatial variability of CDD is presented. The biggest decrease is projected in the center and northern part of the Alps for both RCPs scenarios.

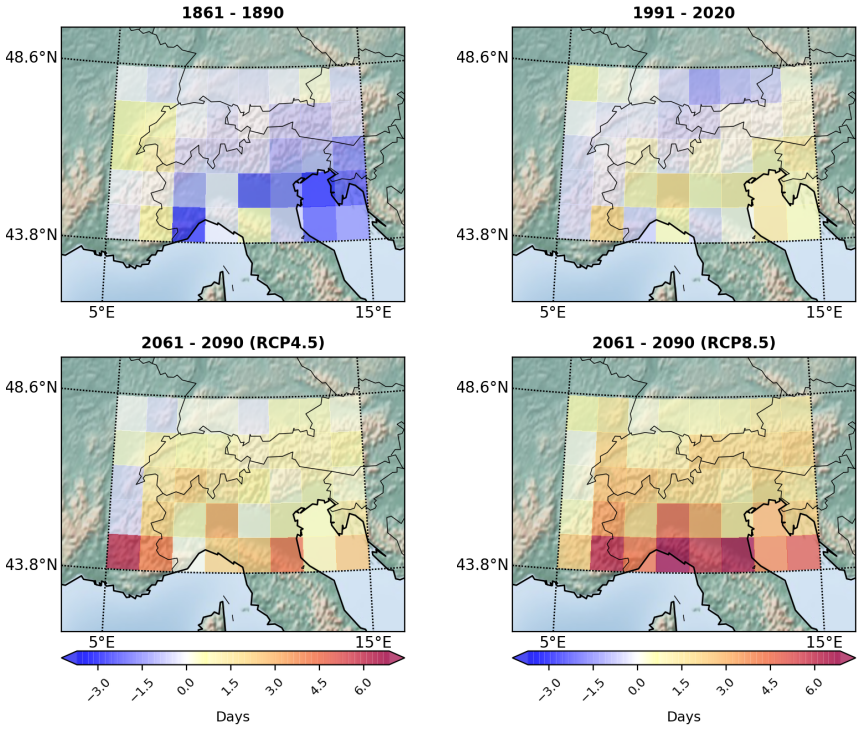

Figure 5.54: The multimodel median of changes in **Wet Days** relative to the reference period for the Alpine region, temporally averaged over the three analyzed time periods.

5.2.24 *Maximum Length Of Wet Spell*

Maximum length is projected to decrease (Figure 5.55, this is consistent with the previous index. In RCP4.5 there is a decrease of 0.3 days and in RCP8.5 a decrease of 1.0 days by the year 2090.

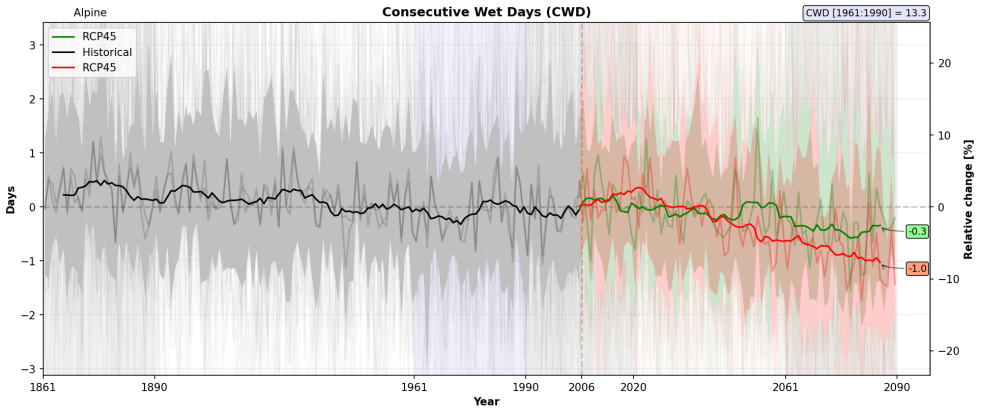

Figure 5.55: The multimodel median of changes in **Maximum Length Of Wet Spell** displayed as differences to the reference period, averaged over the Alpine region.

In Figure 5.56, Spatial variability of CWD is showed. The biggest decrease is projected in the center and southern part of the Alps.

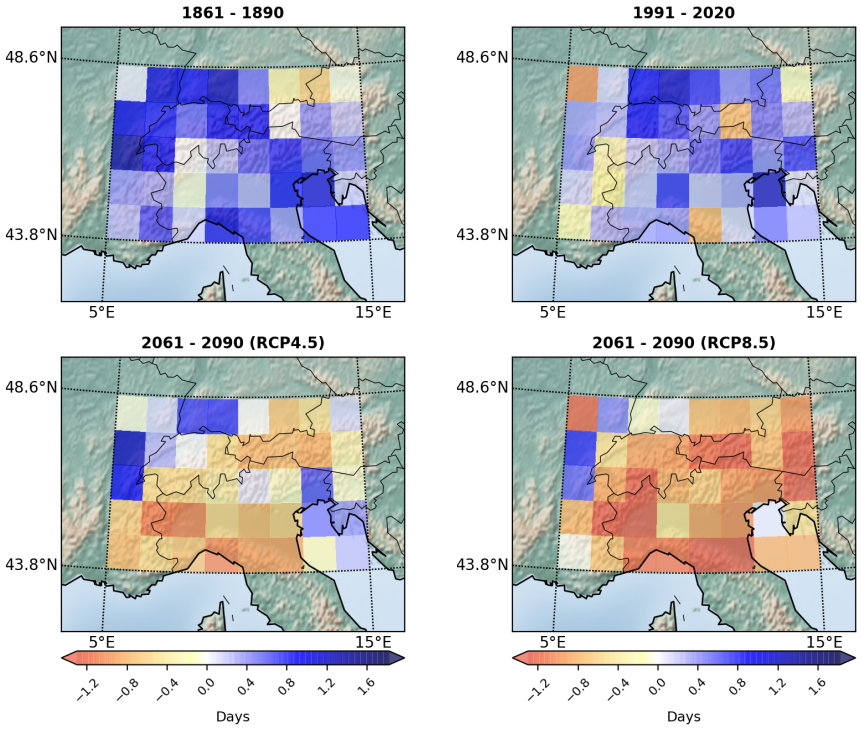

Figure 5.56: The multimodel median of changes in **Maximum Length Of Wet Spell** relative to the reference period for the Alpine region, temporally averaged over the three analyzed time periods.

5.2.25 *Annual Total PRCP When RR > 95p*

Precipitation of very wet days 5.57 is projected to increase in RCP4.5 an increase is projected of 59.9 mm and in RCP8.5 an increase of 69.1 mm by the year 2090.

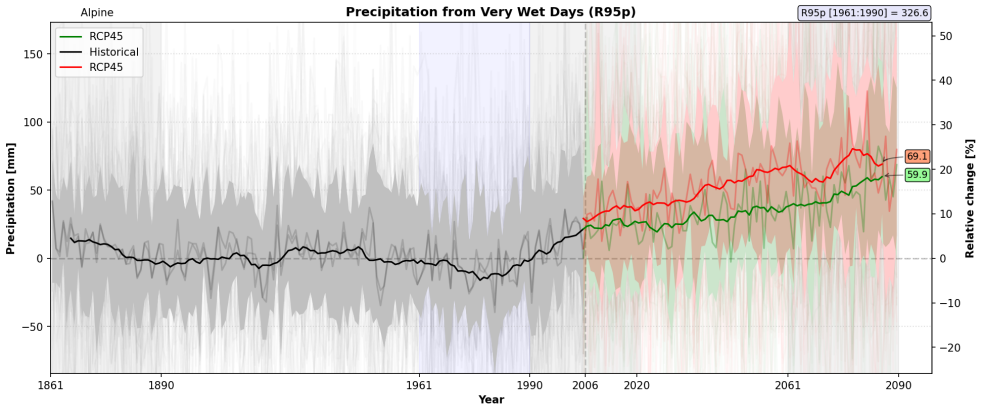

Figure 5.57: The multimodel median of changes in **Precipitation from wet days** displayed as differences to the reference period, averaged over the Alpine region.

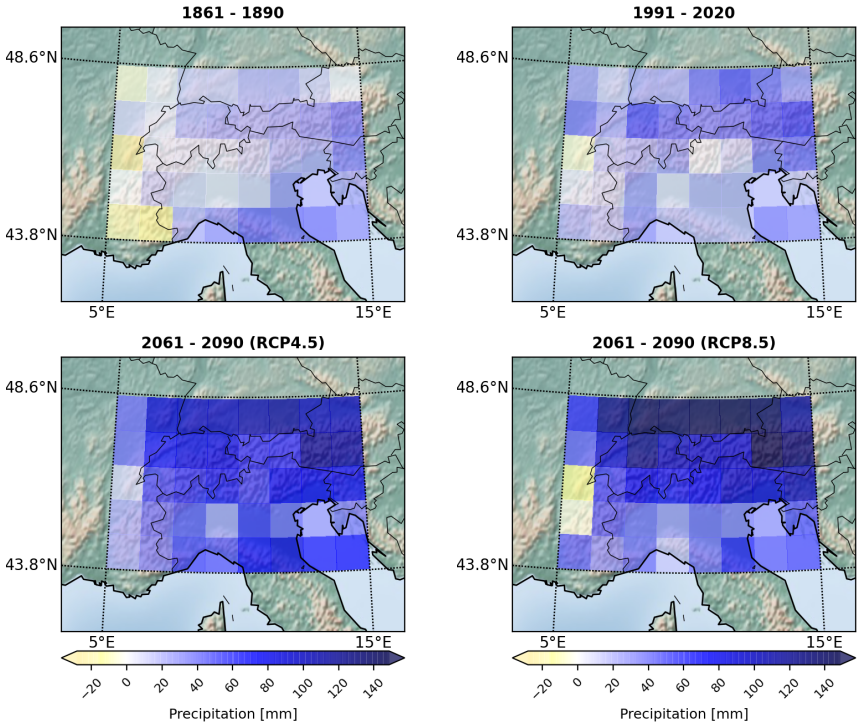

Figure 5.58: The multimodel median of changes in **Maximum Length Of Wet Spell** relative to the reference period for the Alpine region, temporally averaged over the three analyzed time periods.

5.2.26 *Annual Total PRCP When RR > 99p*

Figure 5.59 is showed the precipitation from extremely wet days. Is projected to increase dramatically. In RCP4.5 is expected an increase of 43.1 mm and in RCP8.5 an increase of 53.5 mm by the year 2090.

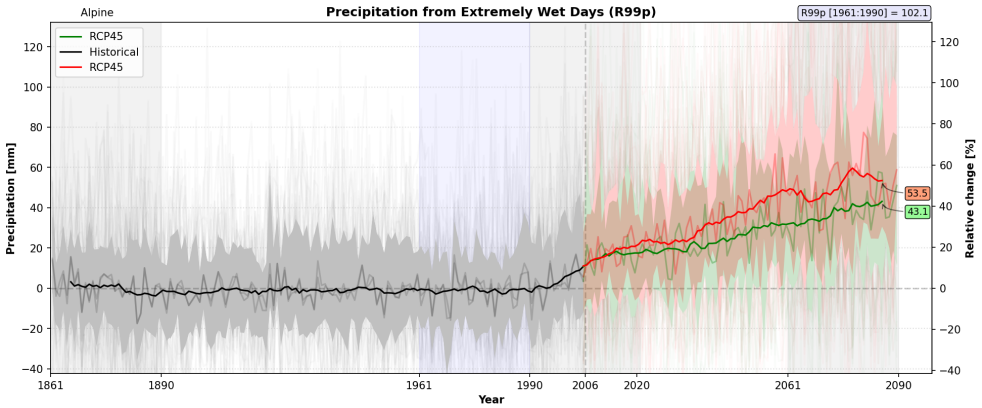

Figure 5.59: The multimodel median of changes in **Precipitation from extremely wet days** displayed as differences to the reference period, averaged over the Alpine region.

As expected from other indices, extremely precipitation is projected to increase in both RCPs scenarios.

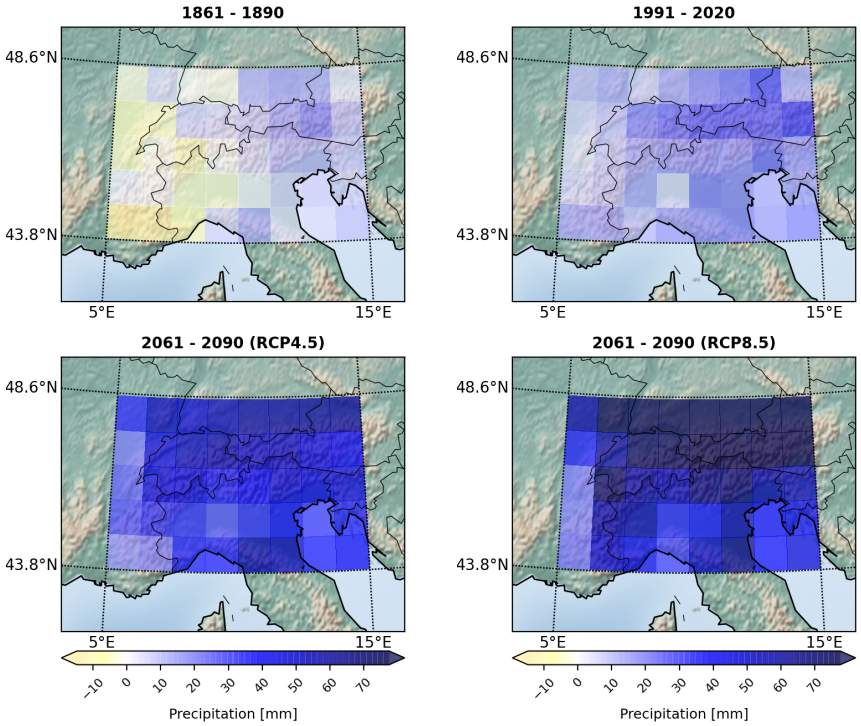

Figure 5.60: The multimodel median of changes in **Maximum Length Of Wet Spell** relative to the reference period for the Alpine region, temporally averaged over the three analyzed time periods.

5.2.27 *Annual Total Precipitation in Wet Days*

Figure 5.61 there are no significant changes in annual total precipitation. In RCP4.5 is expected an increase of 41.3 mm/year and in RCP8.5 a decrease of 9.7 mm/year in 2090.

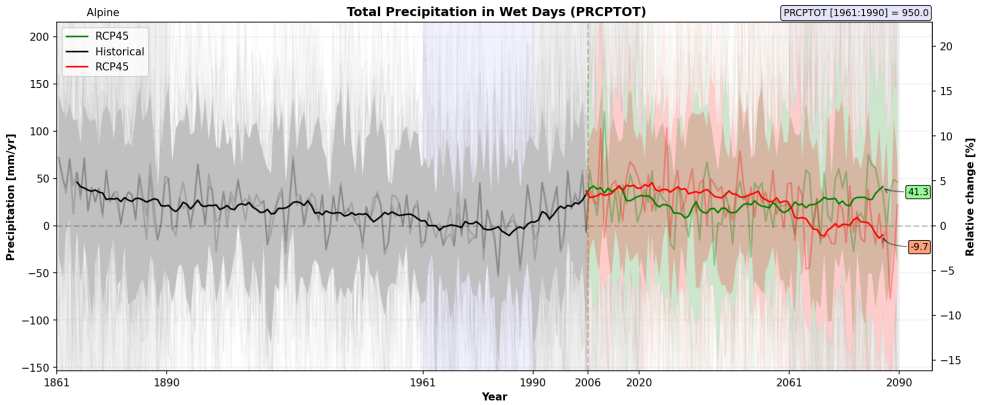

Figure 5.61: The multimodel median of changes in **Total Precipitation in Wet Days** displayed as differences to the reference period, averaged over the Alpine region.

From Figure 5.62 the largest decrease of precipitation is projected in the center and southern part of the Alps for both scenarios.

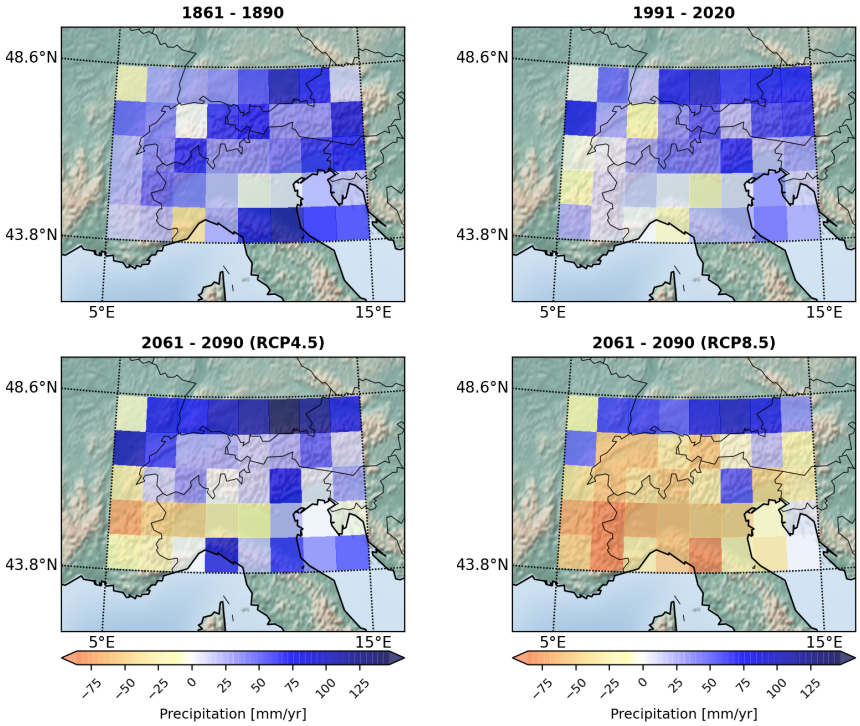

Figure 5.62: The multimodel median of changes in **Total Precipitation in Wet Days** relative to the reference period for the Alpine region, temporally averaged over the three analyzed time periods.

5.3 ETCCDI INDICES IN THE ANDES

5.3.1 *Number of Summer Days*

Figure 5.64 displays the evolution in number of Summer Days. Both scenarios show a clear increasing tendency starting at the beginning of the reference period. By the end of the 21*st* century, the increase corresponds to 84 days (33%) and 61 days (24%) for RCP8.5 and RCP4.5 respectively.
The spatial behaviour is shown in Figure 5.63. The increase is larger in the central region, following the mountains range, where it reaches the maximum values in both RCPs.

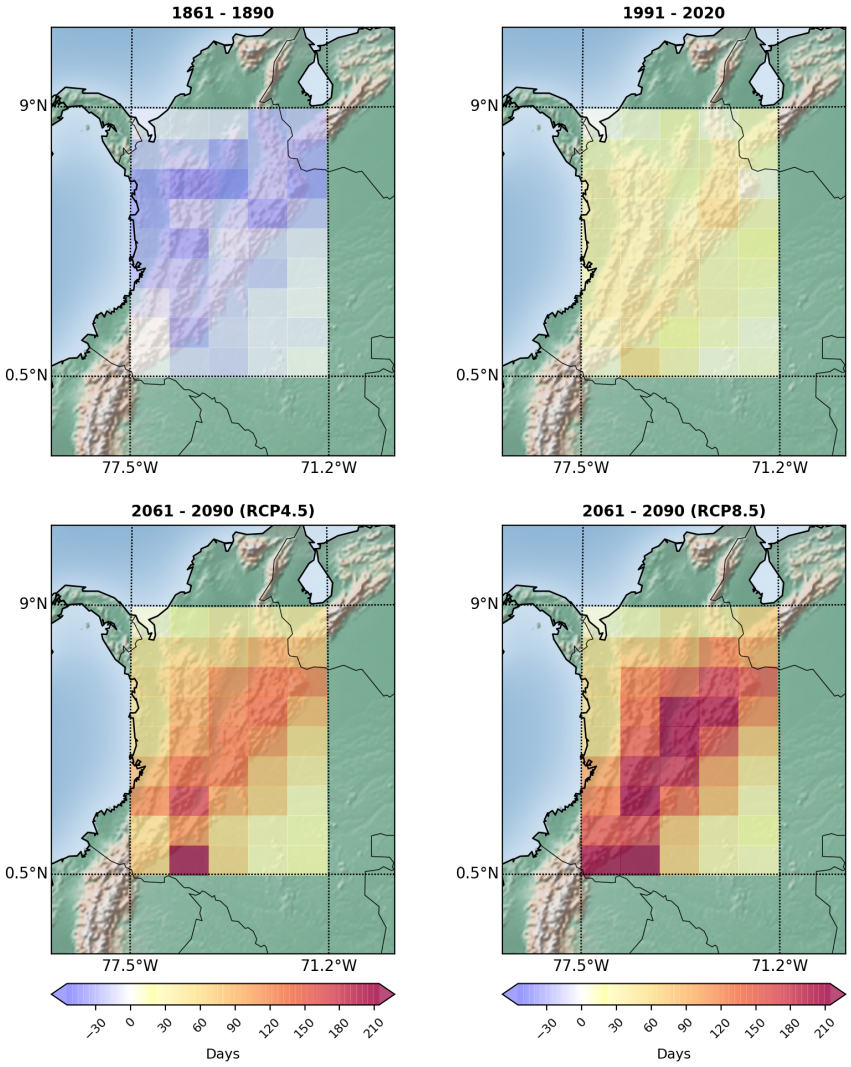

Figure 5.63: The multimodel median of changes in **Summer Days** relative to the reference period for the Andes region, temporally averaged over the three analyzed time periods.

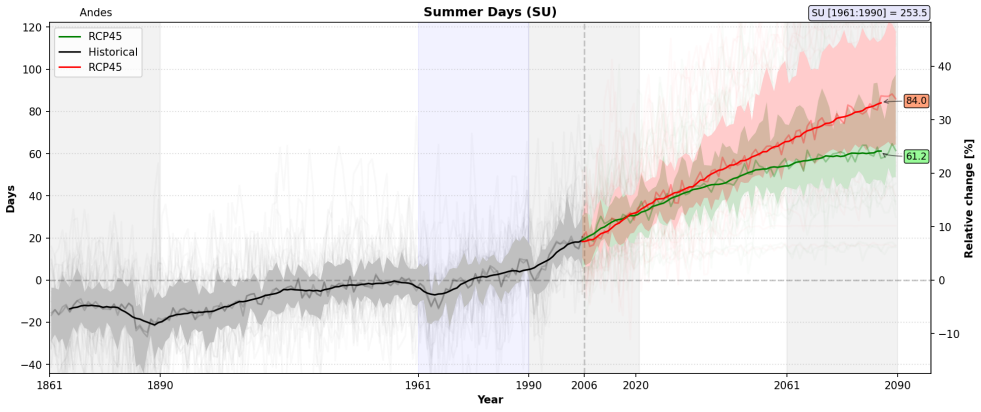

Figure 5.64: The multimodel median of changes in **Summer Days** displayed as differences to the reference period, averaged over the Andes region.

5.3.2 *Number of Tropical Nights*

Similarly to Summer Days, the number of Tropical Nights also increases during the whole 21*st* century, and shows a spatial behaviour governed by higher values in the mountains range. The maximum values are larger than for SD in both days and percentage as it reaches 150 days (85%) and 96 days (54%) for RCP8.5 and RCP4.5 respectively. The time series is shown in Figure 5.65 and the map in Figure 5.66.

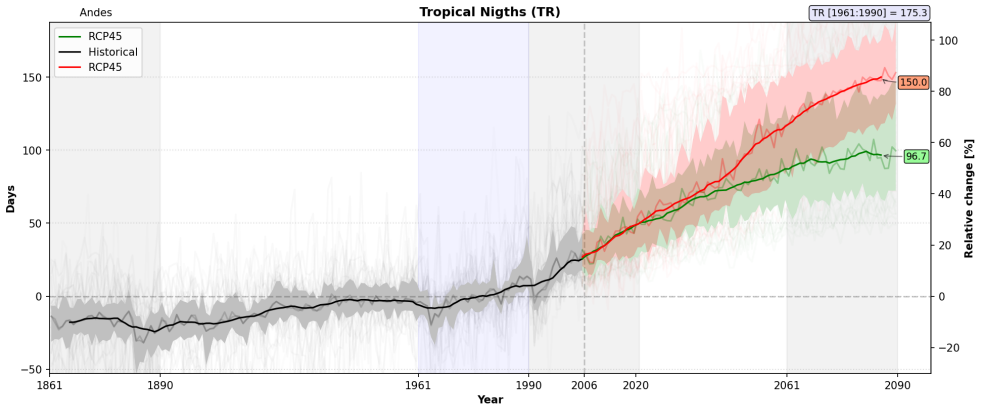

Figure 5.65: The multimodel median of changes in **Tropical Nights** displayed as differences to the reference period, averaged over the Andes region.

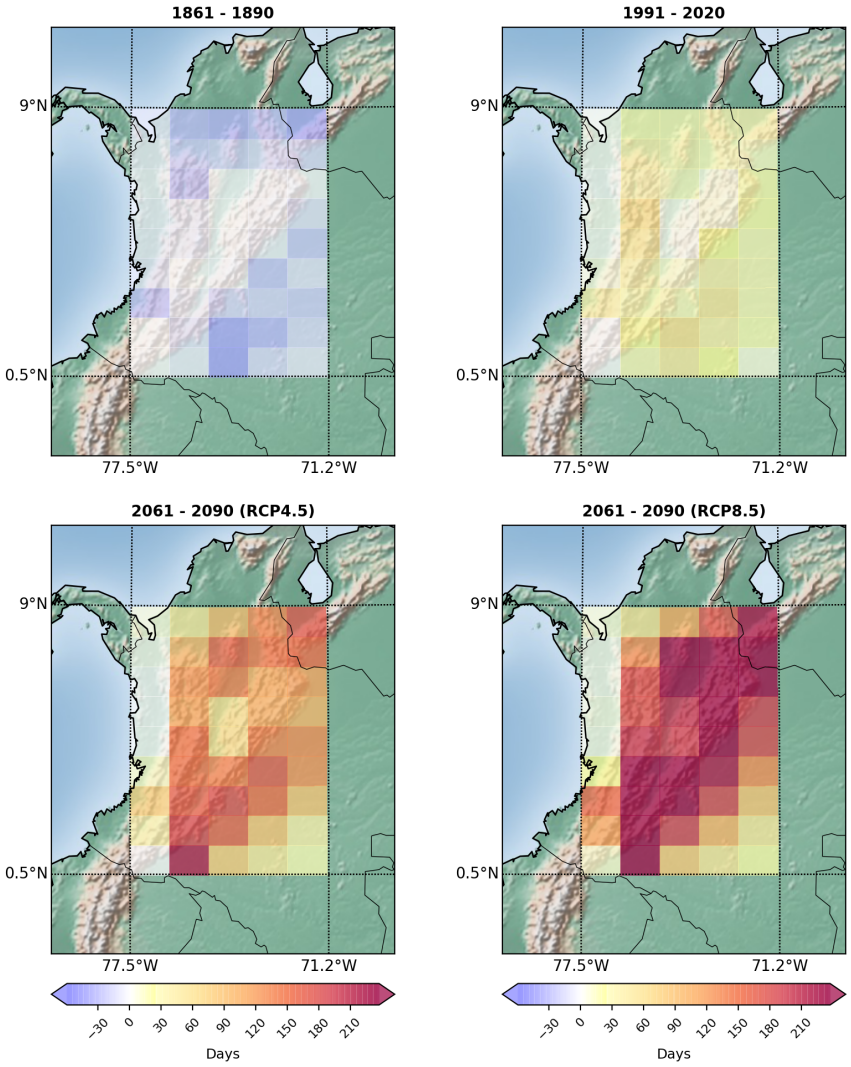

Figure 5.66: The multimodel median of changes in **Tropical Nights** relative to the reference period for the Andes region, temporally averaged over the three analyzed time periods.

5.3.3 *Yearly Maximum Value of Daily Maximum Temperature*

Figure 5.67 shows a continuous increase in TXx, which corresponds to the temperature in the warmest day in the year. The maximum value, by the year 2090 is 5 °C for RCP8.5 and 2.7 °C for RCP4.5.

Figure 5.68 shows the spatial distribution of the changes, with higher values in the north east side of the region, and in the maximum located in the south east.

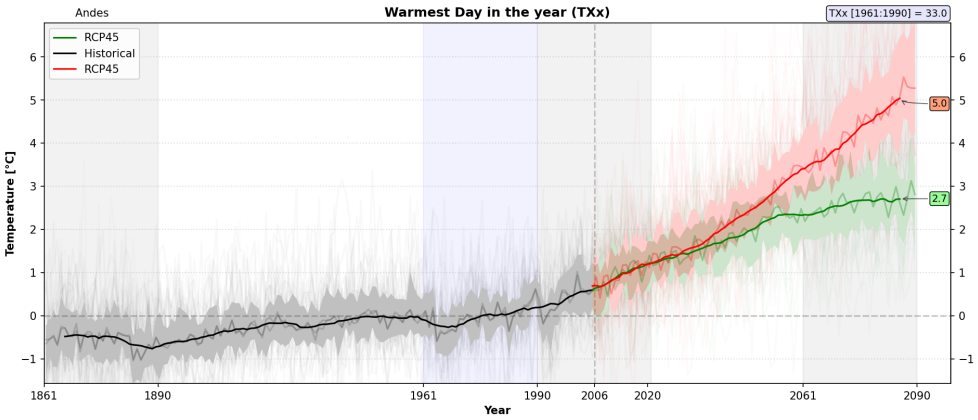

Figure 5.67: The multimodel median of changes in **Yearly Maximum Value of Daily Maximum Temperature** displayed as differences to the reference period, averaged over the Andes region.

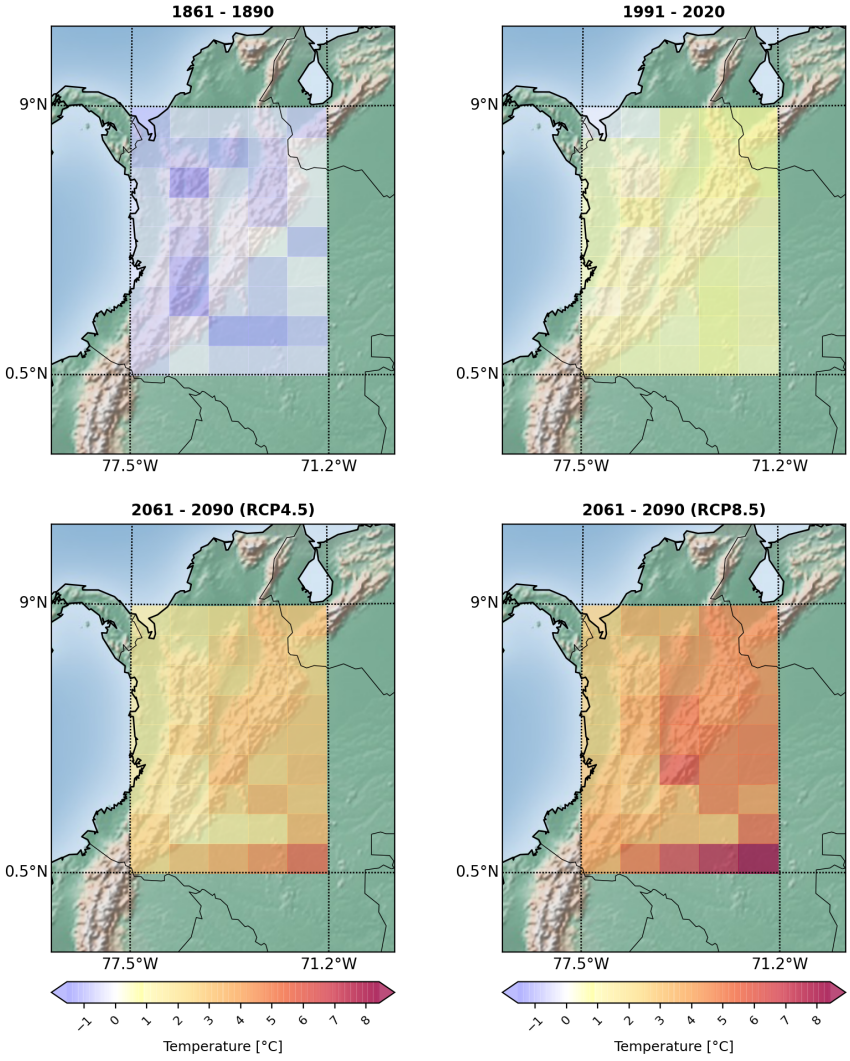

Figure 5.68: The multimodel median of changes in **Yearly Maximum Value of Daily Maximum Temperature** relative to the reference period for the Andes region, temporally averaged over the three analyzed time periods.

5.3.4 *Yearly Maximum Value of Daily Minimum Temperature*

There are very similar changes in TNx, which corresponds to the warmest night in the year. The maximum value, by the year 2090 is 4.7 °C for RCP8.5 and 2.6 °C for RCP4.5 as shown in Figure 5.70

The spatial distribution also shows higher increase in the east side of the region, with maximum values in the north east (Figure 5.69).

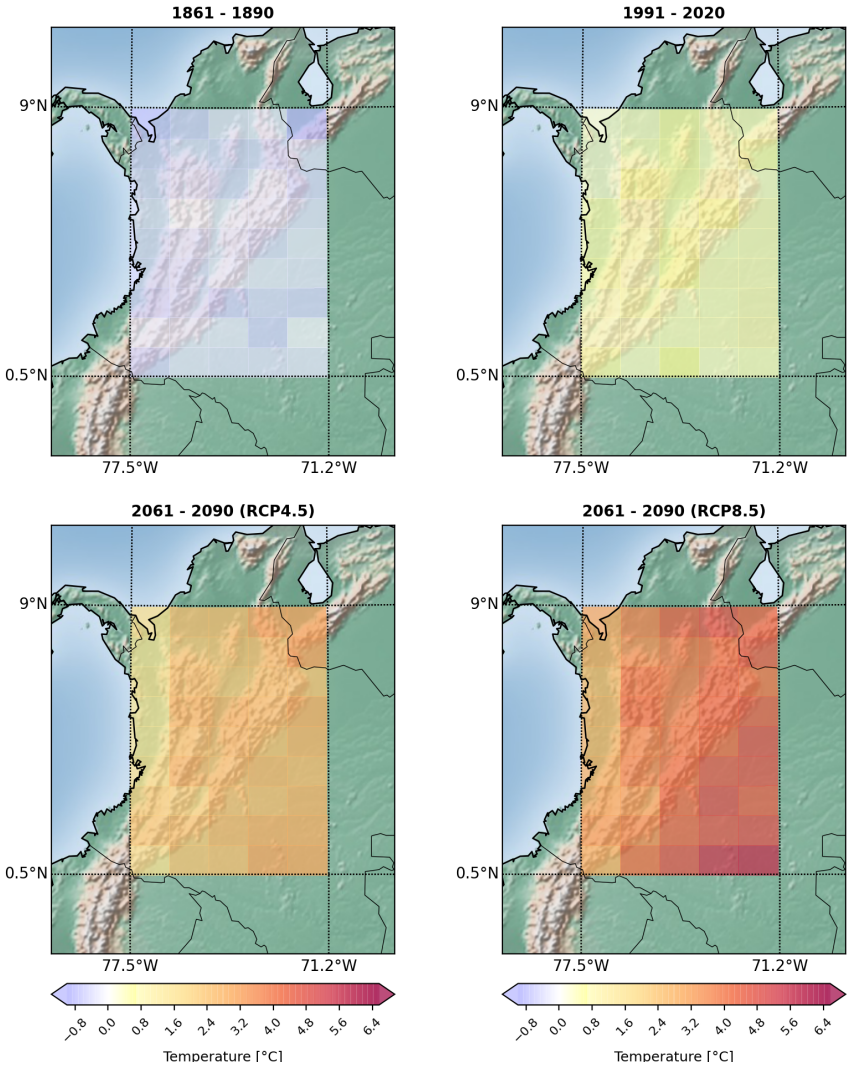

Figure 5.69: The multimodel median of changes in **Yearly Maximum Value of Daily Minimum Temperature** relative to the reference period for the Andes region, temporally averaged over the three analyzed time periods.

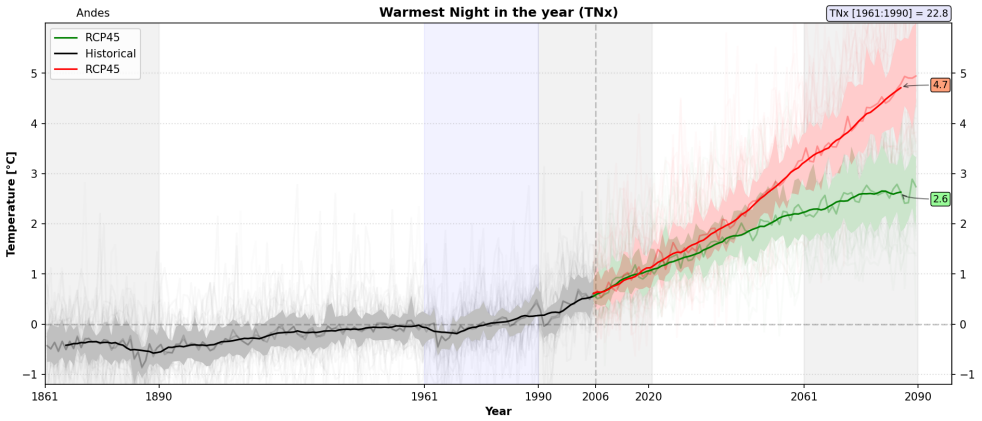

Figure 5.70: The multimodel median of changes in **Yearly Maximum Value of Daily Minimum Temperature** displayed as differences to the reference period, averaged over the Andes region.

5.3.5 *Yearly Minimum Value of Daily Maximum Temperature*

TXn, which corresponds to the coldest day in the year also shows an steady increase in temperature, slightly lower than for the previous two indices. It reaches 3.6 °C for RCP8.5 and 2.9 °C for RCP4.5 by the end of the century.

5.71

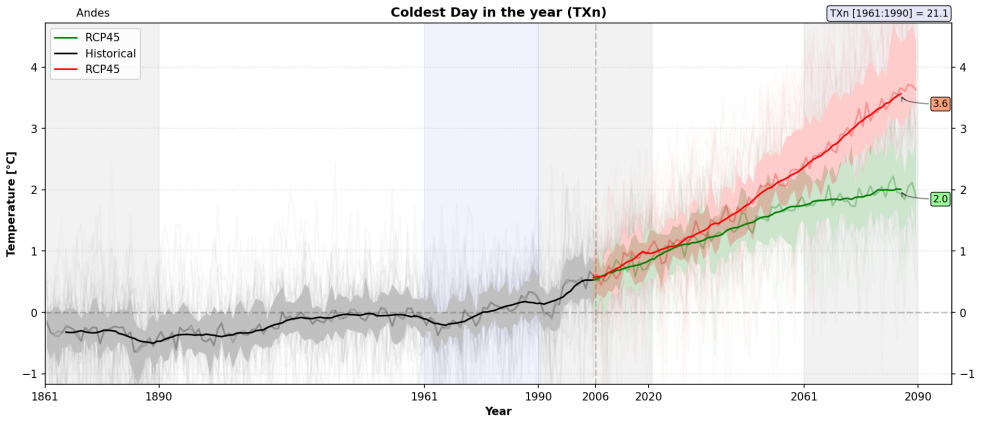

Figure 5.71: The multimodel median of changes in **Yearly Minimum Value of Daily Maximum Temperature** displayed as differences to the reference period, averaged over the Andes region.

In the spatial distribution in Figure 5.72 there is no clear tendency, as most of the maximum values as scattered all over the plot.

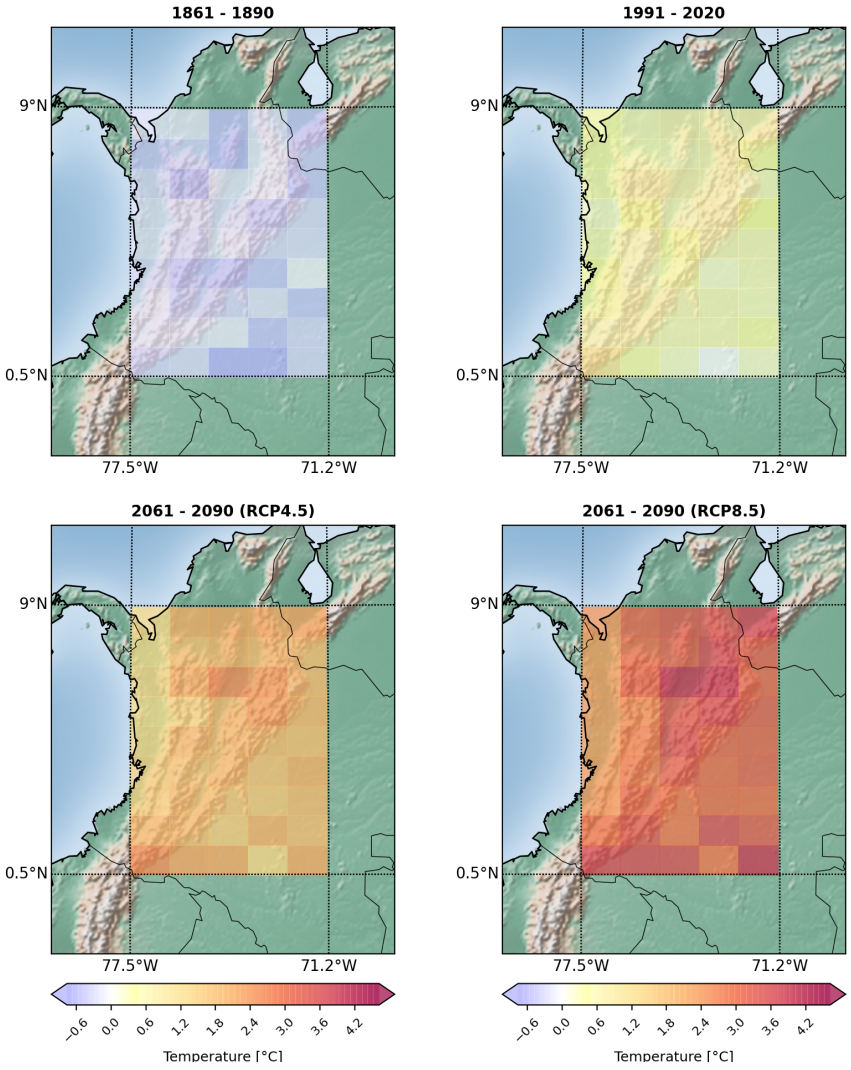

Figure 5.72: The multimodel median of changes in **Yearly Minimum Value of Daily Maximum Temperature** relative to the reference period for the Andes region, temporally averaged over the three analyzed time periods.

5.3.6 *Yearly Minimum Value of Daily Minimum Temperature*

Figure 5.73) illustrates the evolution of TNn, the temperature in the coldest night of the year. Again, the slope is pretty constant. The values reached by the end of the century are 4.8°C and 2.7°C for RCP8.5 and RCP4.5 respectively. The spatial distribution in Figure 5.74 shows higher values in the north east of the region for both RCP scenarios.

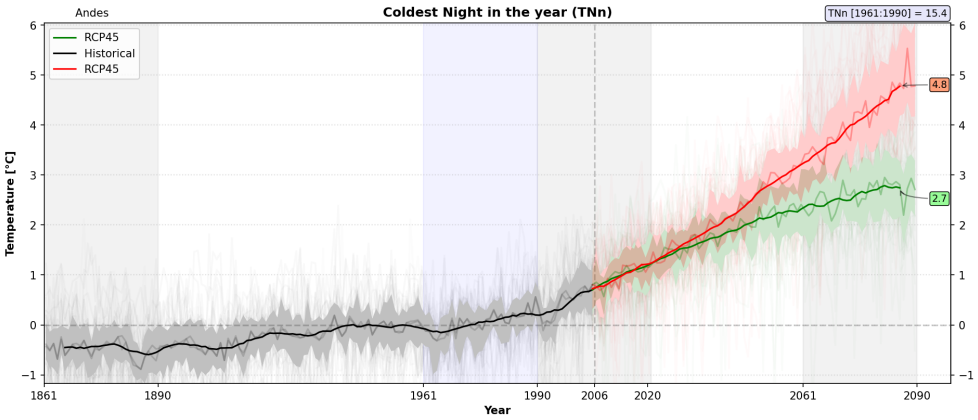

Figure 5.73: The multimodel median of changes in **Yearly Minimum value of Daily Minimum Temperature** displayed as differences to the reference period, averaged over the Andes region.

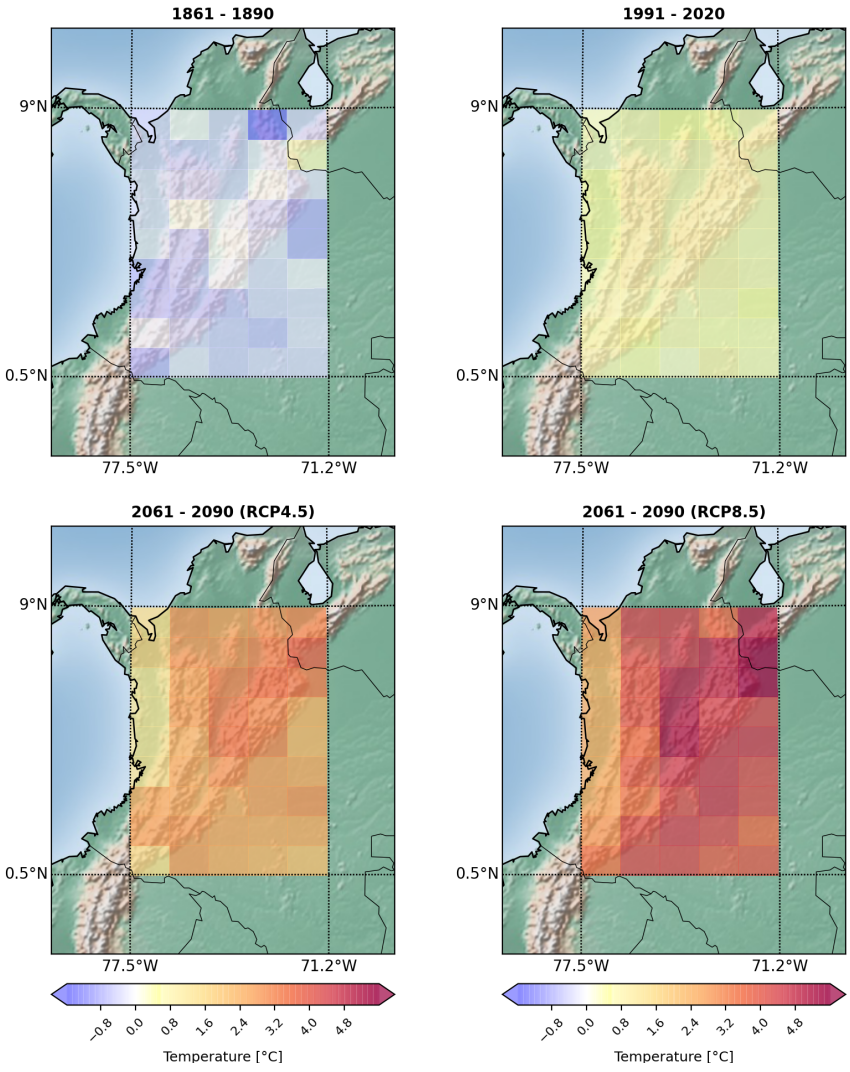

Figure 5.74: The multimodel median of changes in **Yearly Minimum Value of Daily Minimum Temperature** relative to the reference period for the Andes region, temporally averaged over the three analyzed time periods.

5.3.7 *Percentage of Days when TN < 10th Percentile*

The number of Cold Nights shows a decreasing tendency during the whole period of study, reaching virtually zero exceedance rate by the year 2061, which means none of the nights in the future would be considered cold by the reference period's standard. This is true for both RCP scenarios. It is also worth noting that already in the historical simulation, by the year 2006 the number is low, at 2.7%. The time series is depicted in Figure 5.76.

From the time periods averages in Figure 5.75, we can observe the huge difference in the values from the past, present and the two RCP scenarios. Because the values are given as exceedance rate, the maps are very homogeneous.

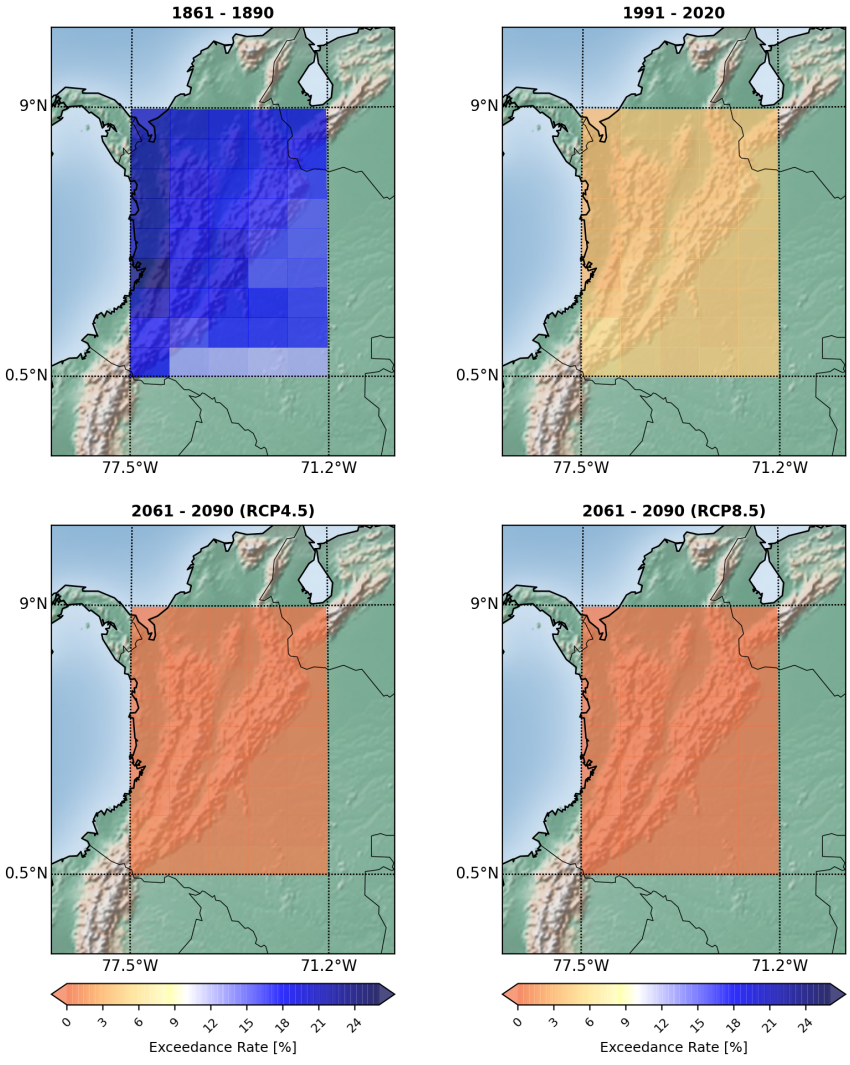

Figure 5.75: The multimodel median of changes in **Percentage of Days when Daily Minimum Temperature is lower than 10th Percentile** relative to the reference period for the Andes region, temporally averaged over the three analyzed time periods.

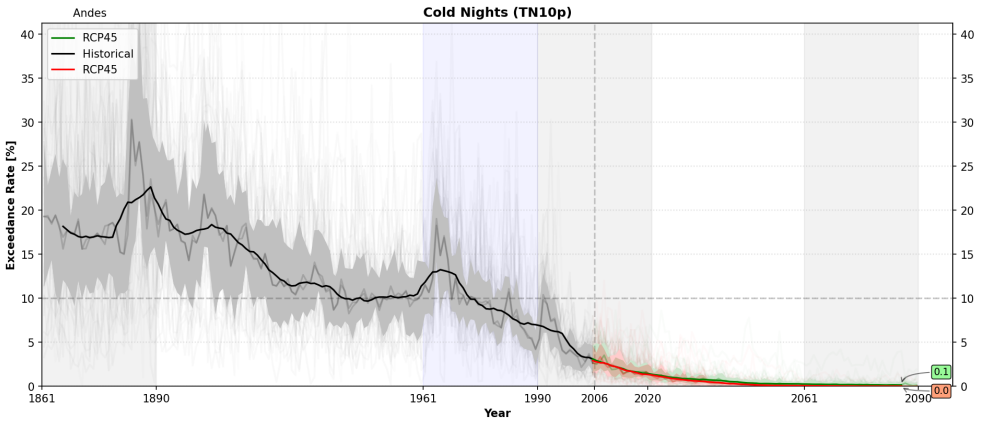

Figure 5.76: The multimodel median of changes in **Percentage of Days when Daily Minimum Temperature is lower than the 10th Percentile** displayed as differences to the reference period, averaged over the Andes region.

5.3.8 *Percentage of Days when TX < 10th Percentile*

The same tendency be can seen for the number of cold days in Figure 5.77, although the value for the RCP4.5 simulation does not reach the zero, and remains constant at 0.9% from 2060 onwards. As for Tn10p the maps are very homogeneous (Figure 5.78)

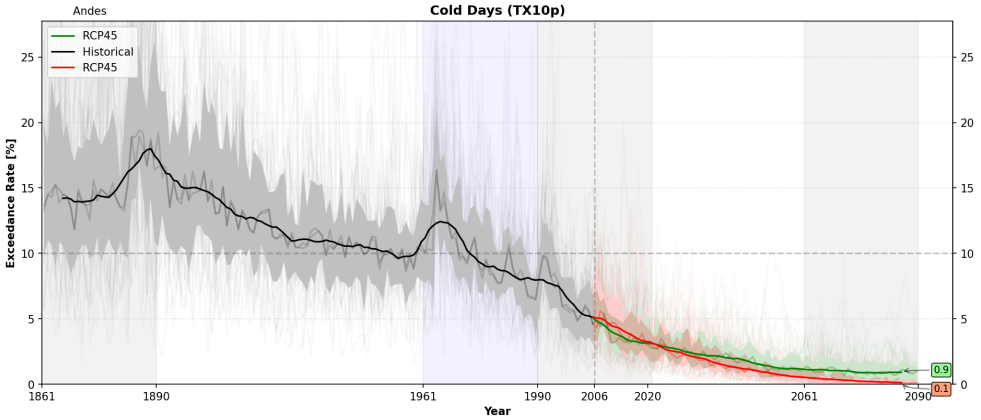

Figure 5.77: The multimodel median of changes in **Percentage of Days when Daily Maximum Temperature is lower than the 10th Percentile** displayed as differences to the reference period, averaged over the Andes region.

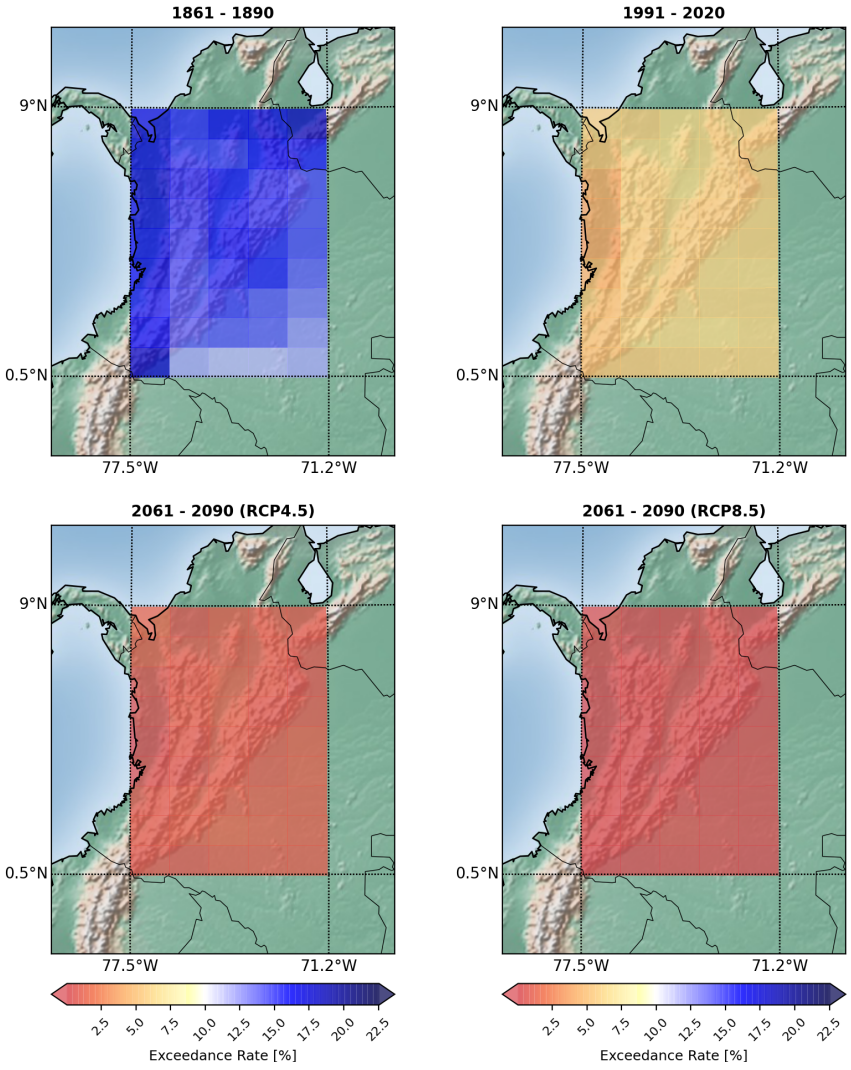

Figure 5.78: The multimodel median of changes in **Percentage of Days when Daily Maximum Temperature is lower than 10th Percentile** relative to the reference period for the Andes region, temporally averaged over the three analyzed time periods.

5.3.9 *Percentage of Days when TN > 90th Percentile*

The number of warm nights increases dramatically, reaching 87% for RCP4.5 and saturating at 99% for RCP8.5 which means under this scenario, all nights in the future are considered warm. This is consistent with the decrease to zero percent in cold nights. The time series is depicted in Figure 5.79. The maps, depicted in Figure 5.80 are very homogeneous.

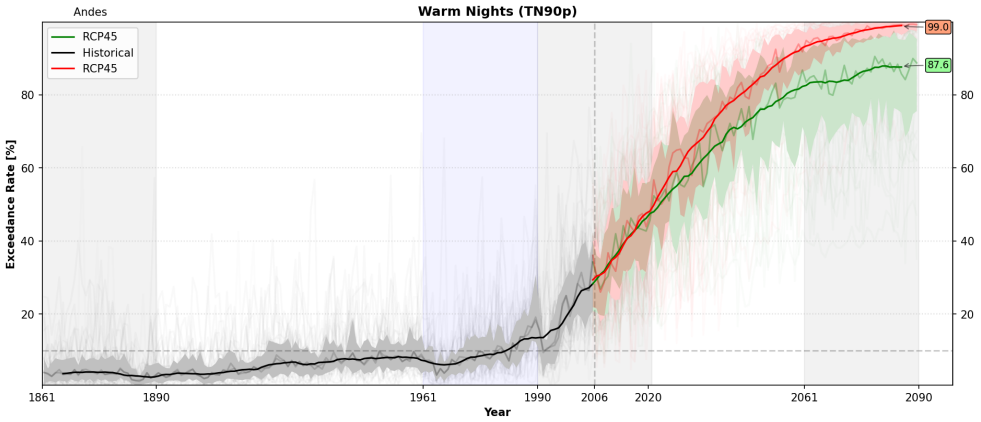

Figure 5.79: The multimodel median of changes in **Percentage of Days when Daily Minimum Temperature is greater than the 10th Percentile** displayed as differences to the reference period, averaged over the Andes region.

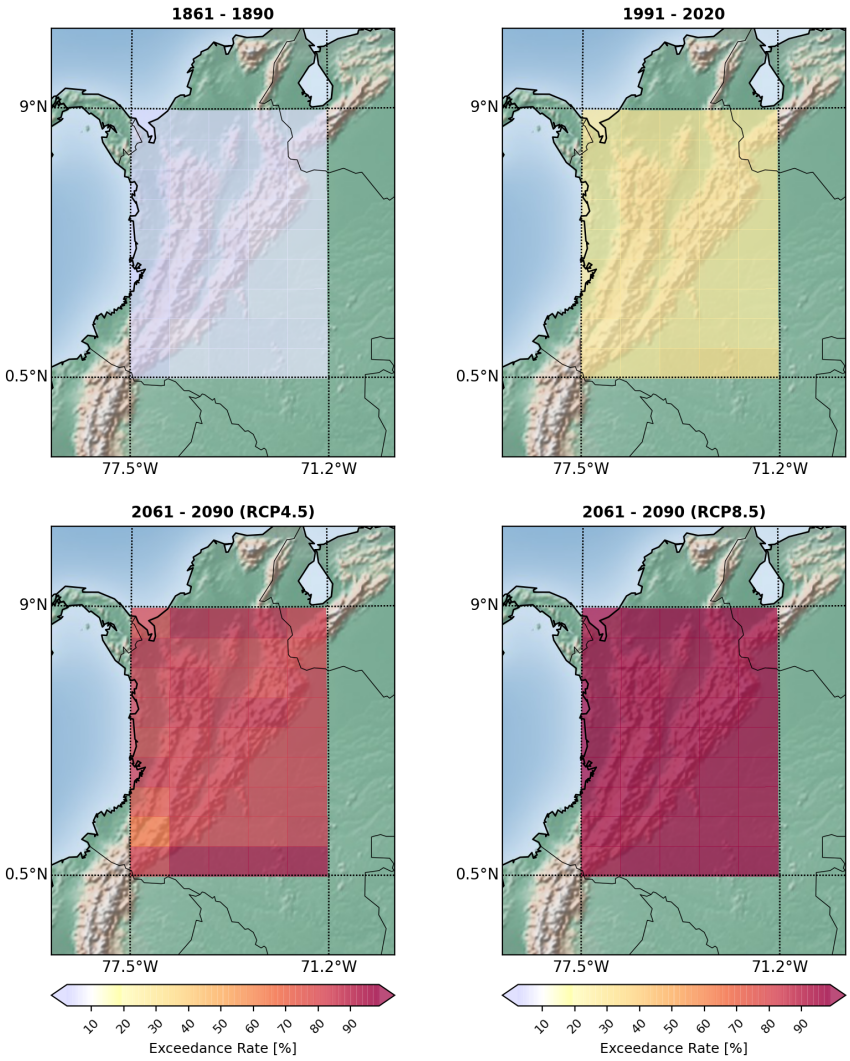

Figure 5.80: The multimodel median of changes in **Percentage of Days when Daily Minimum Temperature is greater than 90th Percentile** relative to the reference period for the Andes region, temporally averaged over the three analyzed time periods.

5.3.10 *Percentage of days when TX > 90th percentile*

The increase in warm days is not as high as for warm nights, which is consistent with results from previous indices (Tropical Nights vs Summer Days). The maximum value reached in RCP8.5 is 84% and in rcpc is 61%. The evolution is shown in Figure 5.82. The maps in Figure 5.82 show a slightly higher values towards the south regions, but are in gereral very homogeneous.

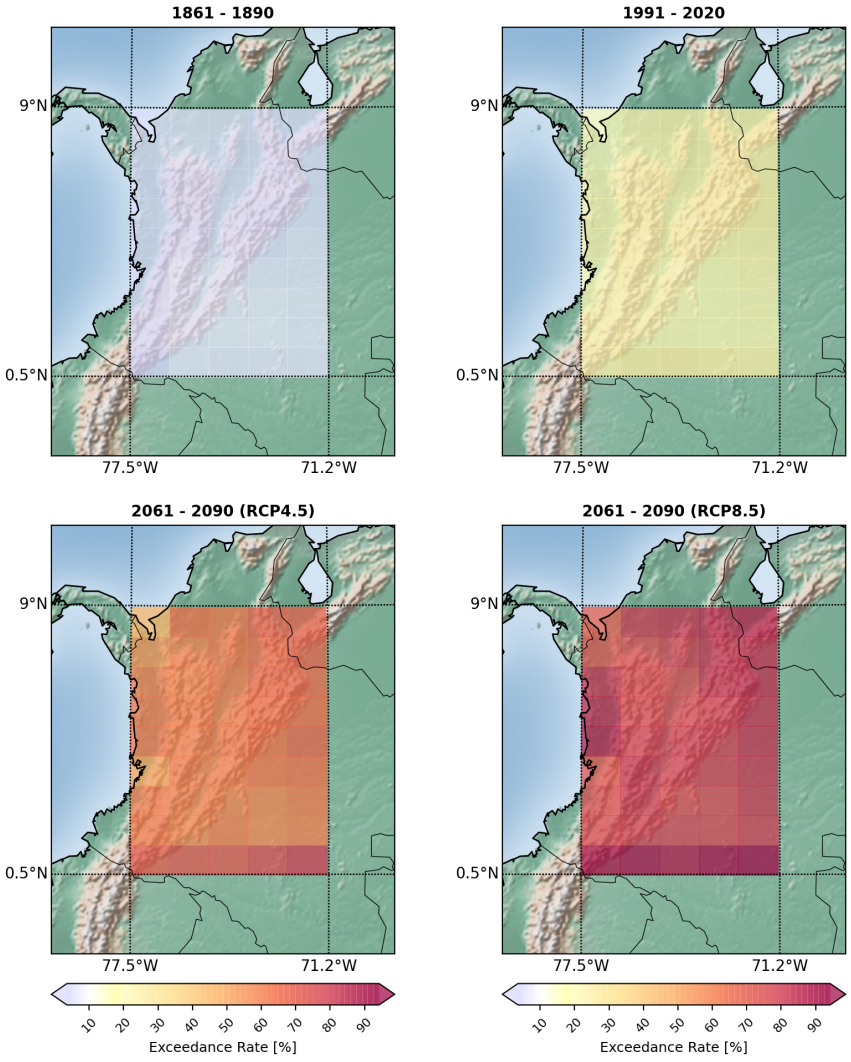

Figure 5.81: The multimodel median of changes in **Percentage of Days when Daily Maximum Temperature is greater than 90th Percentile** relative to the reference period for the Andes region, temporally averaged over the three analyzed time periods.

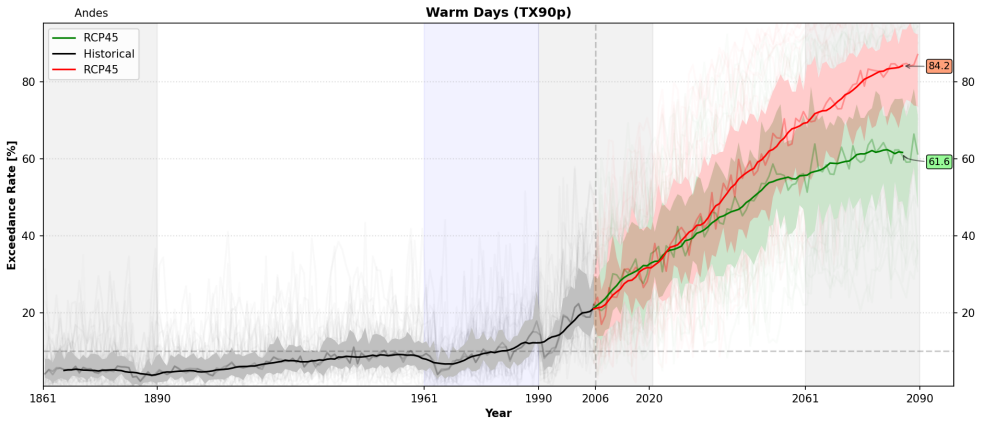

Figure 5.82: The multimodel median of changes in **Percentage of Days when Daily Maximum Temperature is greater than the 90th Percentile** displayed as differences to the reference period, averaged over the Andes region.

5.3.11 *Warm Spell Duration Index*

Similarly to previous temperature indices, the WSDI increases dramatically in both RCP scenarios. Additionally it is important to notice that in this case, the values were very low and constant before the 1990. RCP8.5 maximum value is 265 days while for RCP4.5 is 143. This is shown in figure 5.83).

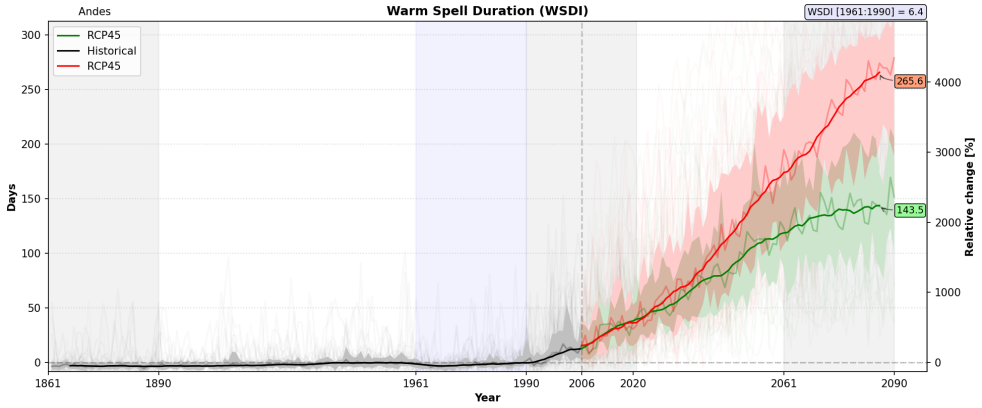

Figure 5.83: The multimodel median of changes in **Warm Spell Duration Index** displayed as differences to the reference period, averaged over the Andes region.

In Figure 5.84 the spatial variability is shown. The higher values correspond to the flats in the region, while the mountain range has slightly lower WSDI.

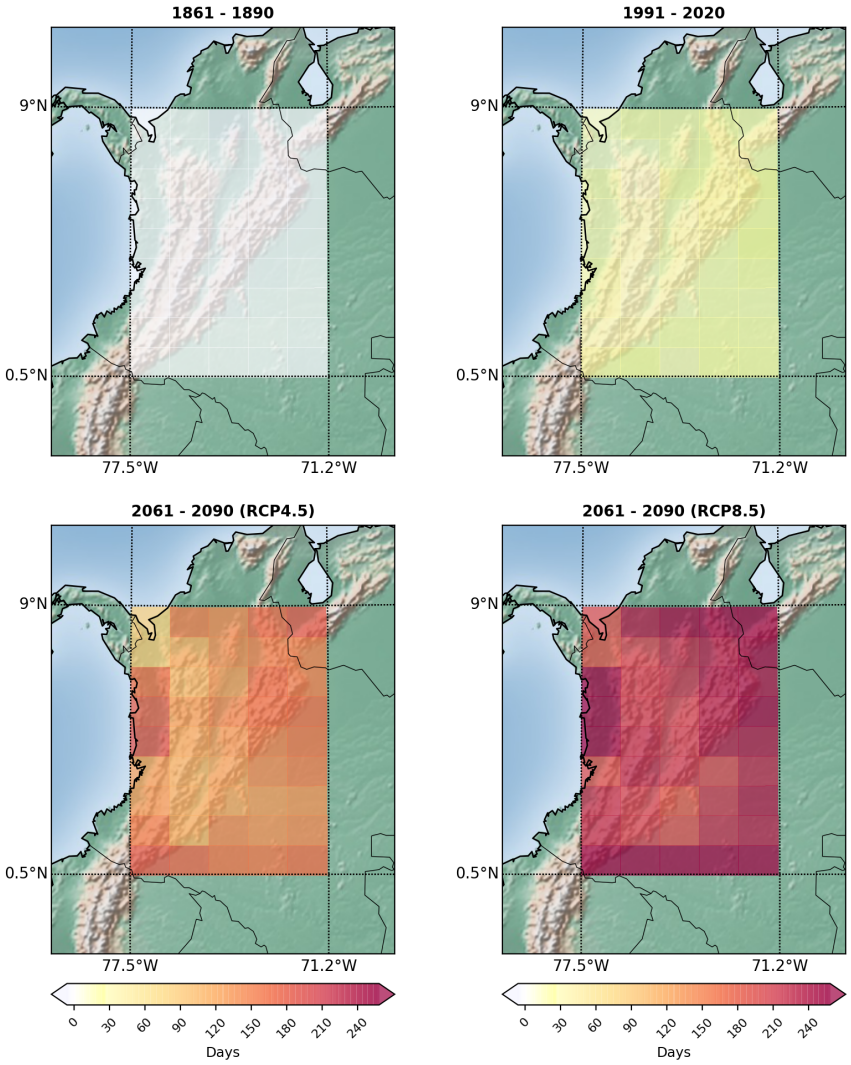

Figure 5.84: The multimodel median of changes in **Warm Spell Duration Index** relative to the reference period for the Andes region, temporally averaged over the three analyzed time periods.

5.3.12 *Cold Spell Duration Index*

Figure 5.85) depicts the decrease in CSDI, that seems low, −3.3 days for both indices, but the value in the reference period was only 3.9 to begin with as it corresponds to a tropical region. The maps in Figure 5.86 are completely homogeneous for present and future, and only the past period shows some variability, with the highest values towards the north west.

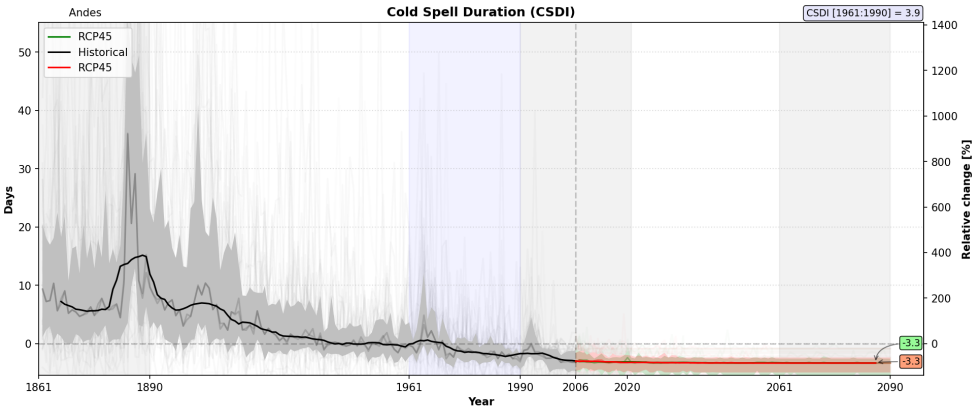

Figure 5.85: The multimodel median of changes in **Cold Spell Duration Index** displayed as differences to the reference period, averaged over the Andes region.

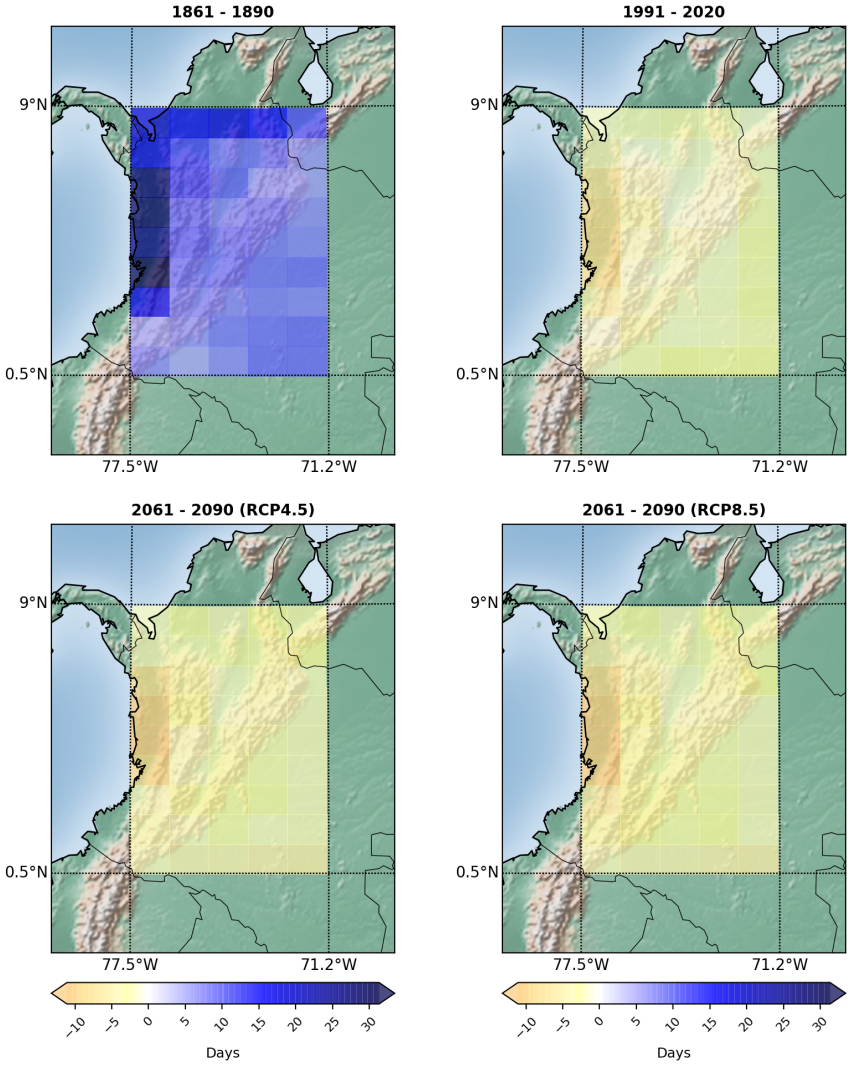

Figure 5.86: The multimodel median of changes in **Cold Spell Duration Index** relative to the reference period for the Andes region, temporally averaged over the three analyzed time periods.

5.3.13 *Daily Temperature Range*

The DTR, depicted in Figure 5.88 shows great variability among the models in the whole time span. The ensemble value remains very close to zero during the projections, only with a small tendency towards negative values, meaning the median increase in minimum temperature is higher than the median increase in maximum temperature. The maps also show very large spatial variability, as can be observed in Figure 5.87.

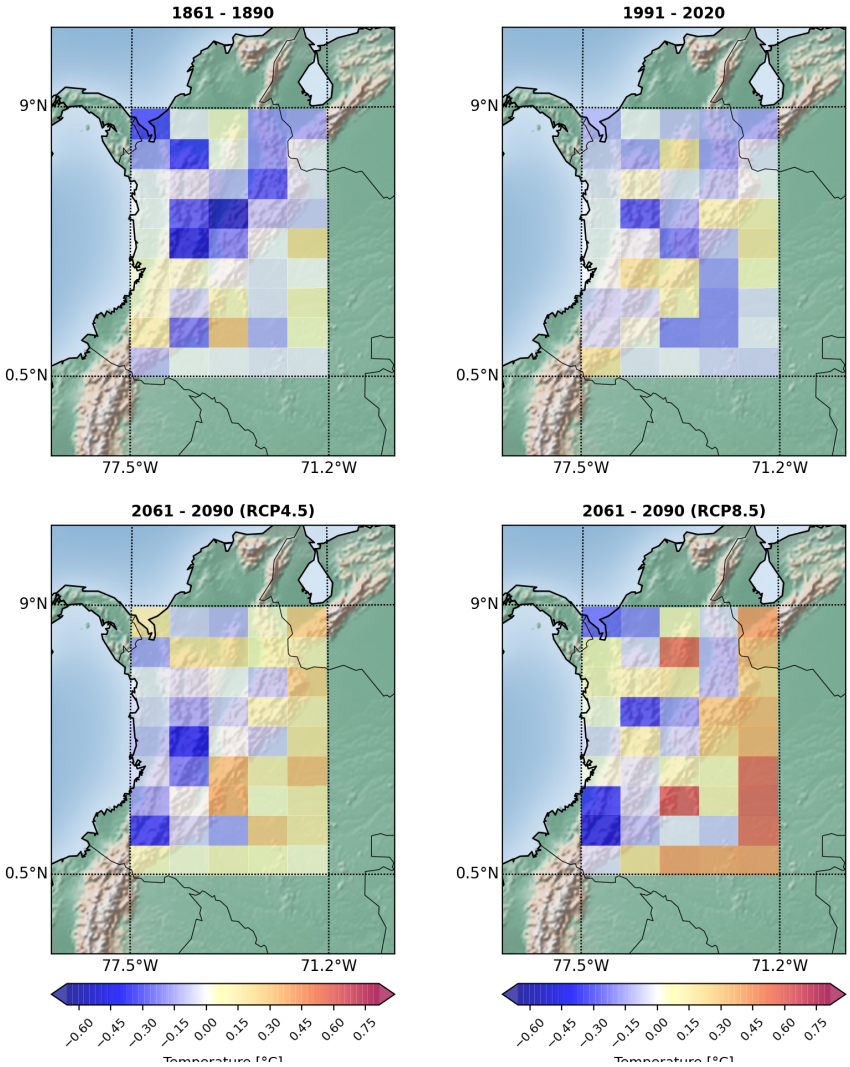

Figure 5.87: The multimodel median of changes in **Daily Temperature Range** relative to the reference period for the Andes region, temporally averaged over the three analyzed time periods.

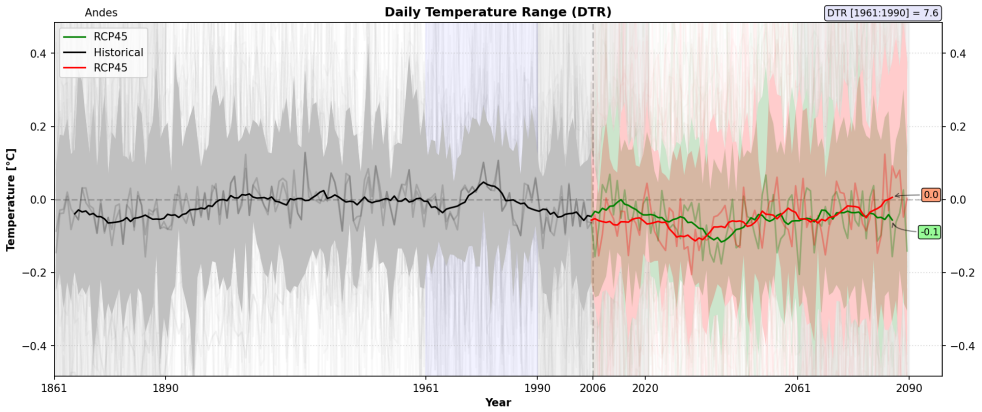

Figure 5.88: The multimodel median of changes in **Daily Temperature Range** displayed as differences to the reference period, averaged over the Andes region.

5.3.14 *Yearly Maximum* 1-*Day Precipitation*

After 1990 an small but steady increase is observed in Figure 5.89. The increase is higher for RCP8.5 which reaches a final value of 10.8*mm* (18%). There is high variability among the models, specially by the end of the simulation. The maps in Figure 5.90 show great spatial variability, with maximum values concentrated in the west coast of the region.

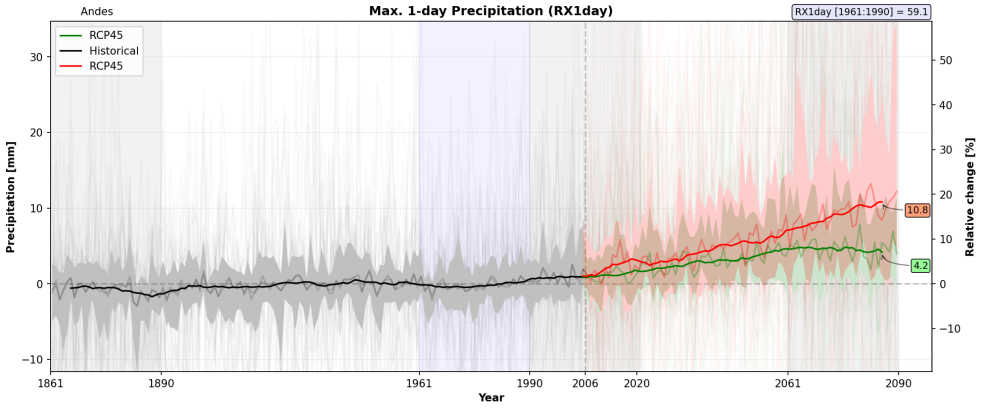

Figure 5.89: The multimodel median of changes in **Yearly Maximum 1-Day Precipitation** displayed as differences to the reference period, averaged over the Andes region.

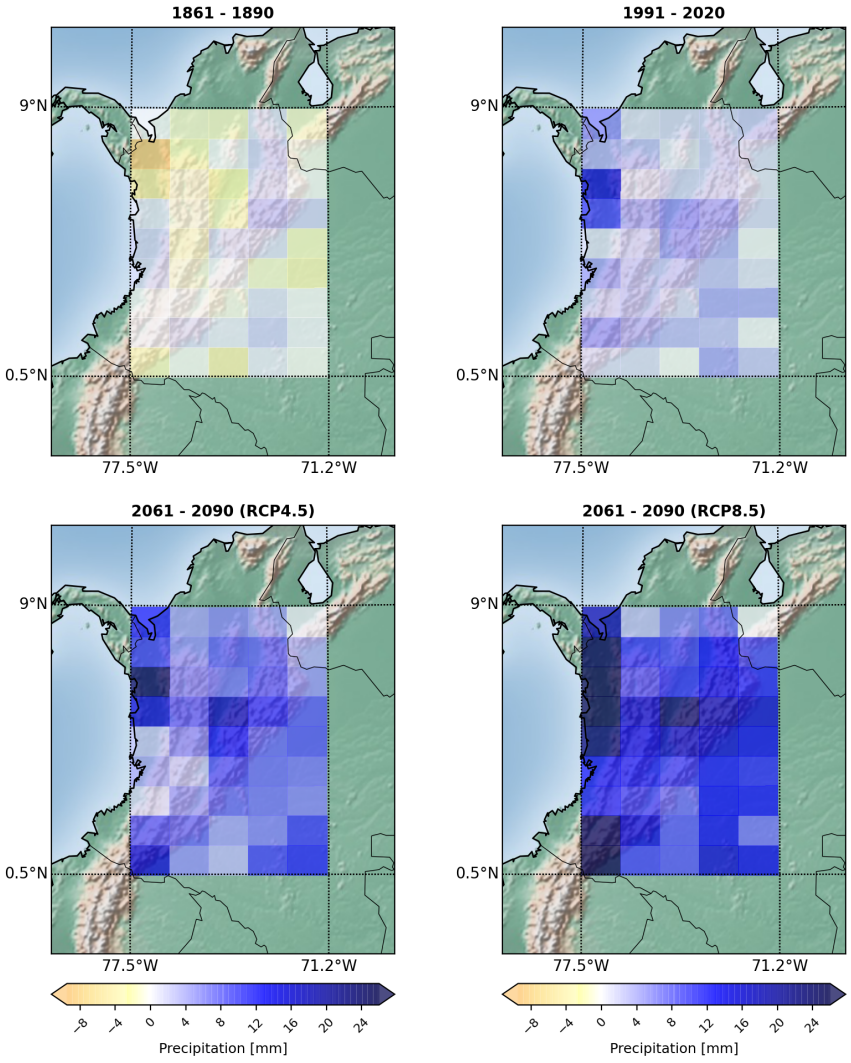

Figure 5.90: The multimodel median of changes in **Yearly Maximum 1-Day Precipitation** relative to the reference period for the Andes region, temporally averaged over the three analyzed time periods.

5.3.15 *Yearly Maximum 5-Day Precipitation*

High variability between models is observed in Figure 5.91. There is a steady increase in the precipitation value, and the maximum value for RCP8.5 reaches 19.6 which corresponds to a 13% relative change. As for Rx1day, in the case of Rx5day the maps show the higher values close to the west coast of the region, as can be observed in Figure 5.92.

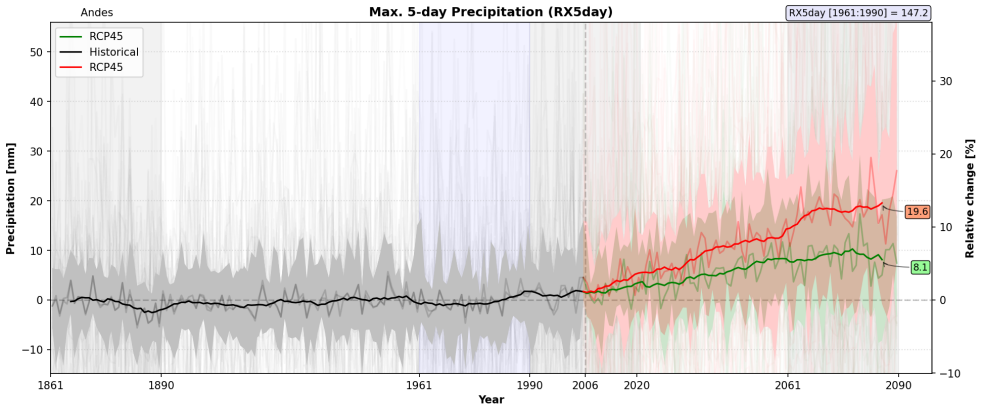

Figure 5.91: The multimodel median of changes in **Maximum 5-Day Precipitation** displayed as differences to the reference period, averaged over the Andes region.

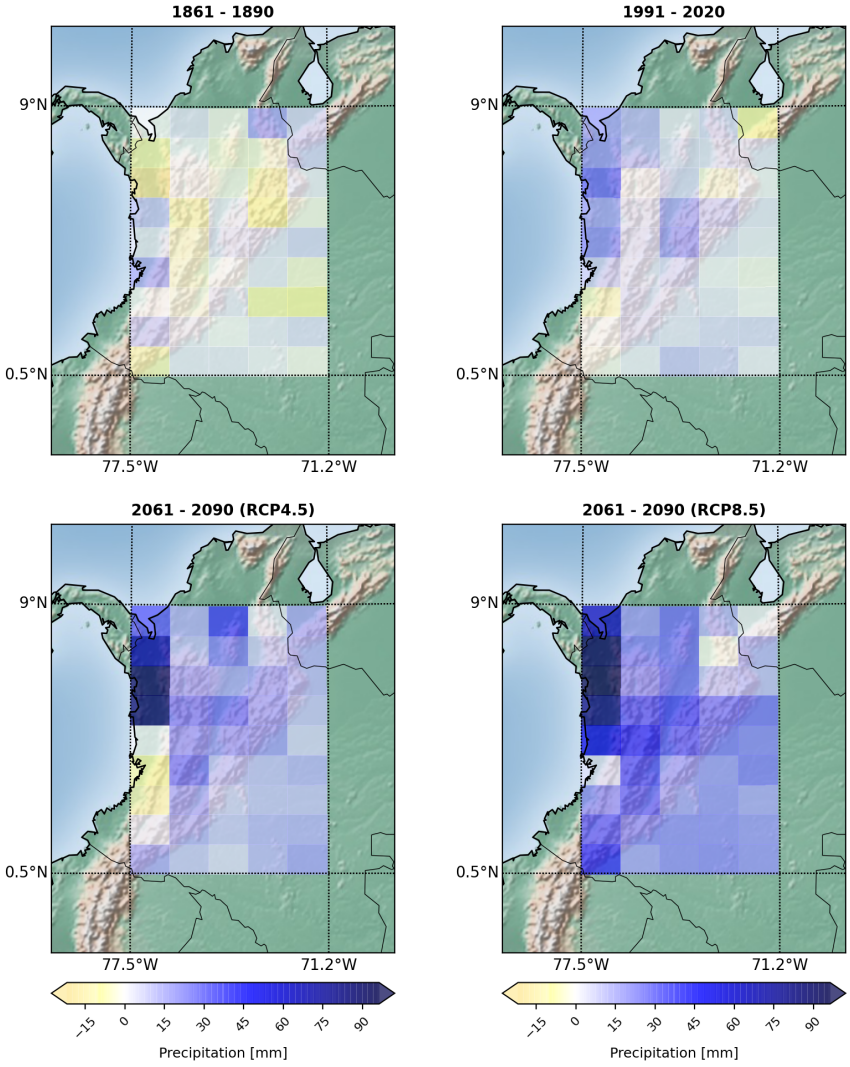

Figure 5.92: The multimodel median of changes in **Maximum 5-Day Precipitation** relative to the reference period for the Andes region, temporally averaged over the three analyzed time periods.

5.3.16 *Simple Precipitation Intensity Index*

The SDII shows some small increase in the future projections, reaching values of 6% of relative change in the RCP8.5 scenario. Again, the models show high variability. (Figure 5.94)

The maps in Figure 5.93 show large variability across the region, with higher values located in the west side of the Colombian Andes.

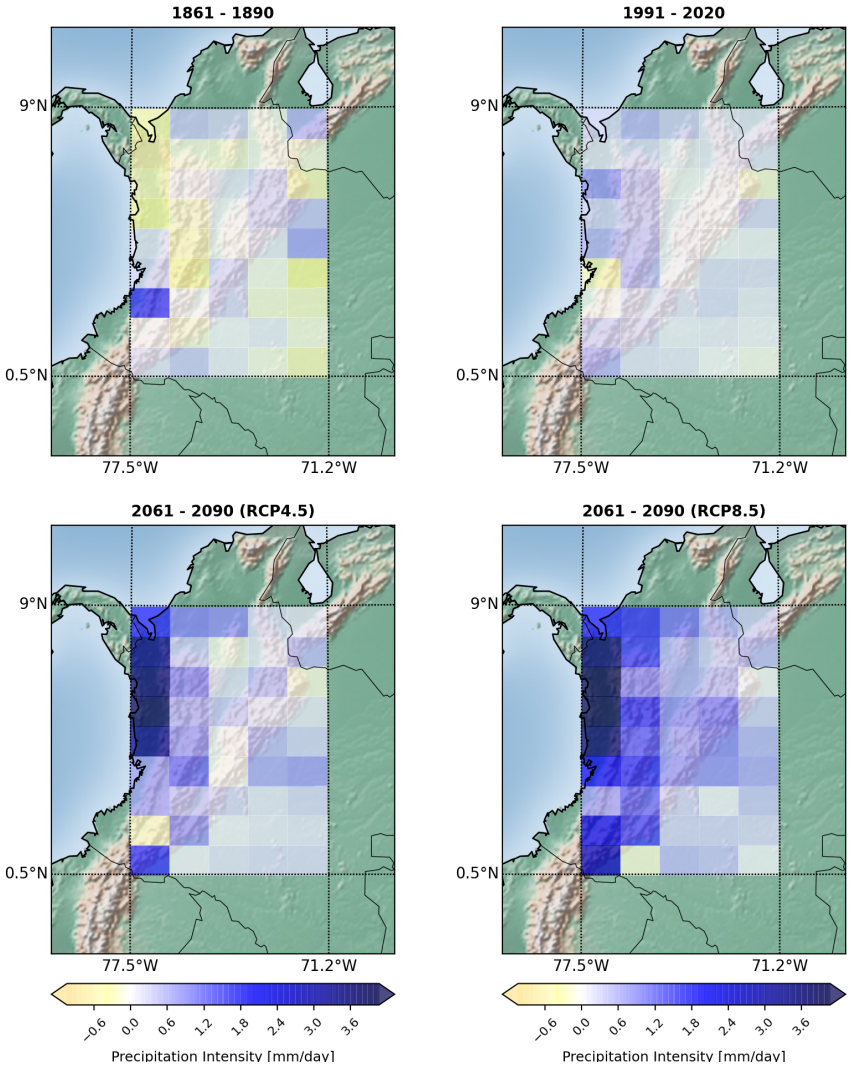

Figure 5.93: The multimodel median of changes in **Simple Daily Intensity** relative to the reference period for the Andes region, temporally averaged over the three analyzed time periods.

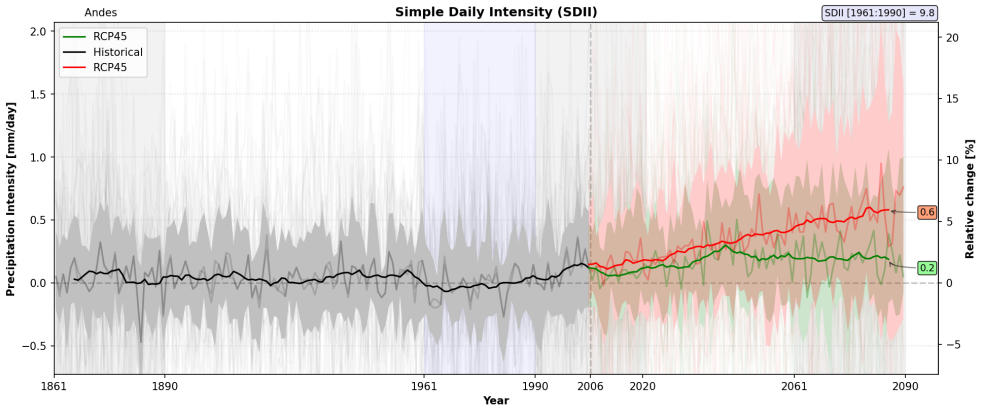

Figure 5.94: The multimodel median of changes in **Simple Daily Intensity** displayed as differences to the reference period, averaged over the Andes region.

5.3.17 *Annual count of days when PRCP* $\geqslant$ 10 *mm*

This index shows very low changes for future projections with respect to the reference period, and high intermodel variability during the whole time span (Figure 5.95) Similarly, the maps show high heterogeneity across the region (Figure 5.96)

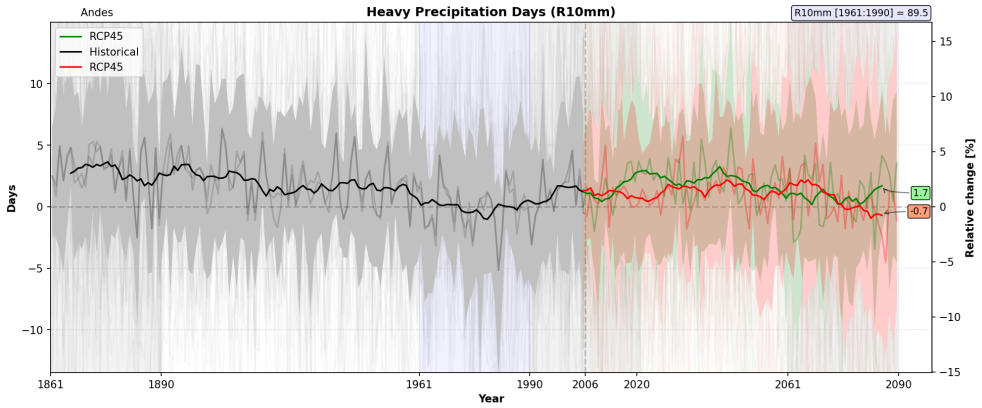

Figure 5.95: The multimodel median of changes in **Annual count of days when PRCP** $\geqslant$ 10 **mm** displayed as differences to the reference period, averaged over the Andes region.

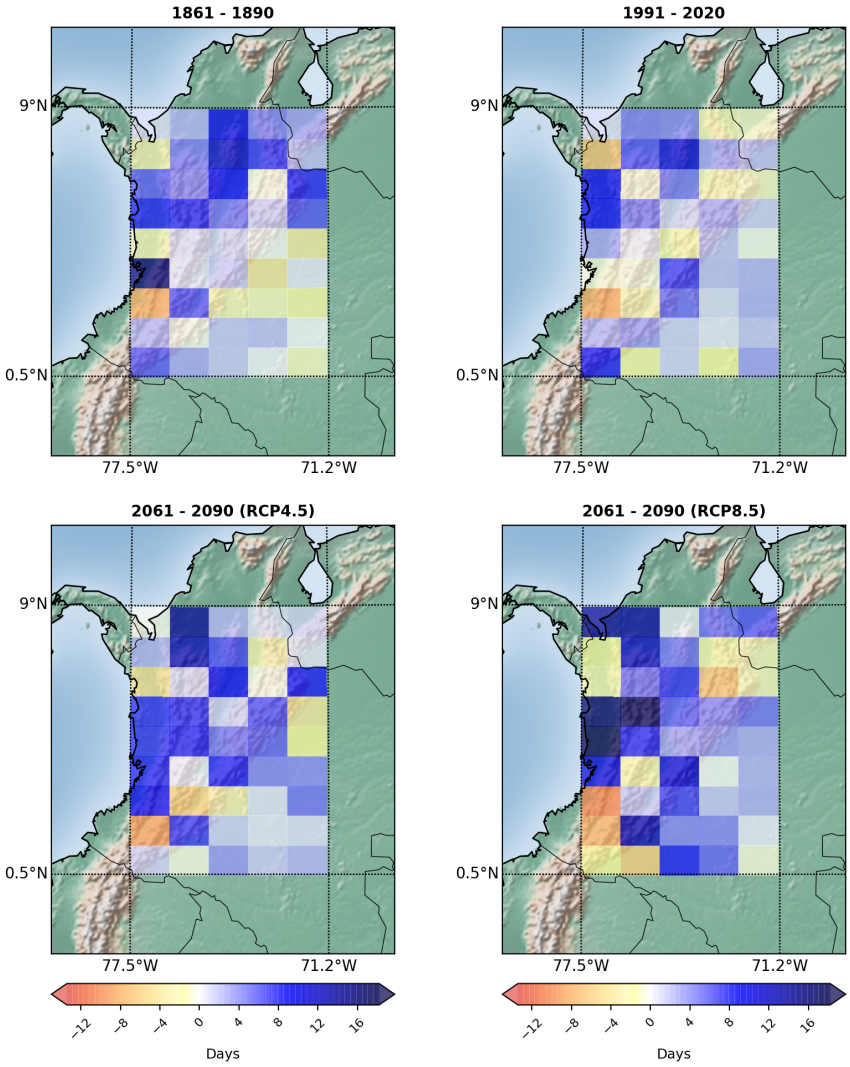

Figure 5.96: The multimodel median of changes in **Annual count of days when PRCP** $\geqslant$ 10 **mm** relative to the reference period for the Andes region, temporally averaged over the three analyzed time periods.

5.3.18 *Annual count of days when PRCP* $\geqslant$ 20 *mm*

Similarly to R10mm, this index shows very low changes for future projections and high variability in the time period of study. (Figure 5.97). In the maps high variability is observed, with the maximum values towards the west of the region (Figure 5.98)

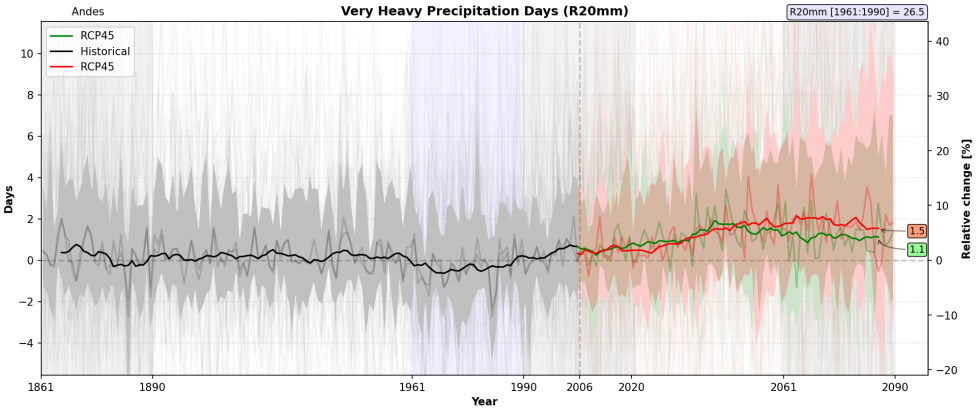

Figure 5.97: The multimodel median of changes in **Annual count of days when PRCP** $\geqslant$ 20 **mm** displayed as differences to the reference period, averaged over the Andes region.

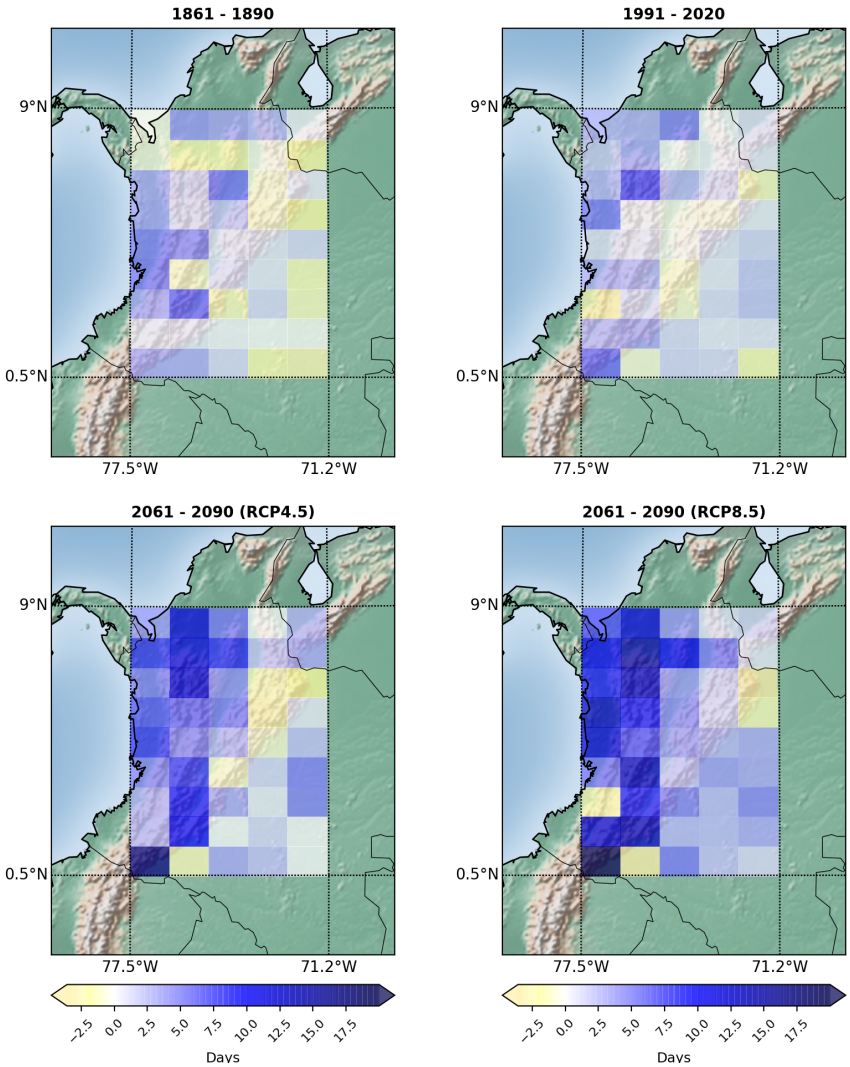

Figure 5.98: The multimodel median of changes in **Annual count of days when PRCP** $\geqslant$ 20 **mm** relative to the reference period for the Andes region, temporally averaged over the three analyzed time periods.

5.3.19 *Annual count of days when PRCP ⩾ 1 mm*

Contrary to previous indices, R1mm shows an small decrease in both projections. The high intermodel variability however is still high, as well as the spatial heterogeneity across the region (Figures 5.100 and 5.99)

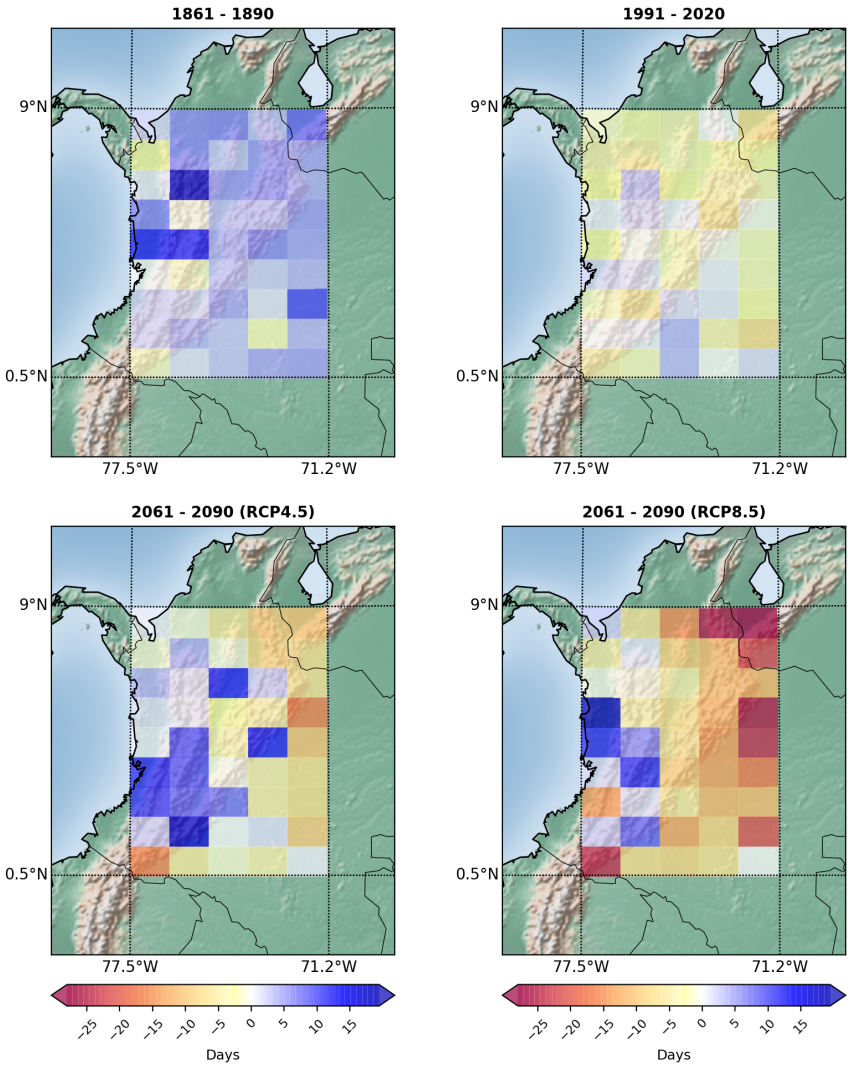

Figure 5.99: The multimodel median of changes in **Annual count of days when PRCP ⩾ 1 mm** relative to the reference period for the Andes region, temporally averaged over the three analyzed time periods.

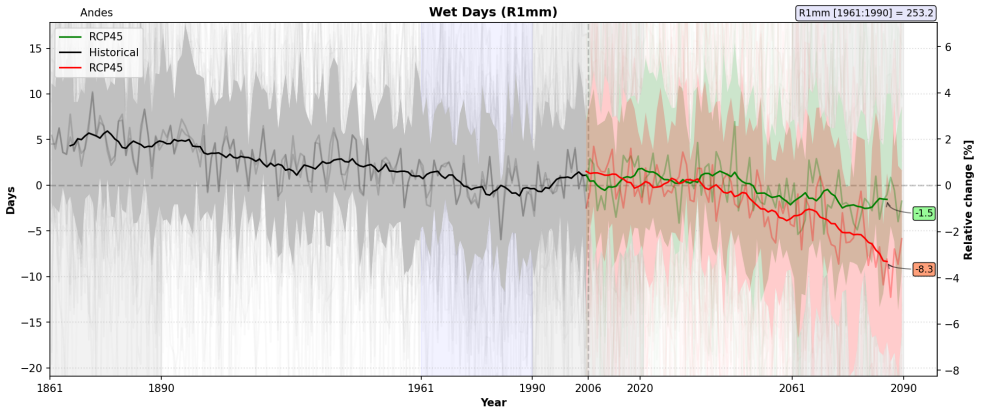

Figure 5.100: The multimodel median of changes in **Annual count of days when PRCP** $\geqslant$ 1 **mm** displayed as differences to the reference period, averaged over the Andes region.

5.3.20 *Maximum length of dry spell*

The CDD is shown in Figures 5.101 and 5.102. The timeseries shows no changes, and the maps high variability.

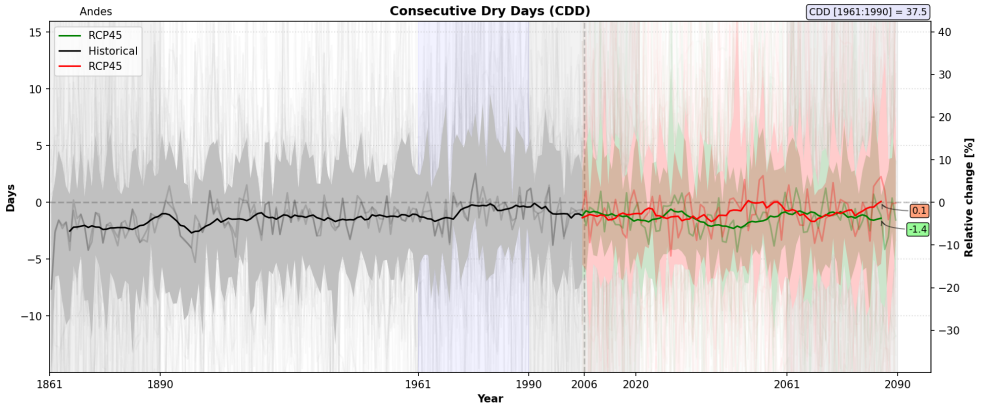

Figure 5.101: The multimodel median of changes in **Maximum length of dry spell** displayed as differences to the reference period, averaged over the Andes region.

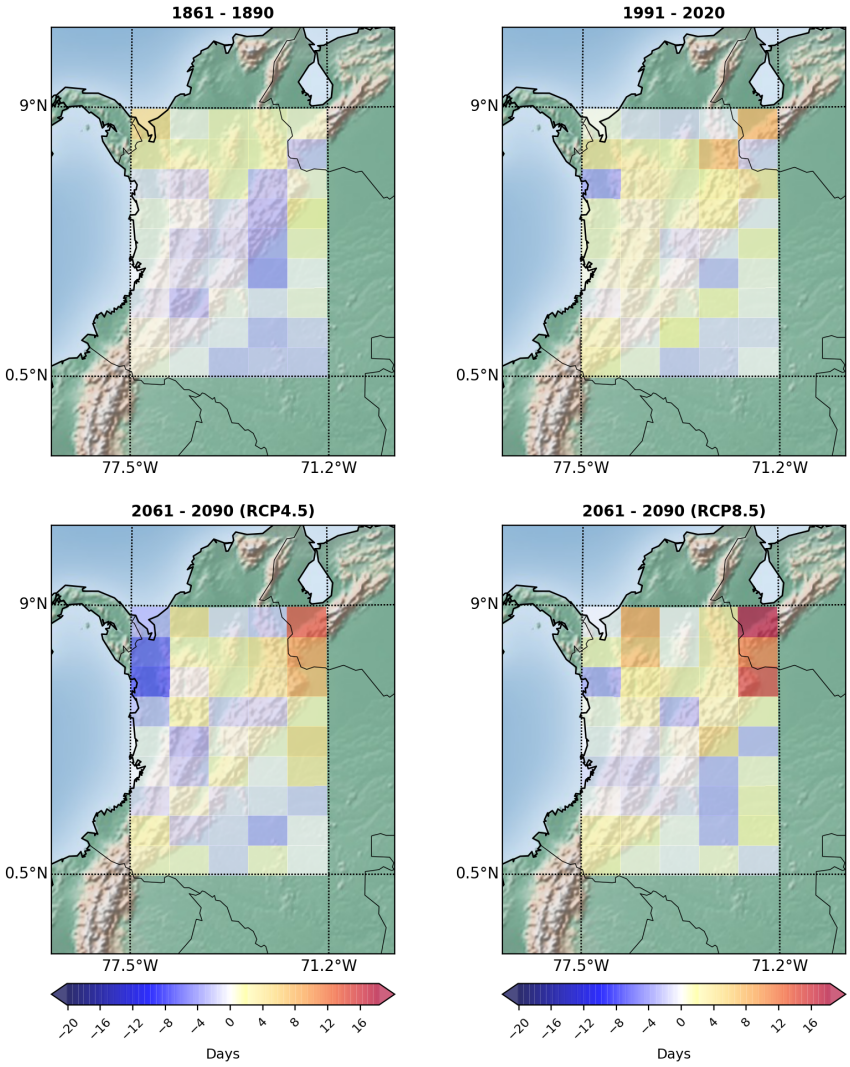

Figure 5.102: The multimodel median of changes in **Maximum length of dry spell** relative to the reference period for the Andes region, temporally averaged over the three analyzed time periods.

5.3.21 *Maximum length of wet spell*

The CWD is shown in Figures 5.104 and 5.103. The timeseries shows some decrease by the end of the century. The maps show high variability.

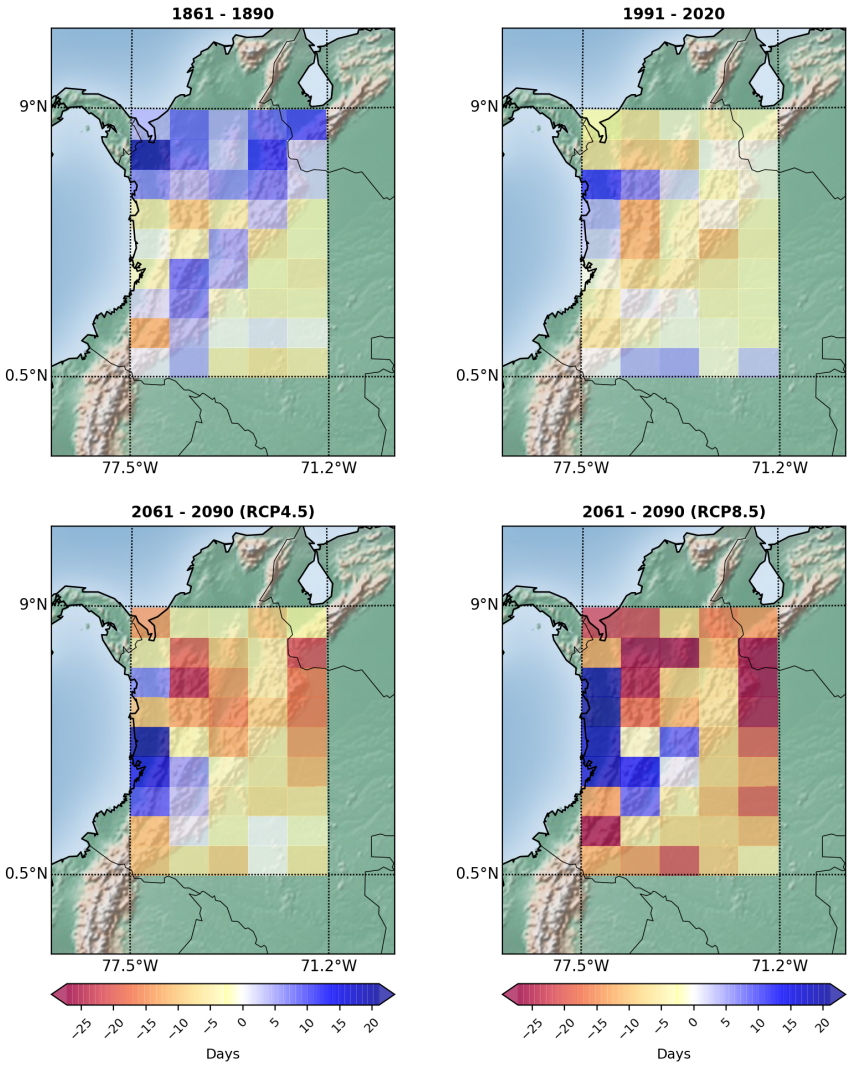

Figure 5.103: The multimodel median of changes in **Maximum length of wet spell** relative to the reference period for the Andes region, temporally averaged over the three analyzed time periods.

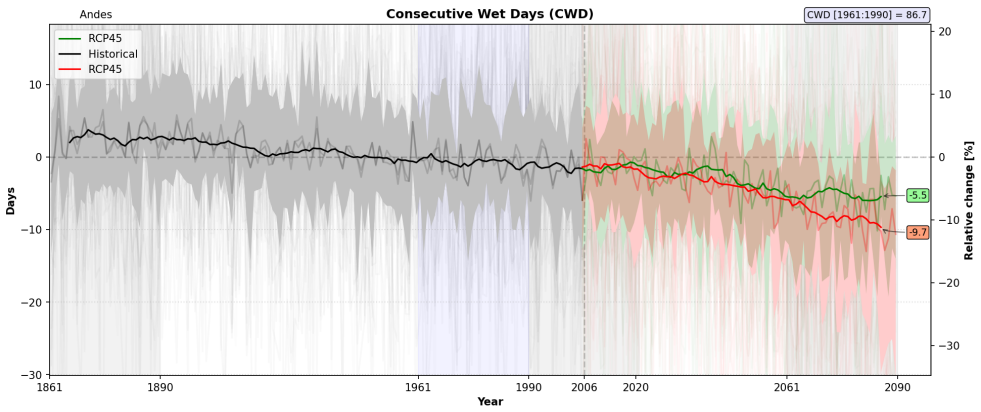

Figure 5.104: The multimodel median of changes in **Maximum length of wet spell** displayed as differences to the reference period, averaged over the Andes region.

5.3.22 *Annual total PRCP when RR > 95p*

The r95pTOT is shown in Figure 5.105 and 5.106. There is an increasing tendency in the time series, and in the map, the highest values are in the west coast.

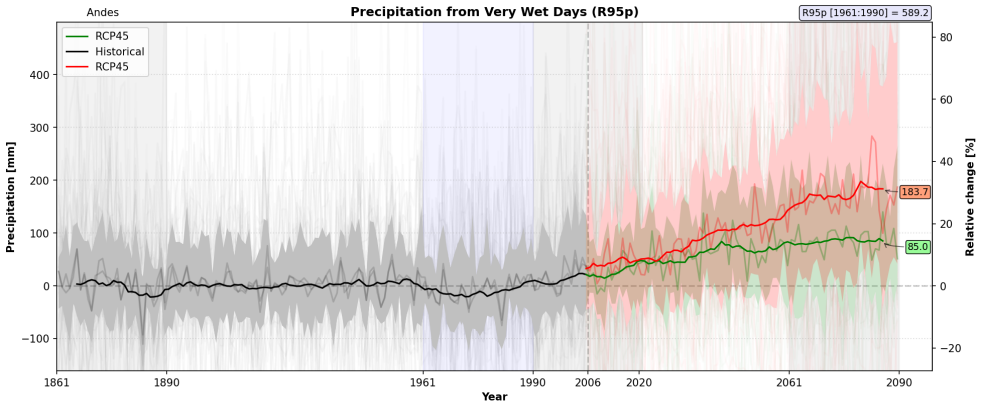

Figure 5.105: The multimodel median of changes in **Precipitation from wet days** displayed as differences to the reference period, averaged over the Andes region.

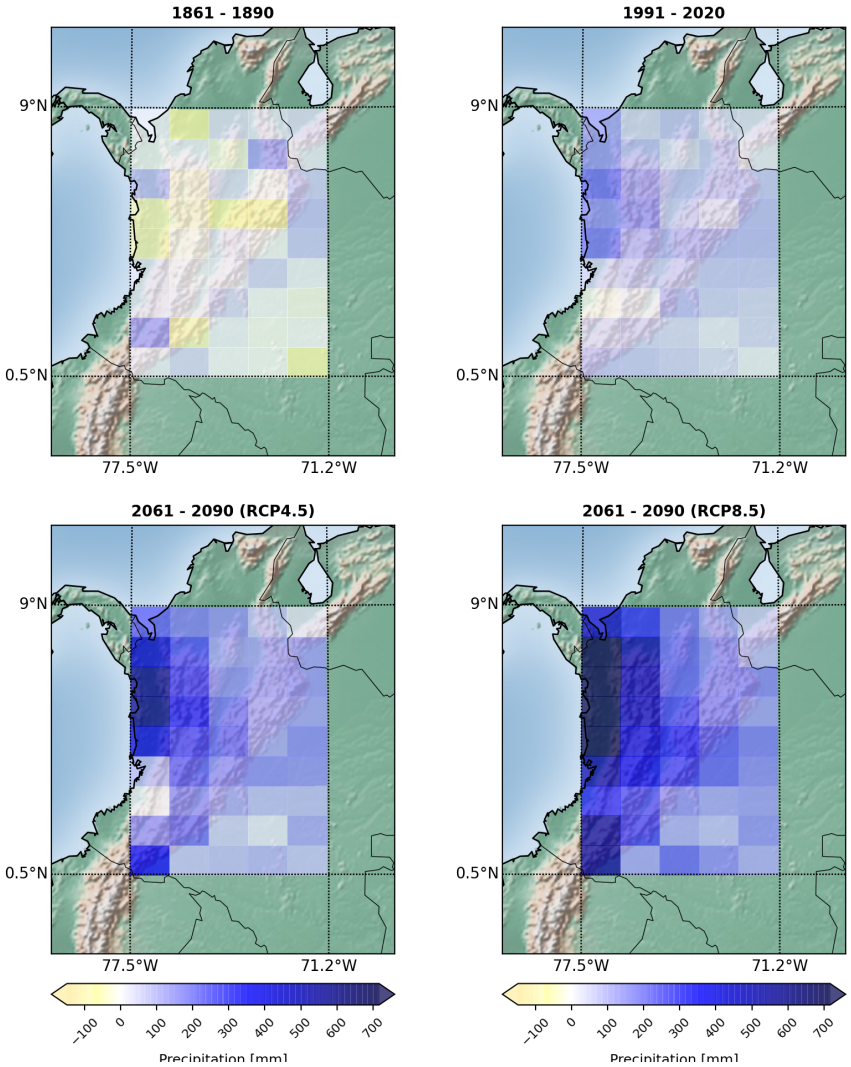

Figure 5.106: The multimodel median of changes in **Precipitation from wet days** relative to the reference period for the Andes region, temporally averaged over the three analyzed time periods.

5.3.23 *Annual total PRCP when RR > 99p*

The r99pTOT is shown in Figure 5.107 and 5.108. There is an increasing tendency in the time series, and in the map, the highest values are in the west coast.

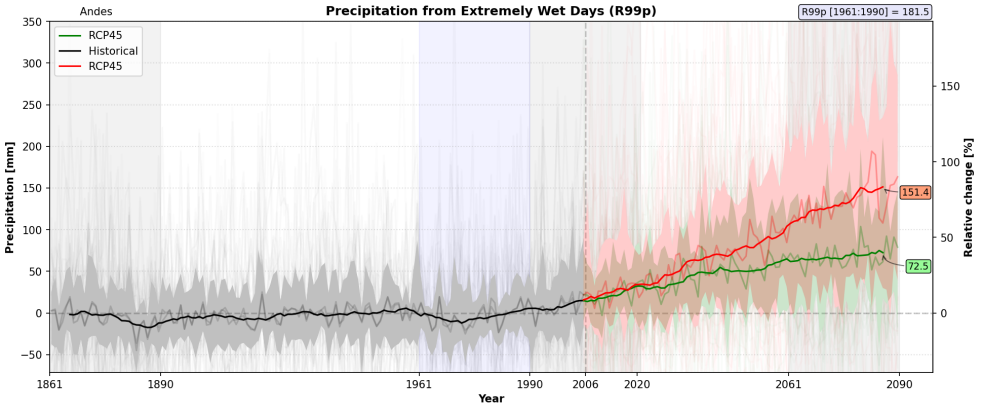

Figure 5.107: The multimodel median of changes in **Precipitation from extremely wet days** displayed as differences to the reference period, averaged over the Andes region.

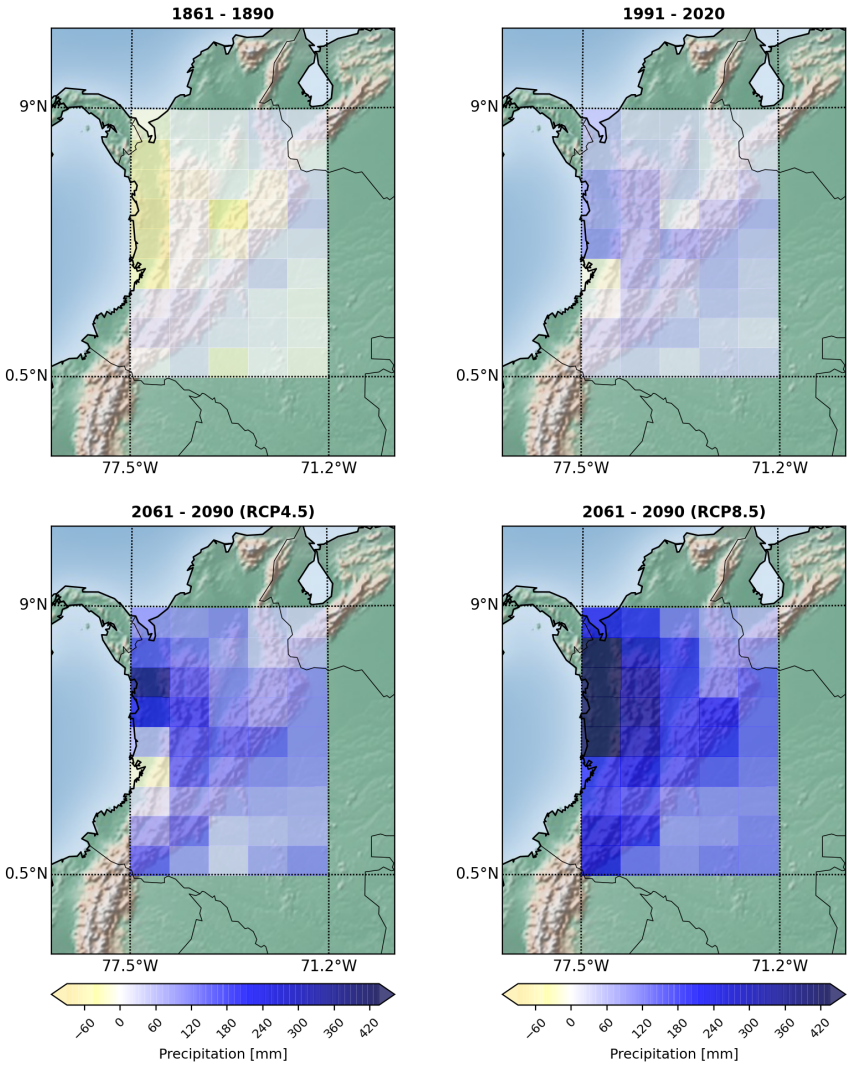

Figure 5.108: The multimodel median of changes in **Precipitation from extremely wet days** relative to the reference period for the Andes region, temporally averaged over the three analyzed time periods.

5.3.24 *Annual total precipitation in wet days*

The Annual total precipitation is shown in Figure 5.107 and 5.108. There is no clear tendency in the time series, and in the map, the highest values are in the west coast.

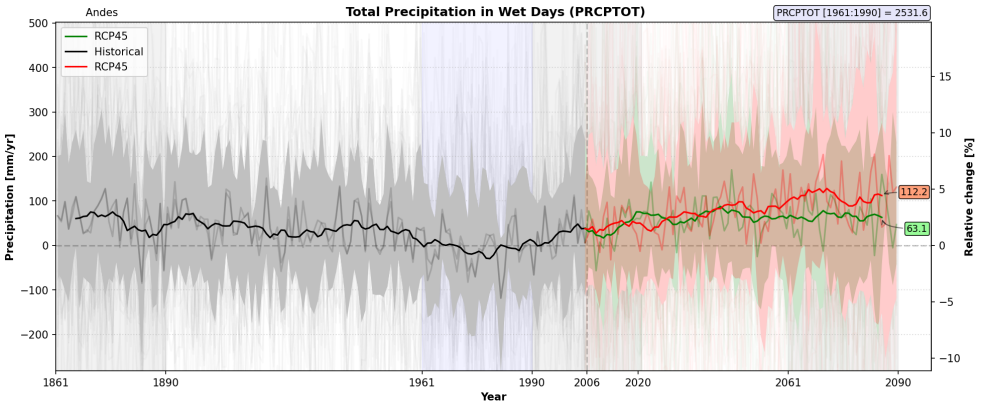

Figure 5.109: The multimodel median of changes in **Total precipitation in wet days** displayed as differences to the reference period, averaged over the Andes region.

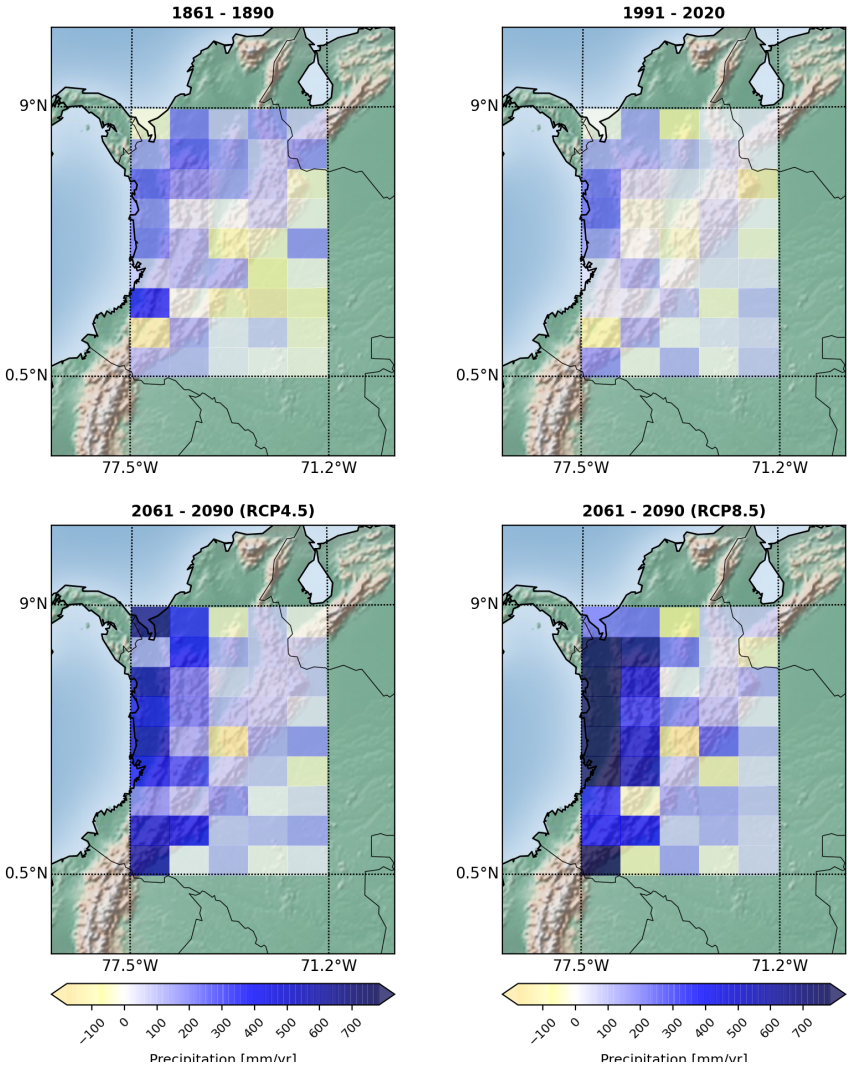

Figure 5.110: The multimodel median of changes in **Total precipitation in wet days** relative to the reference period for the Andes region, temporally averaged over the three analyzed time periods.

6

DISCUSSION AND CONCLUSIONS

The core of this thesis is to investigate climate changes by using daily minimum and maximum temperature and daily precipitation from the CMIP5 project, and the 27 ETCCDI climate indices.
Tables 6.1 and 6.2 it is presented an overview of all indices calculated for Alpine and Andes region, and the results related to global data obtained from the KNMI Climate Explorer [15]. We follow with a more detailed discussion on different sets of related indices along side their respective bar plots to illustrate better the results. Lastly, we present the final conclusions.

Table 6.1: Comparative summary for temperature indices.

Index	**Global**		**Alps**		**Andes**		**Concluding Remarks**
	RCP4.5	**RCP8.5**	**RCP4.5**	**RCP8.5**	**RCP4.5**	**RCP8.5**	
FD [days]	−10	−20	−29.1	−44.7	NA	N.A	• FD, TR, and GSL in Alps are significantly higher compared to the increase at global scale. • DTR remains constant, which means increases in maximum and minimum temperatures are comparable.
SU [days]	30	50	36.0	66.1	61.2	84.0	
ID [days]	−7.8	−14	−11.6	−15.0	N.A	N.A	
TR [days]	22	45	15.9	37.6	96.7	150	
GSL [days]	10	20	35.8	59.0	N.A	N.A	
DTR [°C]	−0.09	−0.18	0.3	0.5	−0.1	0	
TXx [°C]	2.0	4.2	3.8	7.2	2.7	5.0	• Higher increases in the Alps compared to Andes and global scale. • Higher increasing in TX than TN in the Alps and the Andes, contrary to global scale
TNx [°C]	2.0	4.0	3.2	6.1	2.6	4.7	
TXn [°C]	2.5	5.2	3.6	5, 6	2.0	3.6	
TNn [°C]	2.8	5.5	4.5	6.6	2.7	4.8	
Tx10p [%]	0.2	0.1	1.9	0.5	0.9	0.1	• For all regions changes in TN10p are larger than TX10p. • In Andes changes in Tx90p and Tn90p are more pronounced than in the Alps, due to the lack of seasons. • There will be virtually no cold days/nights in Andes and Alpine • Virtually all nights are warm in Andes in RCP8.5
TN90p [%]	49	70	38.4	54.5	87.6	99.0	
TX90p [%]	47	67	39.0	56.3	61.6	84.2	
TN10p [%]	1.0	0.1	1.7	0.4	0.1	0.0	
WSDI [days]	158	250	68.7	250.0	143.5	265.6	
CSDI [days]	−7	−7	−4.7	−5.4	−3.3	−3.3	

Table 6.2: Comparative summary for precipitation indices.

Index	Global		Alps		Andes		Concluding Remarks
	RCP4.5	RCP8.5	RCP4.5	RCP8.5	RCP4.5	RCP8.5	
RX1day [mm]	4.2	9.2	4.2	6.2	4.2	10.8	• No significant changes in total precipitation • Intensification in precipitation extremes • Fewer wet days • Longer consecutive dry days • High variability in the Andes region
RX5day [mm]	7.7	15	6.3	7.5	8.1	19.6	
SDII [mm/day]	0.33	0.62	0.4	0.6	0.2	0.6	
R10mm [days]	1.5	2.5	2.7	1.1	1.7	−0.7	
R20mm [days]	0.95	1.6	1.2	1.4	1.2	1.4	
R1mm [days]	−0.5	−2.4	−0.4	−2.5	−1.5	−8.3	
CDD [days]	1.25	3.3	−4.4	−16.6	−1.4	0.1	
CWD [days]	0.28	0.15	0.9	4.1	−5.5	−9.7	
R95pTOT [mm/yr]	50	100	59.9	69.1	85	183.7	
R99pTOT [mm/yr]	29	65	43.1	53.5	72.5	151.4	
PRCPTOT [mm/yr]	42	75	41.3	−9.7	72.5	72.5	

6.1 DISCUSSION

From Figure 6.1 it can be observed the changes in Frost Days for the Alps and on a global scale. The median decrease of frost days (FD) in the Alps is significantly higher under the two RCPs compared to FD on a global scale. The relative change in the RCP8.5 projection shows that more than half of the Frost Days will be lost by the year 2090.

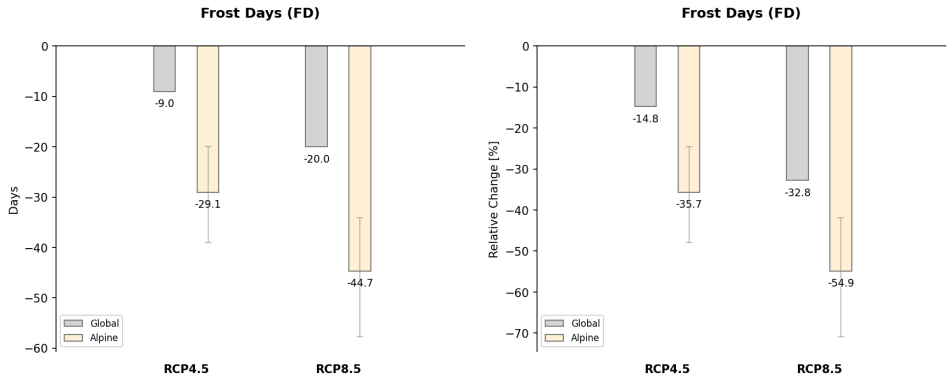

Figure 6.1: Changes in **Frost Days** in the year 2090. On the left the changes in the index's Units. On the Right, changes in percentage.

For what concerns the number of Icing Days lost 6.2 is lower than the number of FD lost. However, because by definition there are more Frost Days than Icing Days in a year (In fact, Frost Days include the Icing Days), this difference is expected. It is better to look instead at the relative scale, which shows the decrease is larger in ID, as it reaches the −67% of change.

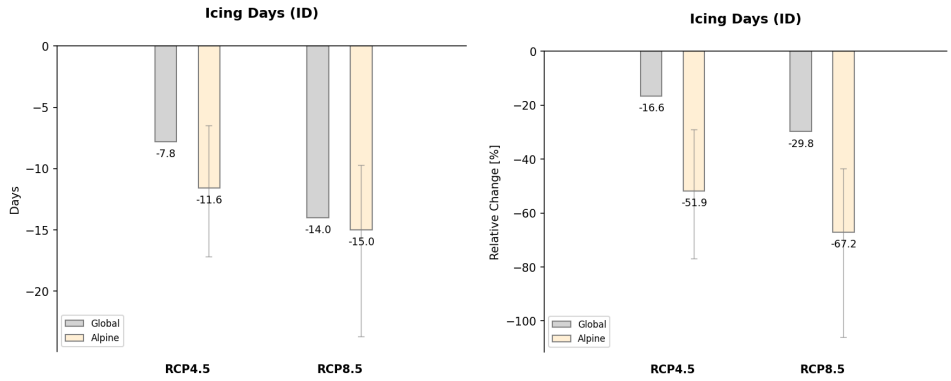

Figure 6.2: Changes in **Icing Days** in the year 2090. On the left the changes in the index's Units. On the Right, changes in percentage.

As for the summer days index (Figure 6.3), there is a general increase in both regions. There is a higher increasing of days in the Andes, because it is located in a tropical region with no seasonality, so the expected number of summer days in a year is higher. If we look the relative changes there is a higher warming in the Alps compared to SU on a global scale and on the Andes region. This increase is critical, because it means in the future some spring and autumn days will reach temperatures to be considered as summer in the past.

In both regions tropical nights (TR) are dramatically greater than on a global scale (Figure 6.4). These increases are larger than their respective counterpart of summer days for Alps and Andes. Whereas for the global data this is not the case as the summer days increase are larger.

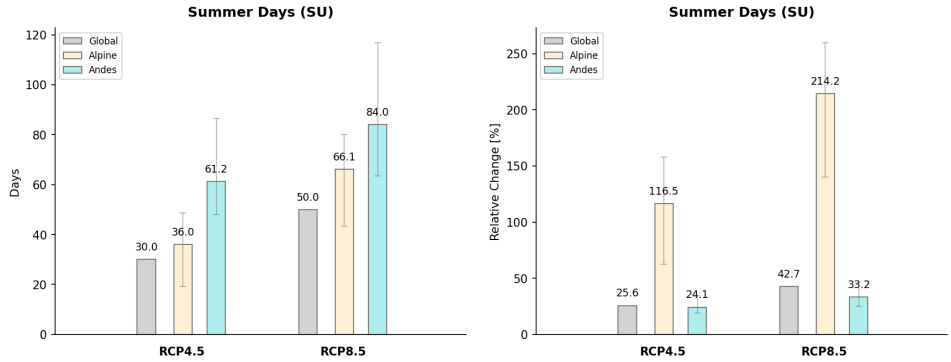

Figure 6.3: Changes in **Summer Days** in the year 2090. On the left the changes in the index's Units. On the Right, changes in percentage.

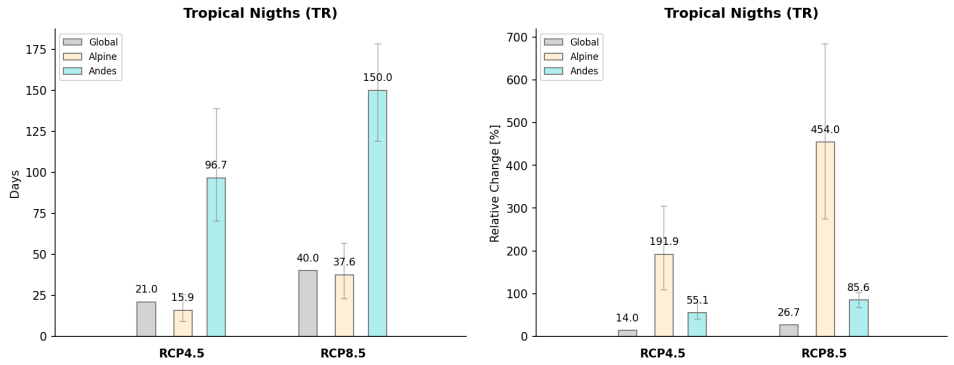

Figure 6.4: Changes in **Tropical Nights** in the year 2090. On the left the changes in the index's Units. On the Right, changes in percentage.

We calculated TXx, TXn, TNx, TNn indices yearly (Figure 6.5). In the Alps these indices can be interpreted as the warmest day in the year, TXn as the coldest day in the year, TNx as the warmest night in the year and TNn as the coldest night in the year. For the Alpine region in particular, we know the warmest day and warmest night of the year occur during the summer, and the coldest day and night during winter. In Andes the warming increase of TXx and TNn are similar to the global increase. In contrast, the Alps indicate stronger warming in comparison to the global scale. This is consistent with what Dake Arndt [13], chief of climate monitoring at the NOAA National Centers for Environmental Information, says: *"the colder places are warming faster than the warmer places"*. In the Alps is projected higher warming in winter nights (TNn) than summer nights (TNx) and higher warming in summer days (TXx) than winter days (TXn).

The warming increase in TNn is greater than TXx in the Alpine region in RCP4.5, and is agree with global data. On the other hand, for RCP8.5 TXx of 7.2°C exceeds the TNn warming of 6.6°C. Therefore if global warming follow the RCP8.5 scenario the Alps will face severe warming in summer. Instead, in Andes (tropical region) the increases in temperature are compatible between TXx and TNn, this is consistent as mentioned Sillmann et al. in his study.

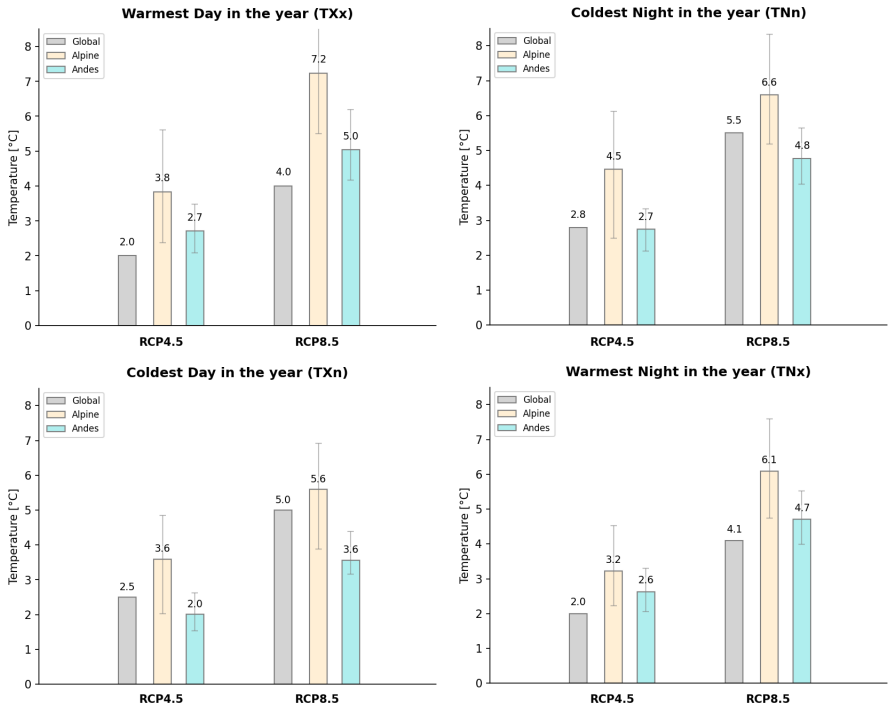

Figure 6.5: Changes in **TXx**, **TNn** (top), **TXn**, **TNx** (bottom), in the year 2090.

As we can see in Figure 6.6 Growing season length is projected to increase further in the Alps compared to the global scale. These increases are of 35.8 days and 59 days in RCP4.5 and RCP8.5 respectively. This mean, is increasing the warm period in the year.

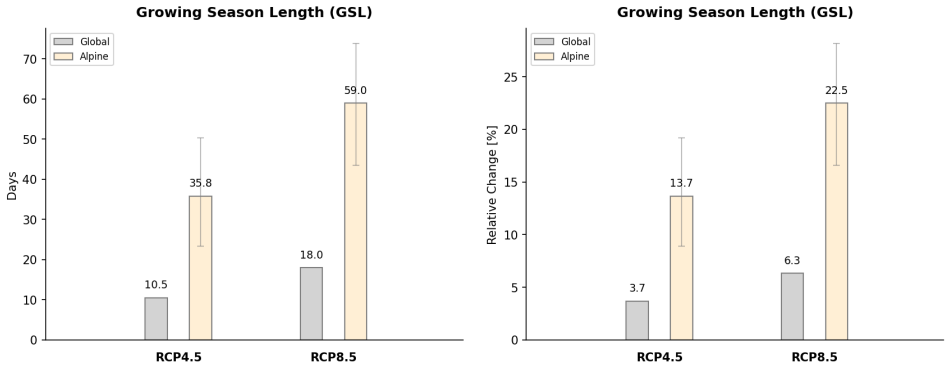

Figure 6.6: Changes in **Growing Season Length** in the year 2090. On the left the changes in the index's Units. On the Right, changes in percentage.

As mentioned by Sillmann et al. [28], by construction the percentile indices represent exceedance rates, relative to the reference period (1961-1990), in which models average to approximately 10%, wich will be the baseline for changes in the future.
All projections in the annual number of cold days (TX10p), cold nights

(TN10p), warm days (TX90p) and warm nights (TN90p) indicate significant warming trends towards the year 2090.

Figure 6.7 shows the exceedance rate for Warm Days and Nights by the year 2090.

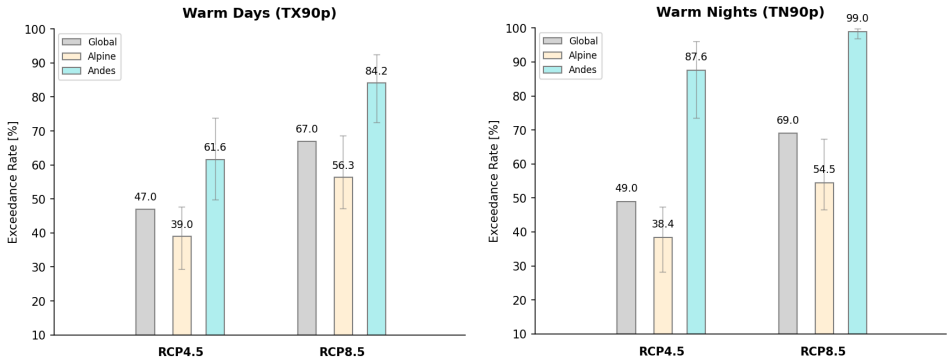

Figure 6.7: Changes in **Warm Days** in the left and **Warm Nights** in the right, in the year 2090.

For warm days and warm nights (TX90p and TN90p) the model simulation indicate a steady increase in both regions and in the global scale. The increase is more pronounced for TN90p than for TX90p in Andes, consistent with the global data. For the Alps the increase is very similar for both indices (slightly larger for warm days than for warm nights).

The Increase in the Alps is lower for both indices and does not reach the 60% of exceedence. This is due to the seasonality of the region. The 90th percentile in the base period corresponds to the warmest days/nights of the year, which are found during the summer. In the future, it is hard that all days/nights in other seasons (specially winter) reach the temperature of those summer days/nights of the reference period.

On the other hand, as the Andes region does not have seasons and therefore has a lower day to day temperature variability, it is more susceptible to increases in percentile based indices. This is observed in the RCP projections, that show values well over 60% of exceedence. This is particularly critical for the TN90p in RCP8.5 which virtually reaches 100%. This means *all* of the days in the future are considered as warm when compared to the days in the base period.

The global data sits between the numbers for the Alps and Andes, for both indices and both RCP scenarios, which is consistent with the fact that it is a global average.

Figure 6.8 shows the exceedance rate for Cold Days and Nights by the year 2090.

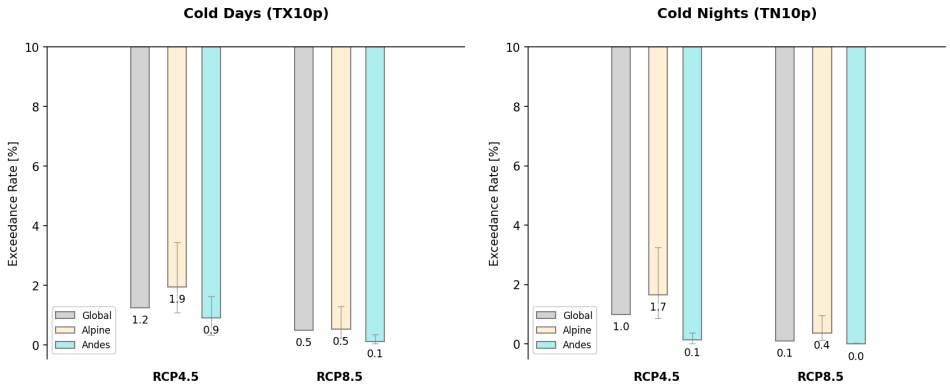

Figure 6.8: Changes in **Cold Days** in the left and **Cold Nights** in the right, in the year 2090.

The median decrease is more pronounced for TN10p than for TX10p in Andes and the Alps, consistent to the global scale whose values fit in the middle of those of the two regions.

The decrease is slightly larger for the Andes region, which as explained above has no seasonality and lower temperature variability. It reaches 0.0% for TN10p and 0.1% for TX10p in RCP8.5 which means there will be virtually no cold days and cold nights as defined in the baseline period.

In the Alps, even for the RCP8.5 projections there is still a small number of days (0.5%) and nights (0.4%). This is a consequence of the seasonality, as during the winter a small percentage of days still qualify as cold.

Warm Spell Duration and Cold Spell Duration indices are shown in Figures 6.9 and 6.10

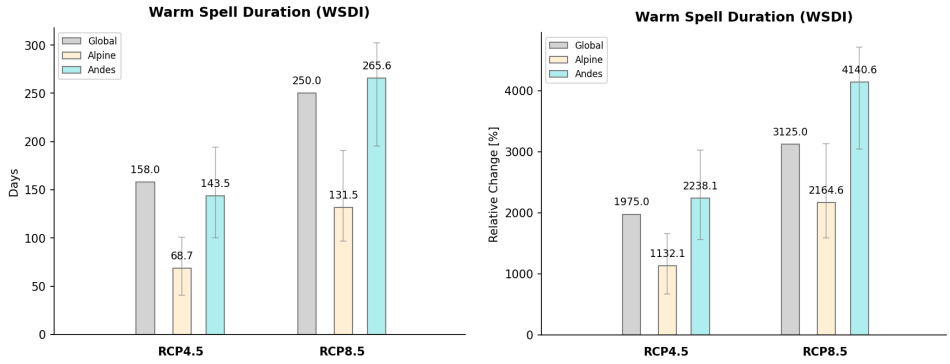

Figure 6.9: Changes in **Warm Spell Duration** in the year 2090. On the left the changes in the index's Units. On the Right, changes in percentage.

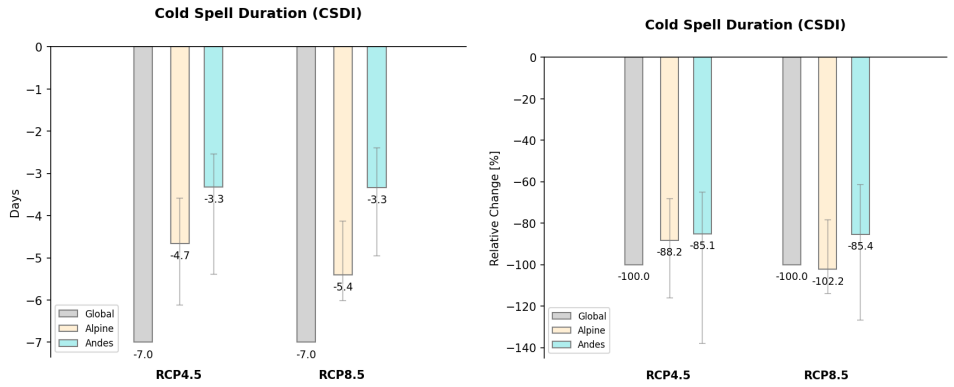

Figure 6.10: Changes in **Cold Spell Duration** in the year 2090. On the left the changes in the index's Units. On the Right, changes in percentage.

Warm spell duration index (WSDI) is expected to increase, according to the temperature rising mentioned before. The largest increase is expected in RCP8.5 and corresponds to 131.5 days (2146% of relative change) and 265.6.6 days (4140.6% of relative change) in Alps and Andes respectively. The increase in the Andes is larger than in the Alps and global data, as it corresponds to a tropical region and therefore has more possibilities to have a continuous number of days with high temperature. On the other hand, the seasonality of the Alps interrupts the warm spells, but even if that is the case, the increase is still significative. The global data sits between the Andes and Alpine values.

The cold spell duration index (CSDI) is projected to decrease in both regions and both scenarios. Even if the number of days seems low, in reality for global data in both scenarios, and in the Alps for RCP8.5 all of the days are lost (decrease of 100%). For Andes and Alpine in RCP4.5 the decrease is also severe (between 80% and 90%)

Figure 6.11 shows the relative change for Highest 1-day precipitation and Highest 5-day precipitation. Changes in heavy and extreme rainfall days are observed in Figure 6.12.

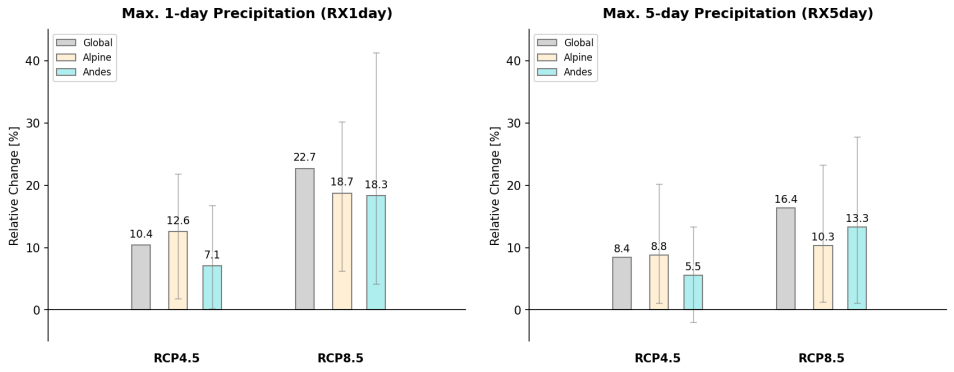

Figure 6.11: Changes in **Highest 1-day precipitation amount** in the left and **Highest 5-day precipitation amount** in the right, in the year 2090.

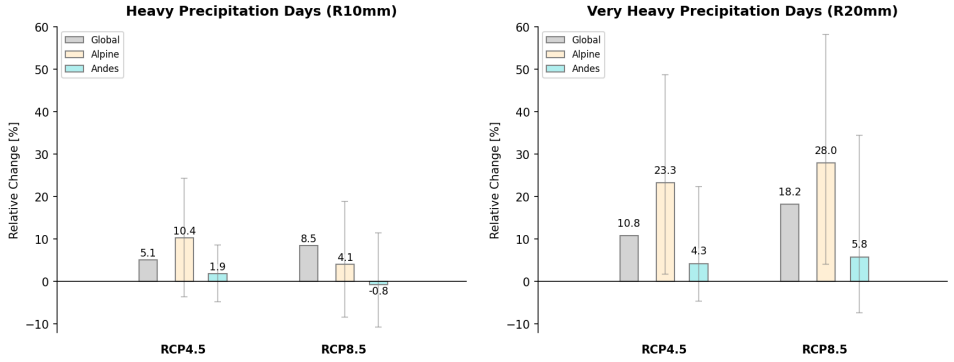

Figure 6.12: Changes in **Heavy Precipitation Days** in the left and **Very Heavy Precipitation Days** in the right, in the year 2090.

The maximum amount of rainfall in a day (RX1day) is projected to increase. In RCP4.5 the largest increase is expected in the Alps by 12.6%. For RCP8.5 similar increases in both regions are expected by about 18%. As for, heavy precipitation (RX5day) is expected to increase to 10% and 13% in Alpine and Andes respectively, if global warming follow the path RCP8.5.
In Alps precipitation extremes (R20mm) are projected to significantly increase in both scenarios, reaching an increase of about 28% in RCP8.5. Although there is a great variability in Andes, there are no significant changes in precipitation extremes.

The Figure below 6.13 show the Precipitation Amount in Wet Days and Precipitacion Intensity by the year 2090.

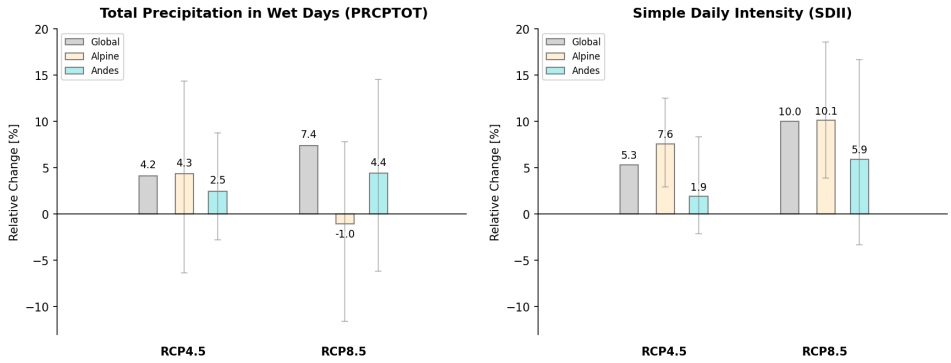

Figure 6.13: Changes in **Precipitation amount due to wet days** in the left and **Intense precipitation** in the right, in the year 2090.

A slight reduction in PRCPTOT is projected in RCP8.5 in the Alps by 1%, instead a small increase is is expected in Andes by 4.4%. Whereas intense precipitation (SDII) is projected to increase significantly in both regions, mainly in the Alps of about 10.1% similarly to the global scale. This indicate that in the Alps in particular, the precipitation does not increase as much, or even decreases, but there is a expected intensification of rainfall.

Changes in consecutive dry/wet days and Wet Days are observed in Figure 6.13 and Figure 6.15 by the year 2090.

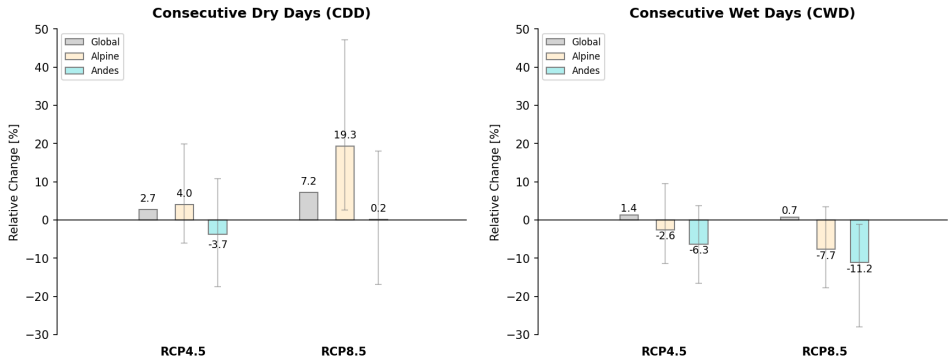

Figure 6.14: Changes in **Consecutive Dry Days** in the left and **Consecutive Wet Days** in the right, in the year 2090.

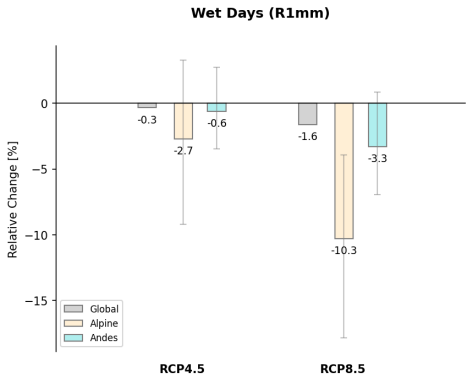

Figure 6.15: Changes in **Wet Days** by the year 2090.

The maximum number of consecutive dry days is projected to significantly increase in Alps by about 19.3% in RCP8.5, particulary in this scenario there is a great uncertainty of how much could variate CDD. This behavior agree with what Sillmann et al. [28] mentioned, *"the regions affected by a decrease in total precipitation (as it is in the Alps), generally coincide with a significant increase in CDD"*.
On the other hand, as a consequence of increasing CDD, a decrease is expected in consecutive wet days (CWD). In Andes there is a great variability in CDD and CWD. However, indicatively shows a reduction in wet days by 11.2% in RCP8.5. In fact, Wet Day index 6.15 reinforces what I mentioned previously. Particularly in the Alps a decrease of 10.3% of wet days is projected in RCP8.5.

Changes in Very Wet Days and Extremely Wet Days are observed in Figure 6.16 by the year 2090.

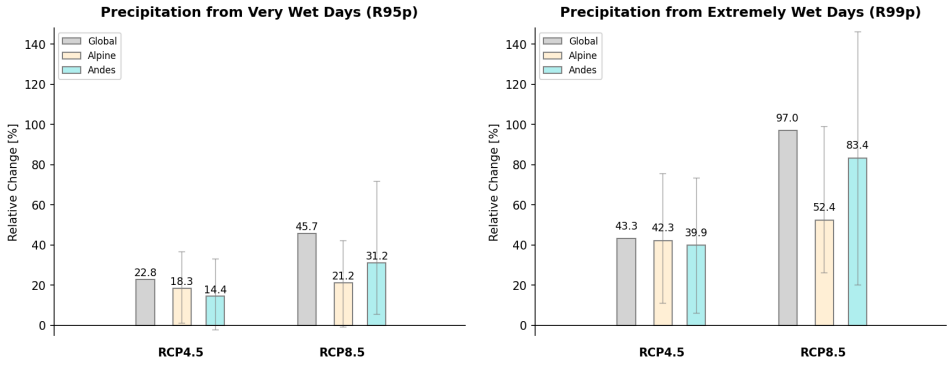

Figure 6.16: Changes in **Precipitation from very Wet Days** in the left and **Precipitation from Extremely Wet Days** in the right, in the year 2090.

Extreme precipitation are projected to increase in both regions and both scenarios. In R99p is expected an increase of about 52.4% and 83.4% in RCP8.5. However, there is large variability in the trend of CMIP5 models

for these indices.

6.2 CONCLUSIONS

In this thesis we presented a climate change study based on the atmospheric variables T_{mean}, T_{max}, T_{min} and Pr, for two regions with different meteorological conditions, in the time span $1860 - 2090$, using historical simulation and two future projections: RCP4.5 and RCP8.5 from the CMIP5 models. We evaluated monthly and daily data using the climate data operators library (CDO).

From monthly data, we found small trends in the T_{mean} values, towards warmer climate in the future. For the Pr, no tendency was found. The monthly data indicated high variability among the used models, and was found to be not very reliable for the objective of this thesis.

Daily data, coupled with the a clear definition of 27 climate extremes from the ETCCDI allowed for a better understanding of future climate projections. Using daily variables T_{max} T_{min} and Pr we were able to show that CMIP5 models can be applied to relatively small regions, without the need for downscaling. The obtained results agree with previous climate studies and suggest an increase in extreme events for both temperature and precipitation.

All of the temperature indices project higher temperatures. The warming started at the end of the 20^{th} century and will continue to increase during the whole 21^{st} century. Due to the different climate conditions on the studied regions, some indices affected one region more than the other. TX90, TN90 and WSDI show a larger increase in the Andes, as this region is located in the tropic and does not have seasons.

Cold temperature indicators like TN10p, TX10p and CSDI show dramatic changes for all regions and both RCPs scenarios, reaching 100% of decrease.

Precipitation indices show no significant changes in annual total precipitation. However the decline in number of wet ($R1mm$) and consecutive wet days (CWD), and the increase in precipitation intensity $SDII$ and consecutive dray days (CDD) indicate that in the future, there will be more days with heavy precipitation, and more days without any precipitation at all which is also indicated by the rise in $R20mm$ and $R99p$. This is consistent with the rise in temperatures, as explained by the Clausius-Clapeyron relation.

The Andes region, in general shows larger variability among the models, even with daily data and using the ETCCDI indices. This is particularly evident for the precipitation projections.

From the same dataset, a deeper analysis could be conducted, examining the seasonal behavior of the Alpine region, to understand in the changes in temperature and precipitation are evenly distributed among the year, or if they are located in a specific season. A similar study could be performed for the Andes, using a bimodal seasonality that fits better with the tropical regions.

Considering that the next year the new *CMIP6* models will be released, further investigations could be performed using the updated simulations and identifying key differences in the results obtained from both projects.

Part II

APPENDIX

A

APPENDIX

A.1 CMIP5 MODELS

Table A.1: CMIP5 global climate models used in this study. For each model it is reported the spatial resolution. CMIP5 models with longitudinal resolution equal to or finer than 1.5° longitude are highlighted in bold.

CMIP5 Model	**Institute and Country of Origin**	**RCP Scenario**		**Spatial Resolution °lat x °lon**
		4.5	**8.5**	
ACCESS1.0	CSIRO-BOM, Australia	x	x	1.25 x 1.87
ACCESS1.3	CSIRO-BOM, Australia	x	x	1.25 x 1.87
BCC-CSM1.1	BCC, CMA, China	x	x	2.79 x 2.81
BCC-CSM1.1(m)	BCC, CMA, China	x	x	2.79 x 2.81
BNU-ESM	BNU, China	x	x	2.79 x 2.81
CanCM4	CCCMA, Canada	x	-	2.79 x 2.81
CanESM2	CCCMA, Canada	x	x	2.79 x 2.81
CCSM4	NCAR, USA	x	x	**0.94 x 1.25**
CESM1(BGC)	NSF-DOE-NCAR, US	x	x	**0.94 x 1.25**
CESM1(CAM5)	NSF-DOE-NCAR, USA	x	x	**0.94 x 1.25**
CESM1(FASTCHEM)	NSF-DOE-NCAR, USA	-	-	**0.94 x 1.25**
CESM1(WACCM)	NSF-DOE-NCAR, USA	x	x	1.88 x 2.50
CMCC-CESM	CMCC, Italy	-	x	3.43 x 3.75
CMCC-CM	CMCC, Italy	x	x	**0.74 x 0.75**
CMCC-CMS	CMCC, Italy	x	x	3.71 x 3.75
CNRM-CM5	CNRM-CERFACS, France	x	x	**1.40 x 1.40**
CNRM-CM5-2	CNRM-CERFACS, France	-	-	**1.40 x 1.40**
CSIRO-Mk3-6-0	CSIRO-QCCCE, Australia	x	x	1.86 x 1.87
CSIRO-Mk3L-1-2	CSIRO-QCCCE, Australia	x	-	3.18 x 5.62
EC-EARTH	EC-EARTH, Europe	x	x	**1.12 x 1.12**
FGOALS-g2	FIO, SOA, China	x	x	2.79 x 2.81
FGOALS-s2	FIO, SOA, China	x	x	4.10 x 5.00
FIO-ESM	FIO, SOA, China	x	x	2.80 x 2.80
GFDL-CM2.1	NOAA, GFDL, USA	x	-	2.02 x 2.50
GFDL-CM3	NOAA, GFDL, USA	x	x	2.00 x 2.50
GFDL-ESM2G	NOAA, GFDL, USA	x	x	2.02 x 2.50
GFDL-ESM2M	NOAA, GFDL, USA	x	x	2.02 x 2.50

Table A.1: CMIP5 global climate models used in this study. For each model it is reported the spatial resolution. CMIP5 models with longitudinal resolution equal to or finer than 1.5° longitude are highlighted in bold.

CMIP5 Model	**Institute and Country of Origin**	**RCP Scenario**		**Spatial Resolution**
		4.5	**8.5**	**°lat x °lon**
GISS-E2-H	NASA/GISS, NY, USA	x	x	2.00 x 2.50
GISS-E2-H-CC	NASA/GISS, NY, USA	x	x	2.00 x 2.50
GISS-E2-R	NASA/GISS, NY, USA	x	x	2.00 x 2.50
GISS-E2-R-CC	NASA/GISS, NY, USA	x	x	2.00 x 2.50
HadCM3	MOHC, UK	x	-	2.50 x 3.75
HadGEM2-AO	NIMR-KMA, Korea	x	x	1.25 x 1.87
HadGEM2-CC	MOHC, UK	x	x	1.25 x 1.87
HadGEM2-ES	MOHC, UK	x	x	1.25 x 1.87
INMCM4	INM, Russia	x	x	1.50 x 2.00
IPSL-CM5A-LR	IPSL, France	x	x	1.89 x 3.75
IPSL-CM5A-MR	IPSL, France	x	x	1.26 x 2.50
IPSL-CM5B-LR	IPSL, France	x	x	1.89 x 3.75
MIROC4h	JAMSTEC, Japan	x	-	**0.56 x 0.56**
MIROC5	JAMSTEC, Japan	x	x	**1.40 x 1.40**
MIROC-ESM	JAMSTEC, Japan	x	x	2.79 x 2.81
MIROC-ESM-CHEM	JAMSTEC, Japan	x	x	2.79 x 2.81
MPI-ESM-LR	MPI-N, Germany	x	x	1.86 x 1.87
MPI-ESM-MR	MPI-N, Germany	x	x	1.86 x 1.87
MPI-ESM-P	MPI-N, Germany	-	-	1.86 x 1.87
MRI-CGCM3	MPI-N, Germany	x	x	**1.12 x 1.12**
MRI-ESM1	MRI, Japan	-	x	**1.12 x 1.12**
NorESM1-M	NCC, Norway	x	x	1.89 x 2.50
NorESM1-ME	NCC, Norway	x	x	1.89 x 2.50

Table A.2: Core Set of 27 Extreme Indices Recommended by the ETCCDI.

ID	Index Name	Variable	Units
FD	Number of frost days	tasmin	Days
SU	Number of summer days	tasmax	Days
ID	Number of icing days	tasmax	Days
TR	Number of tropical nights	tasmin	Days
GSL	Growing season length	tasmin, tasmax	Days
TXx	Monthly maximum value of daily maximum temperature	tasmax	Temperature [°C]
TNx	Monthly maximum value of daily minimum temperature	tasmin	Temperature [°C]
TXn	Monthly minimum value of daily maximum temperature	tasmax	Temperature [°C]
TNn	Monthly minimum value of daily minimum temperature	tasmin	Temperature [°C]
TN10p	Percentage of days when TN<10^{th} percentile	tasmin	Exceedance Rate [%]
TX10p	Percentage of days when TX10^{th} percentile	tasmax	Exceedance Rate [%]
TN90p	Percentage of days when TN>90^{th} percentile	tasmin	Exceedance Rate [%]
TX90p	Percentage of days when TX>90^{th} percentile	tasmax	Exceedance Rate [%]
WSDI	Warm spell duration index	tasmax	Days
CSDI	Cold spell duration index	tasmin	Days
DTR	Daily temperature range	tasmin, tasmax	Days
Rx1day	Monthly maximum 1-day precipitation	pr	Precipitation [mm]
Rx5day	Monthly maximum consecutive 5-day precipitation	pr	Precipitation [mm]

Table A.2: Core Set of 27 Extreme Indices Recommended by the ETCCDI.

ID	Index Name	Variable	Units
SDII	Simple precipitation intensity index	pr	Intensity [mm/day]
R10mm	Annual count of days when PRCP>= 10mm	pr	Days
R20mm	Annual count of days when PRCP>= 20mm	pr	Days
Rnnmm	Annual count of days when PRCP>= nnmm	pr	Days
CDD	Maximum length of dry spell	pr	Days
CWD	Maximum length of wet spell	pr	Days
R95pTOT	Annual total PRCP when RR > 95p	pr	Precipitation [mm]
R99pTOT	Annual total PRCP when RR > 99p	pr	Precipitation [mm]
PRCPTOT	Annual total precipitation in wet days	pr	Precipitation [mm]

BIBLIOGRAPHY

[1] 21st century climate change in the European Alps A review. "21st century climate change in the European Alps - A review." In: *Science of the Total Environment* 493.2 (2013), pp. 1138–1151. DOI: 10.1016/j.scitotenv.2013.07.050. eprint: http://dx.doi.org/10.1016/j.scitotenv.2013.07.050.

[3] M. Beniston. "Extreme climatic events: examples from the alpine region." In: *J. Phys. IV France* 121 (2004), pp. 139–1149. DOI: 10.1051/jp4:2004121008. URL: https://doi.org/10.1051/jp4:2004121008.

[4] S. Brönnimann, J. Rajczak, E. M. Fischer, C. C. Raible, M. Rohrer, and C. Schär. "Changing seasonality of moderate and extreme precipitation events in the Alps." In: *Natural Hazards and Earth System Sciences* 18.7 (2018), pp. 2047–2056. DOI: 10.5194/nhess-18-2047-2018. URL: https://www.nat-hazards-earth-syst-sci.net/18/2047/2018/.

[6] Silvia Chersich, K. Rejšek, Valerie Vranová, Massimiliano Bordoni, and Claudia Meisina. "Climate change impacts on the Alpine ecosystem: an overview with focus on the soil." In: *Journal of Forest Science* 61 (Nov. 2015), pp. 496–514. DOI: 10.17221/47/2015-JFS.

[10] Jhan Carlo Espinoza, René Garreaud, Germán Poveda, Paola A. Arias, Jorge Molina-Carpio, Mariano Masiokas, Maximiliano Viale, and Lucia Scaff. "Hydroclimate of the Andes Part I: Main Climatic Features." In: *Frontiers in Earth Science* 8 (2020), p. 64. ISSN: 2296-6463. DOI: 10.3389/feart.2020.00064. URL: https://www.frontiersin.org/article/10.3389/feart.2020.00064.

[11] Field et al. *Managing the Risks of Extreme Events and Disasters to Advance Climate Change Adaptation. A Special Report of Working Groups I and II of the Intergovernmental Panel on Climate Change*. Cambridge University Press, Cambridge, United Kingdom and New York, NY, USA, 2012, p. 582.

[16] Jascha Lehmann, Dim Coumou, and Katja Frieler. "Increased record-breaking precipitation events under global warming." In: *Climatic Change* 132 (Aug. 2015). DOI: 10.1007/s10584-015-1466-3.

[17] Collins M. et al. *Long-term Climate Change: Projections, Commitments and Irreversibility. In:The Physical Science Basis Contribution of Working Group I to the Fifth Assessment Report of the Intergovernmental Panel on Climate Change*. Cambridge University Press, Cambridge, United Kingdom and New York, NY, USA, 2013, pp. 1029–1136. DOI: 10.1017/CBO9781107415324.004.

[18] Guillermo Murray-Tortarolo, Victor J Jaramillo, Manuel Maass, Pierre Friedlingstein, and Stephen Sitch. "The decreasing range between dry- and wet- season precipitation over land and its effect on vegetation primary productivity." In: *PLOS ONE* 12 (2017), pp. 1–11. DOI: 10.1371/journal.pone.0190304. URL: https://doi.org/10.1371/journal.pone.0190304.

[21] C. Pabón et al. "Observed and Projected Hydroclimate Changes in the Andes." In: *Frontiers in Earth Science* 8 (2020), p. 61. ISSN: 2296-6463. DOI: 10.3389/feart.2020.00061. URL: https://www.frontiersin.org/article/10.3389/feart.2020.00061.

[22] R. Palomino, S Córdoba, Gámiz S, Castro Y, and Esteban M. "Summer precipitation projections over northwestern South America from CMIP5 models." In: *Global and Planetary Change* 131 (2015), pp. 11–23. DOI: doi.org/10.1016/j.gloplacha.2015.05.004.

[23] J. Rajczak, P. Pall, and C. Schär. "Projections of extreme precipitation events in regional climate simulations for Europe and the Alpine Region." In: *Journal of Geophysical Research: Atmospheres* 118 (2013), pp. 3610–3626. DOI: 10.1002/jgrd.50297.

[24] T. Schoolmeester, M. Saravia, M. Andresen, J. Postigo, A. Valverde, B. Jurek M.and Alfthan, and S. Giada. *Outlook on Climate Change Adaptation in the Tropical Andes Mountains*. UN Environment, GRID-Arendal., 2016.

[25] Uwe Schulzweida. *CDO User Guide*. Oct. 2019. DOI: 10.5281/zenodo.3539275. URL: https://doi.org/10.5281/zenodo.3539275.

[27] Juan P. Sierra, Paola A. Arias, and Sara C. Vieira. "Precipitation over Northern South America and Its Seasonal Variability as Simulated by the CMIP5 Models." In: *Hindawi Publishing Corporation* (2015), p. 22. DOI: doi.org/10.1155/2015/634720.

[28] J. Sillmann, V. V. Kharin, F. W. Zwiers, X. Zhang, and D. Bronaugh. "Climate extremes indices in the CMIP5 multimodel ensemble: Part 2. Future climate projections." In: *Journal of Geophysical Research: Atmospheres* 118.6 (), pp. 2473–2493. DOI: 10.1002/jgrd.50188. URL: https://agupubs.onlinelibrary.wiley.com/doi/abs/10.1002/jgrd.50188.

[29] Sebastian Dominik Sippel. "Climate Extremes and Their Impact On Ecosystem-Atmosphere Interaction." PhD thesis. ETH Zurich, 2017.

[30] A. Soncini and D. Bocchiola. "Assessment of future snowfall regimes within the Italian Alps using general circulation models." In: *Cold Regions Science and Technology* 68.3 (2011), pp. 113 –123. ISSN: 0165-232X. DOI: https://doi.org/10.1016/j.coldregions.2011.06.011. URL: http://www.sciencedirect.com/science/article/pii/S0165232X11001133.

[31] Stocker, T.F., D. Qin, G.-K. Plattner, M. Tignor, S.K. Allen, J. Boschung, A. Nauels, Y. Xia, and V. Bex. *IPPC 2013 Summary for Policymakers in Climate Change 2013: The Physical Science Basis.* Cambridge University Press, Cambridge, United Kingdom and New York, NY, USA, 2013, pp. 1–30. DOI: 10.1017/CBO9781107415324.004.

[32] T.F. Stocker, D. Qin, G.-K. Plattner, M. Tignor, S.K. Allen, J. Boschung, A. Nauels, Y. Xia, V. Bex, and P.M. Midgley (eds.) *IPCC 2013: Climate Change 2013: The Physical Science Basis Contribution of Working Group I to the Fifth Assessment Report of the Intergovernmental Panel on Climate Change*. Cambridge University Press, Cambridge, United Kingdom and New York, NY, USA, 2013, p. 1535. DOI: 10.1017/CBO9781107415324.

[33] K. E. Taylor, R. J. Stouffer, and G. A. Meehll. "An overview of the CMIP5 and the experiment design." In: *Bull. Amer. Meteor. Soc.* 93 (2012), pp. 485–498. DOI: https://doi.org/10.1175/BAMS-D-11-00094.1.

[34] S. Terzago, J. von Hardenberg, E. Palazzi, and A. Provenzale. "Snow water equivalent in the Alps as seen by gridded data sets, CMIP5 and CORDEX climate models." In: *The Cryosphere* 11.4 (2017), pp. 1625–1645. DOI: 10.5194/tc-11-1625-2017. URL: https://www.the-cryosphere.net/11/1625/2017/.

[36] Elias M. Zubler, Andreas M. Fischer, Friederike Fröb, and Mark A. Liniger. "Climate change signals of CMIP5 general circulation models over the Alps - impact of model selection." In: *International Journal of Climatology* 36.8 (2016), pp. 3088–3104. DOI: 10.1002/joc.4538. URL: https://rmets.onlinelibrary.wiley.com/doi/abs/10.1002/joc.4538.

SITOGRAPHY

[2] *Alps*. URL: https://www.britannica.com/place/Alps.

[5] *Cdo rb,py*. URL: https://code.mpimet.mpg.de/projects/cdo/wiki/Cdo%7Brbpy%7D.

[7] *Climate extremes indices (CEI) with CDO's*. URL: https://slides.com/wachsylon/cdoetccdi#/3/1.

[8] 2011 ENES. *CMIP5 Data Structure*. 2011. URL: https://portal.enes.org/data/enes-model-data/cmip5/datastructure.

[9] *Earth System Grid Federation*. URL: https://esgf.llnl.gov/.

[12] Geophysical Fluid Dynamics Laboratory GFDL. *Climate Modeling*. URL: https://www.gfdl.noaa.gov/climate-modeling/.

[13] *How Warming Winters Are Affecting Everything*. 2020. URL: https://www.npr.org/2020/02/18/803125282/how-warming-winters-are-affecting-everything?t=1594566128127&fbclid=IwAR1YUQ2a8RJnWDkvqoHSMkLj2XldoWhgdyeyZGQ-c5cDxtRfgOh0&t=1594566983132.

[14] IPCC. *Data Distribution centre*. URL: https://www.ipcc-data.org/guidelines/pages/gcm_guide.html.

[15] *KNMI Climate Explorer*. URL: https://climexp.knmi.nl/start.cgi?id=42e1a289c2b3adc9769810607787f7f6.

[19] NOAA. *Climate Models*. URL: https://www.climate.gov/maps-data/primer/climate-models.

[20] *Network Common Data Form (NetCDF)*. URL: https://www.unidata.ucar.edu/software/netcdf/.

[26] *Scripts and Instructions to process ETCCDI compliant Climate Extremes Indices with CDOs*. URL: https://gitlab.dkrz.de/k204210/cdo_cei/-/tree/master.

[35] *The Alpine Region*. URL: https://ec.europa.eu/environment/nature/natura2000/biogeog_regions/alpine/index_en.htm#regional_features.

[Notes]